MINISTRY OF EDUCATION & TRAINING   MINISTRY OF NATIONAL DEFENSE

MILITARY TECHNICAL ACADEMY

Le Pham Binh

LINEAR STATIC AND DYNAMIC ANALYSIS OF FGM POROUS NANOPLATES RESTING ON ELASTIC FOUNDATION USING NONLOCAL ELASTICITY THEORY

A Thesis for the Degree of Doctor of Philosophy

HA NOI - 2023

MINISTRY OF EDUCATION & TRAINING   MINISTRY OF NATIONAL DEFENSE

MILITARY TECHNICAL ACADEMY

Le Pham Binh

LINEAR STATIC AND DYNAMIC ANALYSIS OF FGM POROUS NANOPLATES RESTING ON ELASTIC FOUNDATION USING NONLOCAL ELASTICITY THEORY

Specialization: Engineering Mechanics

Specialization code: 9.52.01.01

A Thesis for the Degree of Doctor of Philosophy

SUPERVISORS:

1. Assoc. Prof. Dr. Doan Trac Luat
2. Assoc. Prof. Dr. Le Minh Thai

HA NOI - 2023

CONTENTS

ASSURANCE

I hereby declare that this thesis was carried out by myself under the guidance of my supervisors. The presented results and data in the thesis are reliable and have not been published anywhere in the form of books, monographs, and articles.

Author

Le Pham Binh

ACKNOWLEDGEMENTS

LIST OF SYMBOLS AND ABBREVIATIONS

1. Symbols in Latin letters

a	Lengt
b	Width
c	Ceramic
$\mathbf{C}_e$	Element resistance matrix
E	Young's modulus
h	Thickness
k	Power-law index
$\mathbf{K}_e$	Plate element stiffness matrix
$\mathbf{K}_e^f$	Foundation element stiffness matrix
m	Metallic
$\mathbf{M}_e$	Element mass matrix
$\mathbf{N}$	Shape function
$p(t)$	Load
$\mathbf{q}_e$	Element displacement vector
$\mathbf{q}_i$	Node displacement vector
r_1	Inner diameter
R	Outer diameter
r, s	Natural coordinate
T	Kinetic energy
$\mathbf{u}$	Displacement vector
$\mathbf{u}_0$	Displacement vector at the mid-plane
U	Strain energy
u, v, w	Displacement components

u_0, v_0, w_0	Displacement components at the mid-plane
V	Energy stored in the deformed elastic foundation
W	Work done by applied force
x, y, z	Descactes coordinate

2. Symbols in Greek letters

∇	Laplace operator
ε	Strain vector at any point
ρ	Mass density
μ	Nonlocal factor
ν	Poisson coefficient
ξ	Porosity factor
$\boldsymbol{\sigma}$	Stress vector at any point
φ_x, φ_y	Rotation angles of the cross-section around the *y, x*-axes
ω	Natural frequency

3. Abbreviations

BCs	Boundary conditions
Case 1	Even porosity
Case 2	Uneven porosity
CPT	Classical plate theory
CCS	Completely clamped supported
CSS	Completely simply supported
EF	Elastic Foundation
FEM	Finite Element Method
FGM	Functionally Graded Material
FGP	Functionally Graded Porous Material
FSDT	First-order shear deformation theory

HSDT	Higher-order shear deformation theory
NET	Nonlocal Elasticity Theory
MCST	Modified Couple Stress Theory
MSGT	Modified Strain Gradient Theory
TSDT	Third-order shear deformation theory

LIST OF TABLES

LIST OF FIGURES

INTRODUCTION

1. Motivation

Due to their special mechanical, thermal, electrical, and chemical properties, nanostructures are increasingly used in the fields of medicine, electronics, and so on. Nanoplates are one of the most important structures commonly used as components in thin films, resonators, and sensors. Therefore, studying the vibrations of nanostructures is very important for design and manufacturing.

With nanostructures, the dimensional effect becomes special. The test and simulation results show a significant influence on the mechanical properties when the size of the structure becomes small. When the length of the plate decreases, the influence of the intermolecular forces on the static and dynamic properties is significant and cannot be neglected. Since nano experiments are difficult and the simulation of molecular dynamics is expensive, the development of mathematical models at the nanoscale has become a key issue for evaluating the mechanical behavior of nanostructures.

So the topic *"Linear Static and Dynamic Analysis of FGM Porous Nanoplates Resting on Elastic Foundation Using Nonlocal Elasticity Theory"* is an urgent topic that has scientific and practical significance.

2. Aim of this thesis

In general, studying nanostructures and the mechanical behavior of nanostructures is a large field. Within the framework of the thesis, the author focuses on studying the static and dynamic response of the functionally graded material (FGP) nanoplates using the finite element method (FEM) based on nonlocal elasticity theory (NET) with the following specific objectives:

- Establishing governing equations and algorithms to calculate the stress, strain, and displacement of the FGP nanoplates subjected to static and dynamic loads.

- The calculation programs are established by the Matlab software to analyze displacement, stress, free vibration, and dynamic response of FGP nanoplates resting on an elastic foundation.

- Investigating the influence of some structural factors, materials, and load characteristics on the mechanical behavior of FGP nanoplates.

3. Research objectives and research areas

3.1. Research objectives

a) Structure

- Plates: Consider FGP nanoplates with different shapes such as rectangular, L-shape, annular, and half-annular.

- Porosity distribution with two rules: evenly distributed and unevenly distributed.

- Elastic foundation: The plate is placed on the Winkler-Pasternak foundation with two layers. The first layer is a spring system with a stiffness coefficient of k_1, while the second layer is a surface layer with a shear stiffness of k_2.

b) Load

Consider FGP nanoplates subjected to static and dynamic loads. Nanostructure devices are mainly subjected to high temperature, moisture, pressure, and pulse load. So in the thesis, in the case of dynamic load, the pulse load is considered.

3.2. Research areas

Studying the mechanical behavior of FGP nanoplates subjected to static and dynamic loads by finite element method based on nonlocal elasticity theory and first-order shear deformation theory.

The thesis has three main problems:

- Static bending problem.

- Free vibration problem.

- Forced vibration problem.

4. Research methods

The finite element method, in combination with nonlocal elasticity theory and Hamilton's principle is used to establish governing equations for the static, free vibration, and forced vibration of FGP nanoplates.

The calculation program is established in the Matlab software. The obtained results are compared with those of other published ones to confirm the correctness of the proposed method.

Thesis structure:

The thesis is organized into an introduction, four chapters, conclusions, and recommendations for future studies as follows:

Introduction: Presenting the urgency of the topic, objectives, objects, areas, and research methods of the thesis.

Chapter 1: Research overview.

Chapter 2: Theoretical basic for calculation of FGP nanoplates resting on an elastic foundation.

Chapter 3: Static analysis of FGP nanoplates resting on an elastic foundation.

Chapter 4: Dynamic analysis of FGP nanoplates resting on an elastic foundation.

Conclusions and recommendations: This chapter summarizes the novel contributions of the thesis and suggests recommendations for future studies.

List of publications

Bibliography

Chapter 1 RESEARCH OVERVIEW

1.1. Overview of nanomaterials and nanostructures

1.1.1. The concept of nanomaterials and nanostructures

Nanomaterials are a type of material with a structure of porosities, fibers, tubes, thin sheets, and so on, with very small sizes ranging from 1 to 100 nanometers. Nanotechnology is a technology related to the design, analysis, calculation, fabrication, and application of nanometer-sized structures and devices.

In 1959, the concept of nanotechnology was mentioned by the American physicist Richard Feynman when he mentioned the ability to make matter at a microscopic size from the process of gathering atoms and molecules. In the 1980s, a number of analytical tools came out, such as scanning probe microscopes that could see the size of just a few atoms or molecules. These tools helped people see and understand more in the field of nano.

1.1.2. Properties of nanomaterials, nanostructures

Compared with conventional materials, nanomaterials have superior mechanical, physical, and chemical properties. The advanced properties of nanomaterials are due to their very small size compared to traditional materials. Nanomaterials are between the quantum properties of atoms and the bulk properties of materials. For bulk materials, the critical length of the properties is very small compared to the magnitude of the material, but for nanomaterials that is no longer the case, so the special properties start from this cause [1], [5].

1.1.3. Processing techniques of nanomaterials, nanostructures

Nanomaterials can be manufactured by four common methods, such as wet chemical methods, mechanical methods, thermal evaporation methods, and

gas-phase methods. Each method has its advantages and disadvantages, depending on material requirements, and equipment conditions, to choose the appropriate method.

a) Wet chemical methods

Wet chemical methods include hydrothermal, sol-gel, and co-precipitation methods. Under the influence of temperature, pressure, and pH conditions, solutions containing different ions are mixed in an appropriate proportion, and under the influence of these conditions, nanomaterials are precipitated. After filtration and drying processes, nano-sized materials are obtained.

The advantage of the wet chemical method is that the materials that can be manufactured are very diverse. They can be inorganic, organic, and metal materials. The advantage of this method is that it is cheap and can be used to produce a large number of materials, but it also has the disadvantage that compounds with water molecules can be difficult. It is not high efficiency, and the product is not uniform.

b) Mechanical methods

This method includes grinding and mechanical alloying methods. In this method, the material in powder form is ground to a smaller size. Nowadays, the most commonly used crushers are planetary or rotary crushers. The mechanical method has the advantages of being simple, the tooling is inexpensive, and it can be fabricated with a large amount of material. However, it has the disadvantage that the particles are agglomerated together, the particle size distribution is not uniform, it is easy to get contaminated by the fabrication tools, and it is often difficult to achieve small particles. This method is often used to create non-organic materials such as metals.

c) Thermal evaporation methods

Thermal evaporation methods include lithography and vacuum deposition methods. These methods are effective in fabricating thin films or surface coatings and can also be used to fabricate nanoparticles by creating nanomaterials from shields. However, this method is not very efficient for large-scale fabrication.

d) Gas-phase methods

Gas-phase methods include flame pyrolysis, electro-explosion, laser ablation, and plasma. The principle of these methods is to create nanomaterials from the gas phase. Flame pyrolysis is a long-standing method used to create simple materials such as carbon and silicon. Laser ablation can produce a variety of materials but is limited in the laboratory because of its low efficiency. The plasma methods can be used to produce a wide variety of materials but are not suitable for organic materials because their temperatures can reach 9000^{0}C.

1.1.4. Applications of nanostructures

Nanotechnology allows the fabrication and use of materials at the molecular level, increasing and creating special properties of materials and reducing the size of devices and systems to extremely small sizes. This is considered the industrial revolution, promoting development in all fields, especially biomedical, energy, environment, information technology military, and affecting the whole society [1].

a) In medicine - biology

Nanoparticles are seen as nanorobots that penetrate the body. Enables humans to intervene at the molecular or cellular scale. Currently, humans have created nanoparticles with biological properties that can be used to support disease diagnosis, drug delivery, and cell destruction.

b) Energy

The nanotechnology platform contributes to improving the quality of

solar cells, increasing the efficiency and storage of batteries and supercapacitors, and creating superconductors as electrical conductors for long-distance power transmission.

c) Electronic-mechanical

Nanotechnology helps to manufacture nanoelectronics components with extremely fast processing speeds to integrate into generations of nano-computer or use nanomaterials to make extremely small information recording devices, computer screens, and mobile phone screens. Besides, nanotechnology creates ultra-lightweight, super-strong nanomaterials. Nanomaterials are also used in the manufacture of devices for cars, planes, and spacecraft.

d) Apparel and food

The garment industry has turned a new page when applying silver nanoparticles, which have the ability to attract and destroy bacteria that cause unpleasant odors in clothes. This useful application has been applied to a number of sportswear models. Not stopping there, nanotechnology can make foods taste better and be more nutritious. In addition, nanotechnology will also help store food for many times longer by creating food storage materials that have the ability to kill bacteria.

e) Environment

Nanotechnology helps to replace polluting chemicals, materials, and traditional manufacturing processes with a new process that is compact, energy-efficient and has a reduced impact on the environment. Specifically, it has successfully fabricated nanofiltration membranes that contribute to filtering pollutant molecules; Nano-catalysts and adsorbents are used to treat waste quickly and completely. In which the highlight is the nano water purifier. This is a machine that uses nano technology with pore and micro-sized filters to remove impurities, bacteria, and dirt in the input water. Aside from that, the

membranes will help keep the minerals in the water that is good for the body.

Nanotechnology is truly a turning point in every aspect of life. Currently, nanotechnology is still being researched to discover all the great uses it brings.

1.2. Overview of plate theories and method of plate analysis

1.2.1. Plate theories

a) Classical plate theory

Advantages: This theory is simple and contains only three unknowns.

Disadvantages: It does not consider shear strain, only suitable for the calculation of thin plates.

b) First-order shear deformation theory

Advantages: The shear strain is taken into account, so it is suitable for the calculation of thin and moderate plates.

Disadvantages: The shear stress is constant with the plate thickness, which does not satisfy the condition that the shear stress is zero at the top and bottom faces. Therefore, a shear correction factor is needed, which depends on many conditions such as material, geometrical structure, boundary conditions, etc. (normally taken as 5/6).

c) Higher-order shear deformation theory

Advantages: The shear stress is distributed parabolic along the plate thickness and satisfies the condition that the shear stress is zero at the top and bottom faces. So, it is suitable for the calculation of moderate and thick plates.

Disadvantages: The higher-order shear deformation theory has a complex displacement field. The degree of freedom of the structure increases, resulting in a large amount of computation.

d) Quasi-3D theory

Advantages: The shear stress is distributed parabolic along the plate thickness and satisfies the condition that the shear stress is zero at the top and

bottom faces, considering the strain along the plate thickness, which is closer to the actual stress of the plates. Therefore, it is suitable for calculating both medium and thick structures.

Disadvantages: The higher-order shear deformation theory has a complex displacement field. The degree of freedom of the structure increases, resulting in a large amount of computation.

1.2.2. Method of plate analysis

There are different methods for calculating plates as well as nanoplates, such as analytical methods, numerical methods, and semi-analytical methods. Analytical methods include Navier solution, Lévy solution, Rayleigh-Ritz, Galerkin-Vlasov, and so on. Numerical methods include finite element methods (FEM), smoothed finite element method (S-FEM), finite difference method (FDM), differential quadrature method (DQM), differential element method (DEM), and isometric geometry method (IGA).

The advantage of analytical methods is that they can provide accurate and reliable solutions, but the transformations are quite complicated and are usually only used for simple and symmetrical structures. Numerical methods only give approximate solutions, but this method is effective for complex structures with different boundary conditions and loads. Nowadays, with the development of calculation methods and computer science, the results of numerical methods have been verified through many published works, confirming their reliability and accuracy.

a) Analytical methods

Analytical methods include Navier's solution, Lévy's solution, Rayleigh-Ritz, Galerkin-Vlasov, and so on.

Advantages: Analytical methods can give accurate solutions and high reliability.

Disadvantages: These methods must vary in complexity. Therefore, only used for both simple structures and boundary conditions.

b) Numerical methods

Numerical methods include the finite element method, smoothed finite element method, finite difference method, differential quadrature method, differential element method, and isometric geometry method.

Advantages: Numerical methods can compute complex structures.

Disadvantages: These methods only give approximate solutions.

However, with the development of calculation methods and computer science, the results of numerical methods have been tested through many published works, confirming their reliability and accuracy.

c) Semi-analytical methods.

Combination of analytical methods and numerical solutions.

1.3. Theory deserves nano-size effect

Nowadays, with the development of science and technology, compact devices are required, especially those in medicine, electronics, and aerospace. Nanoplates are one of the important structures commonly used in resonators [6], [7] (Figure 1.1), sensors [8], [9], [10] (Figure 1.2), and thin film elements [11]. As a result of their application, understanding the vibration characteristics of the nanoplates is an important issue. Therefore, the vibration analysis of the nanoplates has become a subject of primary interest in recent studies.
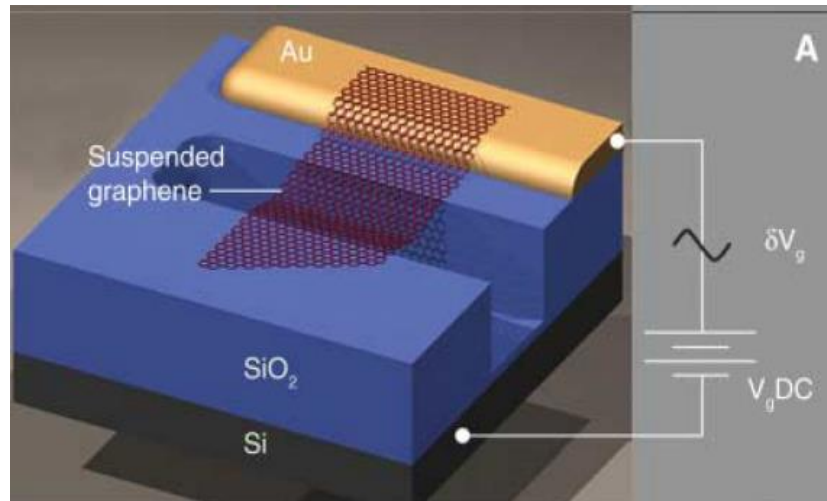
Figure 1.1. Nanoplate is used in the resonator [6].
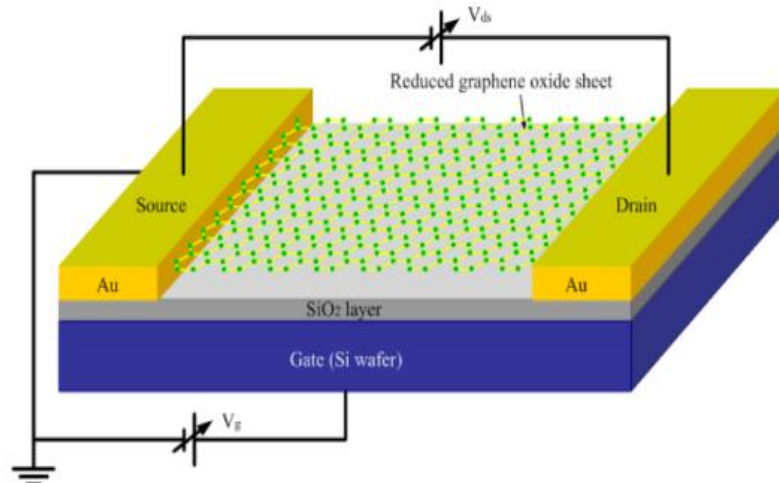
Figure 1.2. Nanoplate is used in the sensor [8].

Theoretical studies and experimental modelings show that the usual calculation theories for structures with sizes of millimeters and above are not accurate for micrometers and nanometers in size. There are three main theories have been proposed to analyze micro/nanostructures, which are the nonlocal elasticity theory, modified couple stress theory, and modified strain gradient theory.

1.3.1. Nonlocal elasticity theory

The nonlocal elasticity theory was initially formulated by Eringen [12],

[13], Eringen and Edelen [14] by means of an integral constitutive equation:

$$\sigma_{ij} = \int_x k(|x - \overline{x}|, \kappa) \sigma_{ij}^L dx \tag{1.1}$$

where

σ_{ij} and σ_{ij}^L are the components of the nonlocal and local stress tensors, respectively.

k is the kernel function determined in terms of nonlocal parameters κ and neighbor distance $|x - \overline{x}|$.

$\kappa = e_0 a$ with a and e_0 are the material constant and the parameter depending on the size ratio of the material, respectively. The value e_0 can be determined either from experiments or simulations.

By considering a specific kernel function k, Eringen [15] reformulated the nonlocal constitutive equation (1.1) in a differential form as follows:

$$\left(1 - \mu \nabla^2\right) \sigma_{ij} = \sigma_{ij}^L \tag{1.2}$$

where $\mu = \kappa^2$, ∇^2 is the Laplace operator.

The research results on nonlocal elasticity theory in the period from 1972 to 2002 were summarized by Eringen in the literature [16].

Compared to the integral model, the differential one is widely used for nanostructures due to its simplicity. More information about the paradoxical behavior of the differential model can be found in the literature [17], [18], [19].

1.3.2. Modified couple stress theory

The modified couple stress theory was proposed by Yang et al. [20] by modifying the classical couple stress theory of Toupin [21], Mindlin [22], Tiersten, and Koiter [23]. By introducing an additional equilibrium condition of moments of couples to enforce the couple stress tensor to be symmetric, the number of additional material length scale parameters in the modified couple

stress theory is reduced from two to one. This makes the modified couple stress theory more advantageous because the determination of the material parameters is a challenging task. The strain energy U is a function of both strain and curvature as follows [23]:

$$U = \frac{1}{2}\int_V \left(\sigma_{ij}\varepsilon_{ij} + m_{ij}\chi_{ij}\right)dV \tag{1.3}$$

where

m_{ij} are the components of the deviatoric part of the symmetric couple stress tensor.

χ_{ij} are the components of the symmetric curvature tensor defined by [23]:

$$\chi_{xx} = \frac{\partial\theta_x}{\partial x}, \; \chi_{yy} = \frac{\partial\theta_y}{\partial y}, \; \chi_{zz} = \frac{\partial\theta_z}{\partial z} \tag{1.4}$$

$$\chi_{xy} = \frac{1}{2}\left(\frac{\partial\theta_x}{\partial y} + \frac{\partial\theta_y}{\partial x}\right), \chi_{xz} = \frac{1}{2}\left(\frac{\partial\theta_x}{\partial z} + \frac{\partial\theta_z}{\partial x}\right), \chi_{yz} = \frac{1}{2}\left(\frac{\partial\theta_y}{\partial z} + \frac{\partial\theta_z}{\partial y}\right) \tag{1.5}$$

For a linear elastic material, m_{ij} are given by

$$m_{ij} = \frac{E}{1+v}l^2\chi_{ij} \tag{1.6}$$

where l is the material length scale parameter. The evaluation and calibration of l can be found in the literature [24], [25].

1.3.3. Modified strain gradient theory

Compared with the modified couple stress theory, the strain energy in the modified strain gradient theory contains two additional gradient parts: the dilatation gradient γ and the deviatoric stretch gradient η , in addition to the symmetric curvature χ_{ij}. Therefore, the strain energy is written by [26]:

$$U = \frac{1}{2}\int_V \left(\sigma_{ij}\varepsilon_{ij} + p_i\gamma_i + \tau_{ijk}\eta_{ijk} + m_{ij}\chi_{ij} \right)dV \qquad (1.7)$$

The ingredients in the formula (1.7) are determined as in [26].

1.3.4. Overview of the works using nonlocal elasticity theory to analyze nanoplates

Combining the above micro and nanostructure theories with different plate theories, we can be solved various problems. In the above theories, the nonlocal elasticity theory is commonly used to calculate nanostructures because it is quite simple and gives quite accurate results with simulations. The thesis uses nonlocal elasticity theory to calculate nanoplates, so in this section, the author summarizes a number of papers on calculating nanostructures based on nonlocal elasticity theory.

1.3.4.1. Nonlocal elasticity theory in combination with the classical plate theory

The classical plate theory has the advantage of simplicity, containing only three unknowns, but this theory ignores the shear strain. So, this theory is only suitable for the calculation of thin structures. Lu et al. [27] used nonlocal elasticity theory based on classical plate theory to study the effect of geometrical parameters on the static and buckling of isotropic nanoplates. Duan and Wang [28] used nonlocal elasticity theory and classical plate theory to derive exact solutions for the axisymmetric bending analysis of circular nanoplates under general loading. Also, using the Lévy solution based on nonlocal elasticity theory and classical plate theory, Aksencer and Aydogdu [29] employed buckling loads and natural frequencies of rectangular nanoplates with two opposite edges being simply supported. Shakouri [30] derived the Galerkin approach to solve the natural frequencies of isotropic nanoplates. Phadikar and Pradhan [31], Ansari et al. [32] were early scientists who used the

finite element method basis on nonlocal elasticity theory to calculate to calculate the mechanical behavior of nanobeams. Based on the classical plate theory and nonlocal elasticity, Phadikar and Pradhan [31] use the finite element method to analyze static bending, free vibration, and buckling of isotropic nanobeams and nanoplates. Nguyen et al. [33] used an isogeometric analysis (IGA) to study FGM nanoplates. Other research findings on static bending, free vibration, mechanical buckling, and thermal buckling of nanostructures using nonlocal elasticity theory and classical plate theory have been published in the works [34]-[36].

1.3.4.2. Nonlocal elasticity theory in combination with the first-order shear deformation theory

The first-order shear deformation theory takes into account the shear strain, so it is suitable for the calculation of thin and moderate structures. However, the shear strain is constant with the plate thickness, which does not satisfy the condition that the shear stress is zero at the top and bottom faces. So, a shear correction factor is needed. This factor depends on some conditions, such as the material, the shape of structures, and the boundary conditions, and usually gets a value of 5/6.

Pradhan and Phadikar combine nonlocal elasticity theory combining with the classical plate theory and the first-order shear deformation theory to analyze free vibration [38] and buckling [39] of nanoplates. Ansari et al. examined the vibration of single-layered graphene sheets [40] and multi-layered graphene sheets [41] with different boundary conditions using the nonlocal elasticity theory, the first-order shear deformation theory, and the differential quadrature method. The nonlocal and first-order shear deformation theories were also proposed for nanoplates made of FG and orthotropic materials. For instance, Hosseini-Hashemi et al. [42] developed a nonlocal

FSDT for FG circular nanoplates. Closed-form solutions for natural frequencies of circular nanoplates under various BCs were also obtained. Anjomshoa and Tahani [43] developed a nonlocal FSDT model for the free vibration analysis of orthotropic circular and elliptical nanoplates embedded in an elastic medium. Golmakani and Rezatalab [44] presented a nonlinear nonlocal FSDT model for the nonlinear bending analysis of orthotropic nanoscale plates embedded in an elastic matrix based on nonlocal continuum mechanics. Dastjerdi et al. [45], [46] presented a nonlinear nonlocal FSDT model for the nonlinear geometric analysis of annular/circular orthotropic embedded SLGSs in which the effect of elevated temperature was considered. Based on first-order shear deformation theory, nonlocal elasticity theory, and an isogeometric analysis, Ansari and Norouzzadeh [47] investigate the buckling of nanoplates.

1.3.4.3. Nonlocal elasticity theory in combination with the third-order shear deformation theory

Aghababbaei and Reddy [48] used the nonlocal elasticity theory and the third-order shear deformation theory to study static bending and free vibration of nanoplates with a simply supported boundary. Also, using nonlocal TSDT, Pradhan and Sahu [49] studied the effect of the nonlocal factor on buckling load and free vibration of simply supported graphene plates. Ansari and Sahmani [51] used a unified nonlocal model with three different theories of the classical plate theory, first-order shear deformation theory, and third-order shear deformation theory. Daneshmehr et al. examined the buckling [52] and free vibration [53] of FG nanoplates. Nami and co-workers [54] investigated the thermal buckling of FG nanoplates by using third-order shear deformation theory.

1.3.4.4. Nonlocal elasticity theory in combination with the higher-order shear deformation theory

The shear stress is distributed parabolic along the plate thickness and satisfies the condition that the shear stress is zero at the top and bottom faces, so it is suitable for the calculation of medium and thick plates. However, the higher-order shear deformation theory has a complex displacement field. Shear locking occurs in the case of thin plates, so some techniques must be used to eliminate this phenomenon, such as using the reduction integral or using an independent shear strain field.

Sobhy [55] presented a combination model of nonlocal elasticity theory and the sinusoidal higher-order shear deformation theory of Thai and Choi [56]. Using analytical methods, Sobhy studied the free vibration, mechanical buckling, and thermal buckling of multilayer graphene plates with different boundary conditions. Developing his research direction, Sobhy [57], [58] analyzed the static bending of single-layer anisotropic, anisotropic graphene plates in a thermal environment. Zenkour and Sobhy [59], Alzahrani et al. [60], Thai et al. [61] have studied thermal buckling, thermo-mechanical buckling of single-layer graphene plates using nonlocal elasticity theory and sinusoidal higher-order shear deformation theory of Touratier [62]. Belkorissat et al. [63] calculated FG nanoplates based on higher-order shear deformation theory hyperbolic format. Phung-Van and his colleagues investigated the static and dynamic responses of functionally graded carbon nanotube-reinforced composite nanoplates based on the nonlocal elastic continuous isogeometric model [64]. Zenkour et al. [65] calculated the thermal buckling of nanoplates on the elastic foundation by using the sinusoidal shear deformation theory. Tran et al. [66] used higher-order shear deformation nonlocal theory for bending, buckling, and free vibration analysis of FGP nanoshells resting on an elastic

foundation. Some other studies on nanostructures were also synthesized in [67], [68], [69].

Nguyen Van Hau [2] used the high-order shear deformation theory, Quasi-3D theory, and the Ritz solution to analyze the static bending, stability, and free vibration of FGM and FGM composite plates under mechanical load and temperature. Pham Cong Hong [3] used the classical plate theory, first-order shear deformation theory, and Reddy's third-order shear deformation theory combined with the Galerkin method for static and dynamic nonlinear analysis and FGM plate resting on an elastic foundation. Nguyen Van Thanh [4] used the classical plate theory, first-order shear deformation theory, and Reddy's third-order shear deformation theory combined with Von Karman's geometric nonlinearity to establish the basic equations of static and dynamic nonlinear of the FG-CNTRC plate. The thesis analyzed the static and dynamic stability of the FG-CNTRC plate under mechanical load and temperature by using an analytical approach and the Galerkin method.

1.4. The main results have been published

Through the analysis of the above works, some conclusions are drawn as follows:

Nowadays, nanostructures are widely applied in many fields. Nanotechnology is a turning point for all aspects of life, so the analysis and calculation of nanostructures is an important issue.

There are three main methods dealing with the mechanical response of nanostructure. The first is the experiment method. The second one is simulation. And the last one is developing mathematical–mechanical models. In which experiment method requires modern equipment, so this is expensive and difficult to conduct. While simulation technics, the model is not the same

as the real one. Besides that, the simulation method can't give an exact solution. So developing mathematical-mechanical models need to be carried out.

Based on this approach, there are three theories have been proposed to analyze micro/nanostructures, including nonlocal elasticity theory, modified couple stress theory, and modified strain gradient theory. In which the nonlocal elasticity theory is used a lot because of its simplicity and gives fairly accurate results with molecular simulations.

There are many different plate theories to calculate structures, such as CPT, FSDT, HSDT, and Quasi-3D theory. Among those theories, the FSDT is commonly used. Nowadays, many scientists are interested in HSDT and Quasi-3D theory due to its accuracy.

There are different methods for calculating nanostructures, such as analytical methods, numerical methods, and semi-analytical methods. The advantage of analytical methods is that they can provide accurate and reliable solutions, but the transformations are quite complex and are usually only used for simple and symmetrical structures. Numerical methods only give approximate solutions, but this method is effective for complex structures under different boundary conditions and loads. Nowadays, with the development of numerical methods and information technology, the obtained results have been tested through many published works, confirming their reliability and accuracy.

Research on nanostructures and microstructures have been of interest to scientists for many years. The published works have focused on building computational theories of nanostructures. Some works use the above theories together with analytical methods to calculate static bending, free vibration, and thermo-mechanical buckling of beams, plates, and nanotubes. Recently, some scientists have used numerical methods to analyze the mechanical behavior of nanostructures.

1.5. Issues that need further research

From the overview of the issues presented above, the author realizes that some problems need further research, which is:

- Studying the static response and forced vibrations of nanoplates and nanoshells with complex shapes subjected to different types of mechanical loads taking into account the influence of temperature using the first-order shear theory and the higher-order shear deformation theories.

- Investigating the static and dynamic buckling response of nanostructures resting on an elastic foundation and viscoelastic environments under the effect of diverse mechanical loads.

- Calculating optimal shape and optimizing materials for nanostructures.

- Analysis of nanomaterial-reinforced structures exposed to various sorts of loads.

- Studying the behavior of nanostructures taking into account the influence of porosity, cracks, and so on.

The summary nanostructure problems are shown in Figure 1.3.

1.6. The main contents of the thesis

From the above conclusions, the thesis combines the finite element method, the nonlocal elasticity theory, and the first-order shear deformation theory to analyze static bending, free vibration, and forced vibration of nanoplates. In which the structure rests on an elastic foundation with different shapes such as rectangular, L-shape, annular, and half-annular. Two types of porosity distribution are considered, which are evenly distributed and unevenly distributed.

The results of the thesis are compared with the published results by analytical solutions to verify the accuracy and reliability of the calculation

method and program. Then, the thesis will investigate some geometrical and material properties, elastic foundation, boundary conditions to the static bending, free vibration, and forced vibration of nanoplates.
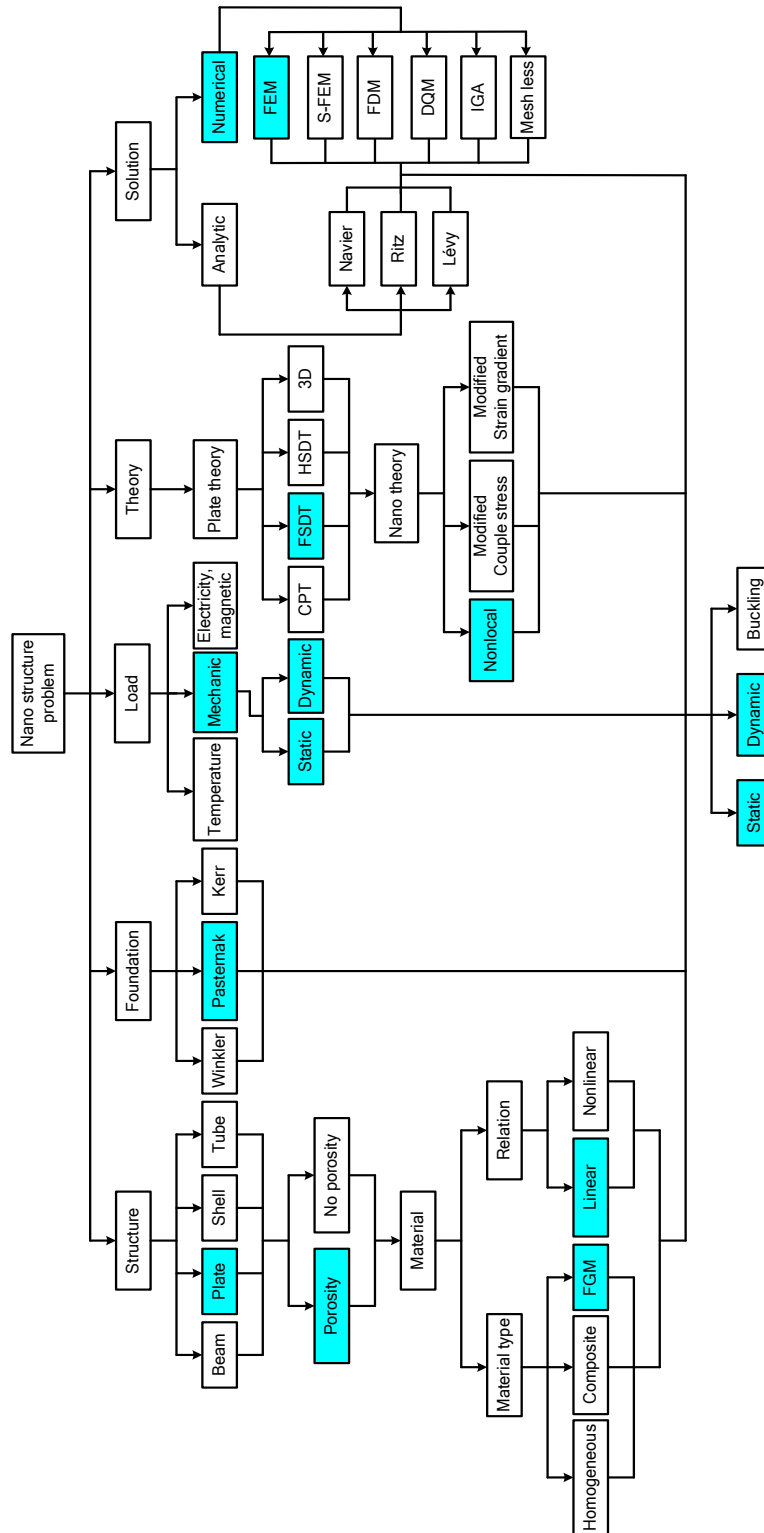
Figure 1.3. The summary of the nanostructure problem.

1.7. Summary of Chapter 1

Due to special mechanical, thermal, electrical, and chemical properties, nanostructures are increasingly used in the fields of medicine, electronics, and so on. Nanoplates are one of the most important structures commonly used as components in thin films, resonators, and sensors. Therefore, studying the vibrations of nanostructures is very important for design and manufacturing.

The mechanical behavior of nanoplates is a very important topic. Therefore, a large number of scientists worldwide are deeply interested, where various different methods, such as analytical methods, semi-analytical methods, numerical methods, and experimental methods, are employed. In the current period, with the strong development of science and technology, especially the application of computers in calculations, the finite element method has many advantages in solving mechanical problems with a huge amount of calculations. Therefore, the topic ***"Linear Static and Dynamic Analysis of FGM Porous Nanoplates Resting on Elastic Foundation Using Nonlocal Elasticity Theory"*** which the thesis sets out, has scientific and practical significance, contributing a novel research direction to investigate static, free vibration, and forced vibration for nanoplates under the influence of other types of loads. Through studying the research works that have been achieved in the current period, to my best knowledge, the author finds that this problem is of scientific and practical significance.

Chapter 2 THEORETICAL BASIC FOR CALCULATION OF FGM POROUS NANOPLATES RESTING ON ELASTIC FOUNDATION

2.1. Material and mechanical models and assumptions

2.1.1. Material and mechanical models

Consider FGP nanoplates with different shapes, such as rectangular, L-shape, annular, and half-annular. The plate is placed on a two-coefficient Winkler-Pasternak elastic foundation with two continuous layers. The first layer is a parallel spring system with a stiffness coefficient k_1, while the second layer is the shear layer with stiffness coefficient k_2. The porosity distribution in nanoplates according to two rules as evenly distributed and unevenly distributed (Figure 2.1). The plate is subjected to static loads and pulsating dynamic loads, which are perpendicular to the plate surface (Figure 2.2).
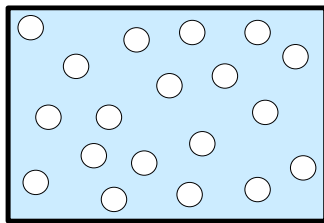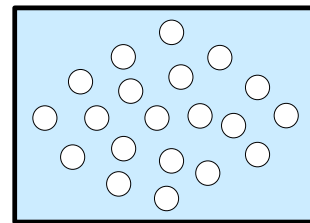
a) Even porosity   *b) Uneven porosity*

Figure 2.1. Two cases of porosities.

a) Rectangular nanoplate

b) L-shape nanoplate

c) Annular nanoplate

d) Half-annular nanoplate
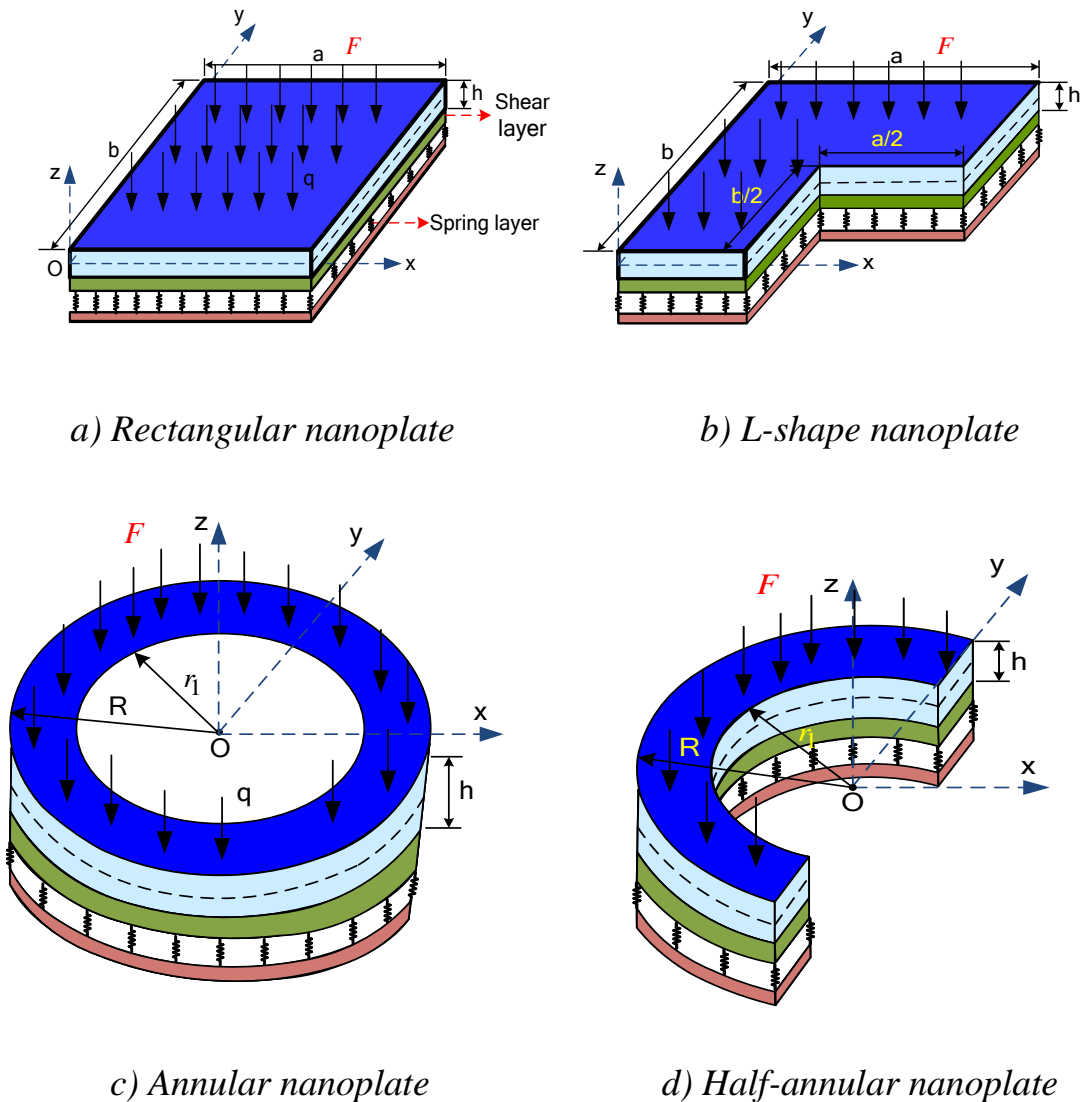
Figure 2.2. The model of FGP nanoplates resting on the elastic foundation.

2.1.2. Assumptions

To establish the mechanical behaviour relations, the thesis uses some assumptions as follows:

- The plate satisfies the Mindlin plate theory with $\varepsilon_z = 0$.

- Displacement of structures is small.

- Material is linear elastic.

2.2. Mechanical properties of materials

The FGP materials with the variation of two constituents and two different distributions of porosity through thickness are determined as follows [70]:

Case 1: Even porosity

$$P(z) = P_m + (P_c - P_m)\left(\frac{z}{h} + 0.5\right)^k - \frac{\xi}{2}(P_c + P_m) \qquad (2.1)$$

Case 2: Uneven porosity

$$P(z) = P_m + (P_c - P_m)\left(\frac{z}{h} + 0.5\right)^k - \frac{\xi}{2}(P_c + P_m)\left(1 - \frac{2|z|}{h}\right) \qquad (2.2)$$

where: P represents material properties such as the elastic modulus E, mass density ρ, and Poisson's ratio ν.

k $(k > 0)$ is the power-law index.

ξ $(0 \leq \xi \leq 0.5)$ is porosity factor.

The symbols m and c represent metal and ceramic components, respectively.

Figure 2.3 illustrates the elastic modulus E of FGP material (Al/Al$_2$O$_3$) in two cases of even and uneven porosity versus the power-law index. Figure 2.4 depicts the distribution of material properties according to the thickness of the nanoplate for the power-law index values $k = 0$, 1, 2, and 4.

a) Even porosity   *(b) Uneven porosity*
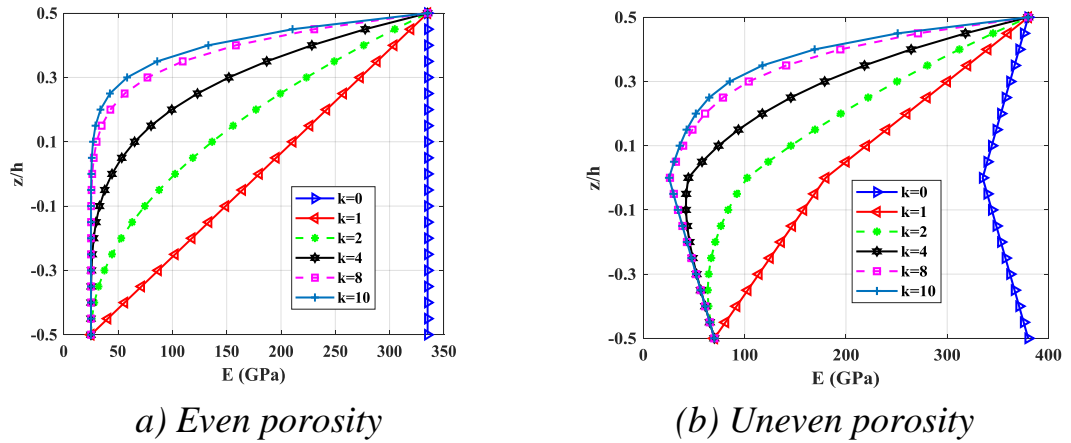
Figure 2.3. Elastic modulus *E* of FGP (Al/Al₂O₃) with different power-law index *k*.

a) k = 0   *b) k =1*

c) k = 2   *d) k = 4*
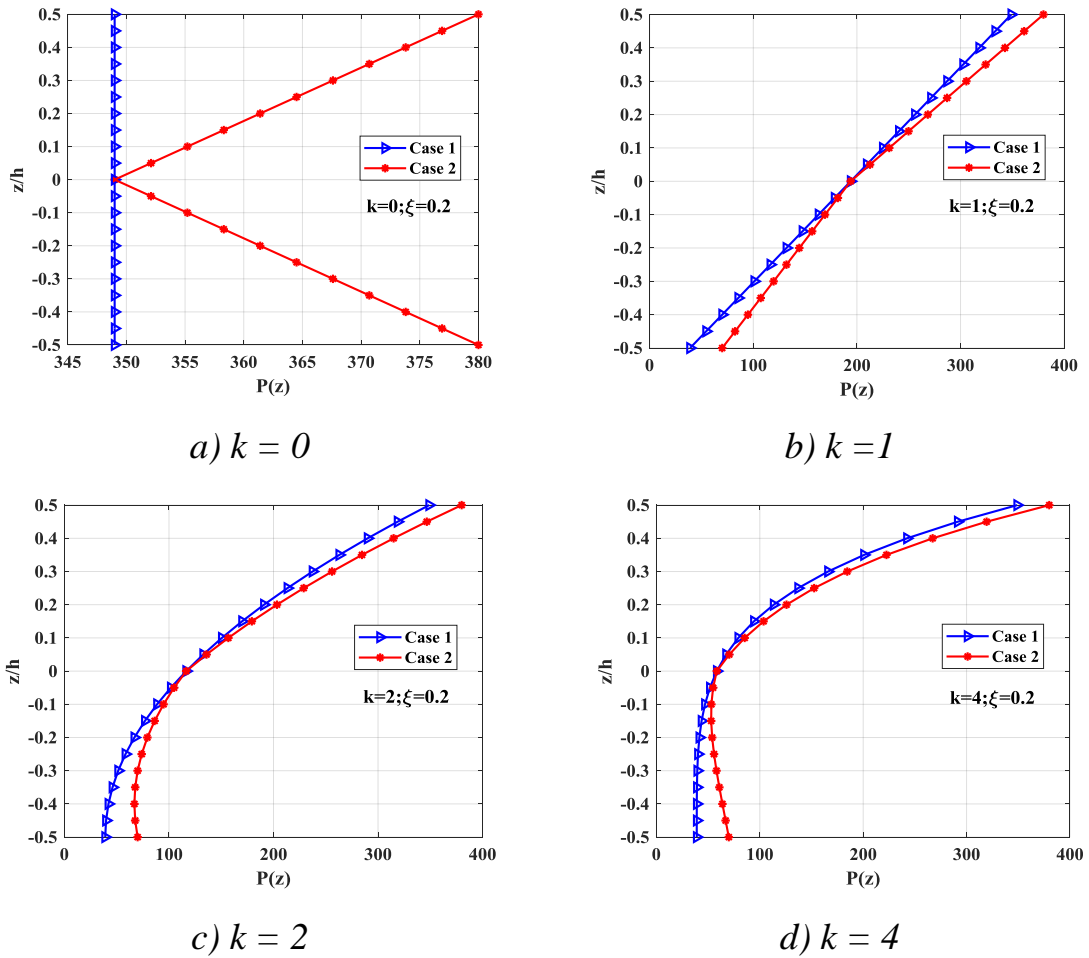
Figure 2.4. Distributions of material properties through thickness of FGP nanoplates.

2.3. The mechanical behavior relations of the plate

2.3.1. The displacement field

Based on the first-order shear deformation theory, the displacement field of the FGP nanoplates is defined by [71]:

$$\begin{cases} u(x,y,z) = u_0(x,y) + z\varphi_x(x,y) \\ v(x,y,z) = v_0(x,y) + z\varphi_y(x,y) \\ w(x,y,z) = w_0(x,y) \end{cases} \tag{2.3}$$

where

u, v, w: are the displacement components at any point (x, y, z);

u_0, v_0, w_0: are the displacement components at the mid-plane ($z = 0$) along x, y, z axis;

φ_x, φ_y: are the rotations of the cross–sections around the y-axis and x-axis, respectively.

2.3.2. Strain – displacement relations

The strain vector of the plate is deduced from the displacement field as follows [71]:

$$\varepsilon = \begin{Bmatrix} \varepsilon_{xx} \\ \varepsilon_{yy} \\ \varepsilon_{xy} \\ \varepsilon_{xz} \\ \varepsilon_{yz} \end{Bmatrix} = \begin{Bmatrix} \dfrac{\partial u}{\partial x} \\ \dfrac{\partial v}{\partial y} \\ \dfrac{\partial u}{\partial y} + \dfrac{\partial v}{\partial x} \\ \dfrac{\partial w}{\partial x} + \dfrac{\partial u}{\partial z} \\ \dfrac{\partial w}{\partial y} + \dfrac{\partial v}{\partial z} \end{Bmatrix} = \begin{Bmatrix} \dfrac{\partial u_0}{\partial x} \\ \dfrac{\partial v_0}{\partial y} \\ \dfrac{\partial u_0}{\partial y} + \dfrac{\partial v_0}{\partial x} \\ \dfrac{\partial w_0}{\partial x} + \varphi_x \\ \dfrac{\partial w_0}{\partial y} + \varphi_y \end{Bmatrix} + z \begin{Bmatrix} \dfrac{\partial \varphi_x}{\partial x} \\ \dfrac{\partial \varphi_y}{\partial y} \\ \dfrac{\partial \varphi_x}{\partial y} + \dfrac{\partial \varphi_y}{\partial x} \\ 0 \\ 0 \end{Bmatrix} \tag{2.4}$$

The equation (2.4) is rewritten by

$$\boldsymbol{\varepsilon} = \left\{ \begin{array}{c} \boldsymbol{\varepsilon}_1 \\ \boldsymbol{\varepsilon}_2 \end{array} \right\} = \left\{ \begin{array}{c} \boldsymbol{\varepsilon}_1^0 + z\boldsymbol{\varepsilon}_1^1 \\ \boldsymbol{\varepsilon}_2^0 \end{array} \right\} \tag{2.5}$$

with

$$\boldsymbol{\varepsilon}_1 = \left\{ \begin{array}{c} \varepsilon_{xx} \\ \varepsilon_{yy} \\ \varepsilon_{xy} \end{array} \right\}; \boldsymbol{\varepsilon}_2 = \left\{ \begin{array}{c} \varepsilon_{xz} \\ \varepsilon_{yz} \end{array} \right\};$$

$$\boldsymbol{\varepsilon}_1^0 = \left\{ \begin{array}{c} \dfrac{\partial u_0}{\partial x} \\[2mm] \dfrac{\partial v_0}{\partial y} \\[2mm] \dfrac{\partial u_0}{\partial y} + \dfrac{\partial v_0}{\partial x} \end{array} \right\}; \boldsymbol{\varepsilon}_1^1 = \left\{ \begin{array}{c} \dfrac{\partial \varphi_x}{\partial x} \\[2mm] \dfrac{\partial \varphi_y}{\partial y} \\[2mm] \dfrac{\partial \varphi_x}{\partial y} + \dfrac{\partial \varphi_y}{\partial x} \end{array} \right\}; \boldsymbol{\varepsilon}_2^0 = \left\{ \begin{array}{c} \dfrac{\partial w_0}{\partial x} + \varphi_x \\[2mm] \dfrac{\partial w_0}{\partial y} + \varphi_y \end{array} \right\} \tag{2.6}$$

2.3.3. Stress-strain relations

According to the nonlocal elasticity theory, the stress-strain relation is determined by [81]

$$\left\{ \begin{array}{c} \sigma_{xx} \\ \sigma_{yy} \\ \sigma_{xy} \\ \sigma_{xz} \\ \sigma_{yz} \end{array} \right\} - \mu \nabla^2 \left\{ \begin{array}{c} \sigma_{xx} \\ \sigma_{yy} \\ \sigma_{xy} \\ \sigma_{xz} \\ \sigma_{yz} \end{array} \right\} = \left[\begin{array}{ccccc} C_{11} & C_{12} & 0 & 0 & 0 \\ C_{12} & C_{22} & 0 & 0 & 0 \\ 0 & 0 & C_{66} & 0 & 0 \\ 0 & 0 & 0 & C_{55} & 0 \\ 0 & 0 & 0 & 0 & C_{44} \end{array} \right] \left\{ \begin{array}{c} \varepsilon_{xx} \\ \varepsilon_{yy} \\ \varepsilon_{xy} \\ \varepsilon_{xz} \\ \varepsilon_{yz} \end{array} \right\} \tag{2.7}$$

The equation (2.7) is rewritten by

$$\boldsymbol{\sigma} - \mu \nabla^2 \boldsymbol{\sigma} = \mathbf{D}\boldsymbol{\varepsilon} \tag{2.8}$$

in which $\mu = (e_0 a)^2$ is nonlocal factor, which represents the small-scale effect in nanostructures, e_0 is a constant, a is an internal characteristic length, and $\nabla^2 = \dfrac{\partial^2}{\partial x^2} + \dfrac{\partial^2}{\partial y^2}$ is the Laplace operator.

$$\mathbf{D} = \begin{bmatrix} \mathbf{D}_b & \mathbf{0}_{3\times 2} \\ \mathbf{0}_{2\times 3} & \mathbf{D}_s \end{bmatrix} \tag{2.9}$$

$$\mathbf{D}_b = \begin{bmatrix} C_{11} & C_{12} & 0 \\ & C_{22} & 0 \\ sym & & C_{66} \end{bmatrix}; \mathbf{D}_s = \begin{bmatrix} C_{55} & 0 \\ 0 & C_{44} \end{bmatrix} \tag{2.10}$$

where

$$
\begin{aligned}
C_{11} &= C_{22} = \frac{E(z)}{[1 - v(z)][1 + v(z)]} \\
C_{12} &= \frac{v(z)E(z)}{[1 - v(z)][1 + v(z)]} \\
C_{66} &= C_{55} = C_{44} = \frac{E(z)}{2[1 + v(z)]}
\end{aligned}
\tag{2.11}
$$

2.3.4. Hamilton principle

To obtain the governing equations of motion of FGP nanoplates, the Hamilton's principle is applied in the form as follows [71]:

$$\int_0^t (\delta U + \delta V - \delta W - \delta T) dt = 0 \tag{2.12}$$

where $\delta U, \delta V, \delta W$ and δT are the variation of the strain energy of plates, the energy stored in the deformed elastic foundation, the work done by applied force, and the kinetic energy, respectively.

The equation (2.12) is rewritten as:

$$\delta H = \delta \int\limits_0^t \left(U + V - W - T \right) dt = 0 \qquad (2.13)$$

The Hamintol principle written for the plate element is as follows:

$$\delta H_e = \delta \int\limits_0^t \left(U_e + V_e - W_e - T_e \right) dt = 0 \qquad (2.14)$$

2.3.4.1. The strain energy of the FGP nanoplates

The variation of the strain energy can be given by [71]:

$$\delta U_e = \int\limits_S \int\limits_{-h/2}^{h/2} \left(\sigma_{xx} \delta \varepsilon_{xx} + \sigma_{yy} \delta \varepsilon_{yy} + \sigma_{xy} \delta \varepsilon_{xy} + \sigma_{xz} \delta \varepsilon_{xz} + \sigma_{yz} \delta \varepsilon_{yz} \right) dz dS \qquad (2.15)$$

$$\delta U_e = \int\limits_S \int\limits_{-h/2}^{h/2} \begin{bmatrix} \sigma_{xx} \left(\dfrac{\partial \delta u_0}{\partial x} + z \dfrac{\partial \delta \varphi_x}{\partial x} \right) + \sigma_{yy} \left(\dfrac{\partial \delta v_0}{\partial y} + z \dfrac{\partial \delta \varphi_y}{\partial y} \right) \\[2mm] + \sigma_{xy} \left(\dfrac{\partial \delta u_0}{\partial y} + \dfrac{\partial \delta v_0}{\partial x} + z \dfrac{\partial \delta \varphi_x}{\partial y} + z \dfrac{\partial \delta \varphi_y}{\partial x} \right) \\[2mm] + \sigma_{xz} \left(\dfrac{\partial \delta w_0}{\partial x} + \partial \varphi_x \right) + \sigma_{yz} \left(\dfrac{\partial \delta w_0}{\partial y} + \partial \varphi_y \right) \end{bmatrix} dz dS \qquad (2.16)$$

$$\delta U_e = \int\limits_S \begin{bmatrix} N_{xx} \dfrac{\partial \delta u_0}{\partial x} + M_{xx} \dfrac{\partial \delta \varphi_x}{\partial x} + N_{yy} \dfrac{\partial \delta v_0}{\partial y} + M_{yy} \dfrac{\partial \delta \varphi_y}{\partial y} \\[2mm] + N_{xy} \left(\dfrac{\partial \delta u_0}{\partial y} + \dfrac{\partial \delta v_0}{\partial x} \right) + M_{xy} \left(\dfrac{\partial \delta \varphi_x}{\partial y} + \dfrac{\partial \delta \varphi_y}{\partial x} \right) \\[2mm] + Q_{xz} \left(\dfrac{\partial \delta w_0}{\partial x} + \partial \varphi_x \right) + Q_{yz} \left(\dfrac{\partial \delta w_0}{\partial y} + \partial \varphi_y \right) \end{bmatrix} dS \qquad (2.17)$$

where the internal force components are calculated as follows:

$$\left\{ N_{ij} ; M_{ij} \right\} = \int\limits_{-h/2}^{h/2} \sigma_{ij} \left\{ 1; z \right\} dz; \quad ij = xx,\ yy,\ xy \qquad (2.18)$$

$$\left\{ Q_{xz} ; Q_{yz} \right\} = \int\limits_{-h/2}^{h/2} \left\{ \sigma_{xz} ; \sigma_{yz} \right\} dz \qquad (2.19)$$

2.3.4.2. The energy stored in the deformed elastic foundation

The variation of the energy stored in the deformed elastic foundation is expressed by [71]:

$$\delta V_e = \int_S R \delta w \, dS \qquad (2.20)$$

where $R = k_1.w - k_2 \nabla^2 w$ is the reaction force of the elastic foundation.

The fomula (2.20) is rewritten as:

$$\delta V_e = \int_S \left(k_1.w - k_2 \nabla^2 w \right) \delta w \, dS = \int_S \left(k_1.w_0 - k_2 \nabla^2 w_0 \right) \delta w_0 \, dS \qquad (2.21)$$

2.3.4.3. The variation of kinetic energy

The velocity of the point with coordinates (x, y, z) at t time is expressed by

$$\begin{cases} \dot{u}(x, y, z, t) = \dot{u}_0(x, y, t) + z\dot{\varphi}_x(x, y, t) \\ \dot{v}(x, y, z, t) = \dot{v}_0(x, y, t) + z\dot{\varphi}_y(x, y, t) \\ \dot{w}(x, y, z, t) = \dot{w}_0(x, y, t) \end{cases} \qquad (2.22)$$

The variation of velocity is expressed by

$$\begin{cases} \delta\dot{u}(x, y, z, t) = \delta\dot{u}_0(x, y, t) + z\delta\dot{\varphi}_x(x, y, t) \\ \delta\dot{v}(x, y, z, t) = \delta\dot{v}_0(x, y, t) + z\delta\dot{\varphi}_y(x, y, t) \\ \delta\dot{w}(x, y, z, t) = \delta\dot{w}_0(x, y, t) \end{cases} \qquad (2.23)$$

The variation of kinetic energy is given by [70]

$$\delta T_e = \int_V \rho(z) \left(\dot{u}\delta\dot{u} + \dot{v}\delta\dot{v} + \dot{w}\delta\dot{w} \right) dV \qquad (2.24)$$

By substituting the fomulas (2.22) and (2.23) into the fomula (2.24)

$$\delta T_e = \int_S \int_{-h/2}^{h/2} \rho(z) \left[\begin{array}{l} \left(\dot{u}_0 + z\dot{\varphi}_x \right) \delta\left(\dot{u}_0 + z\dot{\varphi}_x \right) \\ + \left(\dot{v}_0 + z\dot{\varphi}_y \right) \delta\left(\dot{v}_0 + z\dot{\varphi}_y \right) + \dot{w}_0 \delta\dot{w}_0 \end{array} \right] dz \, dS \qquad (2.25)$$

$$\delta T_e = \int_S \int_{-h/2}^{h/2} \rho(z) \begin{pmatrix} \dot{u}_0 \delta\dot{u}_0 + \dot{u}_0 z \delta\dot{\varphi}_x + z\dot{\varphi}_x \delta\dot{u}_0 + z^2 \dot{\varphi}_x \delta\dot{\varphi}_x \\ +\dot{v}_0 \delta\dot{v}_0 + \dot{v}_0 z \delta\dot{\varphi}_y + z\dot{\varphi}_y \delta\dot{v}_0 + z^2 \dot{\varphi}_y \delta\dot{\varphi}_y + \dot{w}_0 \delta\dot{w}_0 \end{pmatrix} dz dS \qquad (2.26)$$

$$\delta T_e = \int_S \begin{bmatrix} J_0 \left(\dot{u}_0 \delta\dot{u}_0 + \dot{v}_0 \delta\dot{v}_0 + \dot{w}_0 \delta\dot{w}_0 \right) \\ +J_1 \left(\dot{u}_0 \delta\dot{\varphi}_x + \dot{v}_0 \delta\dot{\varphi}_y + \dot{\varphi}_x \delta\dot{u}_0 + \dot{\varphi}_y \delta\dot{v}_0 \right) \\ +J_2 \left(\dot{\varphi}_x \delta\dot{\varphi}_x + \dot{\varphi}_y \delta\dot{\varphi}_y \right) \end{bmatrix} dS \qquad (2.27)$$

where

$$\left(J_0, J_1, J_2 \right) = \int_{-h/2}^{h/2} \left(1, z, z^2 \right) \rho(z) dz \qquad (2.28)$$

2.3.4.4. The work done by applied force

The variation of work done by applied force is expressed by [71]

$$\delta W_e = \int_S F \delta w dS = \int_S F \delta w_0 dS \qquad (2.29)$$

By substituting equations (2.17), (2.21), (2.27) and (2.29) into (2.12) and integrading by part, grouping by terms containing $\delta u_0, \delta v_0, \delta w_0, \delta\varphi_x, \delta\varphi_y$, respectively. The motion equations of FGP nanoplates can be obtained by

$$\delta u_0 : \quad \frac{\partial N_{xx}}{\partial x} + \frac{\partial N_{xy}}{\partial y} = J_0 \ddot{u}_0 + J_1 \ddot{\varphi}_x \qquad (2.30)$$

$$\delta v_0 : \quad \frac{\partial N_{xy}}{\partial x} + \frac{\partial N_{yy}}{\partial y} = J_0 \ddot{v}_0 + J_1 \ddot{\varphi}_y \qquad (2.31)$$

$$\delta w_0 : \quad \frac{\partial Q_{xz}}{\partial x} + \frac{\partial Q_{yz}}{\partial y} + k_1 w_0 - k_2 \nabla^2 w_0 - F = J_0 \ddot{w}_0 \qquad (2.32)$$

$$\delta\varphi_x : \quad \frac{\partial M_{xx}}{\partial x} + \frac{\partial M_{xy}}{\partial y} + Q_{xz} = J_1 \ddot{u}_0 + J_2 \ddot{\varphi}_x \qquad (2.33)$$

$$\delta\varphi_y: \quad \frac{\partial M_{xy}}{\partial x} + \frac{\partial M_{yy}}{\partial y} + Q_{yz} = J_1\ddot{v}_0 + J_2\ddot{\varphi}_y \tag{2.34}$$

Integrating the equation (2.7) following plate thickness, the internal force and moment are determined by

The membrane force is:

$$\begin{Bmatrix} N_{xx} \\ N_{yy} \\ N_{xy} \end{Bmatrix} - \mu\nabla^2 \begin{Bmatrix} N_{xx} \\ N_{yy} \\ N_{xy} \end{Bmatrix} = \begin{bmatrix} A_{11} & A_{12} & 0 \\ A_{21} & A_{22} & 0 \\ 0 & 0 & A_{66} \end{bmatrix} \begin{Bmatrix} \dfrac{\partial u_0}{\partial x} \\ \dfrac{\partial v_0}{\partial x} \\ \dfrac{\partial u_0}{\partial y} + \dfrac{\partial v_0}{\partial x} \end{Bmatrix} + \begin{bmatrix} B_{11} & B_{12} & 0 \\ B_{21} & B_{22} & 0 \\ 0 & 0 & B_{66} \end{bmatrix} \begin{Bmatrix} \dfrac{\partial \varphi_x}{\partial x} \\ \dfrac{\partial \varphi_y}{\partial y} \\ \dfrac{\partial \varphi_x}{\partial y} + \dfrac{\partial \varphi_y}{\partial x} \end{Bmatrix}$$

$$\tag{2.35}$$

The equation (2.35) is abbreviated by

$$(1 - \mu\nabla^2)\{N_{xx} \quad N_{yy} \quad N_{xy}\}^T = \mathbf{A}\varepsilon_1^0 + \mathbf{B}\varepsilon_1^1 \tag{2.36}$$

The shear force is expressed as follows:

$$\begin{Bmatrix} Q_{xz} \\ Q_{yz} \end{Bmatrix} - \mu\nabla^2 \begin{Bmatrix} Q_{xz} \\ Q_{yz} \end{Bmatrix} = \begin{bmatrix} A_{55}^s & 0 \\ 0 & A_{44}^S \end{bmatrix} \begin{Bmatrix} \dfrac{\partial w_0}{\partial x} + \varphi_x \\ \dfrac{\partial w_0}{\partial y} + \varphi_y \end{Bmatrix} \tag{2.37}$$

The equation (2.37) is abbreviated by

$$(1 - \mu\nabla^2)\{Q_{xz} \quad Q_{yz}\}^T = \mathbf{A}^s\varepsilon_2^0 \tag{2.38}$$

The bending and torque of the plate are defined by

$$\begin{Bmatrix} M_{xx} \\ M_{yy} \\ M_{xy} \end{Bmatrix} - \mu\nabla^2 \begin{Bmatrix} M_{xx} \\ M_{yy} \\ M_{xy} \end{Bmatrix} = \begin{bmatrix} B_{11} & B_{12} & 0 \\ B_{21} & B_{22} & 0 \\ 0 & 0 & B_{66} \end{bmatrix} \begin{Bmatrix} \dfrac{\partial u_0}{\partial x} \\ \dfrac{\partial v_0}{\partial x} \\ \dfrac{\partial u_0}{\partial y} + \dfrac{\partial v_0}{\partial x} \end{Bmatrix} + \begin{bmatrix} X_{11} & X_{12} & 0 \\ X_{21} & X_{22} & 0 \\ 0 & 0 & X_{66} \end{bmatrix} \begin{Bmatrix} \dfrac{\partial \varphi_x}{\partial x} \\ \dfrac{\partial \varphi_y}{\partial y} \\ \dfrac{\partial \varphi_x}{\partial y} + \dfrac{\partial \varphi_y}{\partial x} \end{Bmatrix}$$

$$(2.39)$$

The equation (2.39) is abbreviated by

$$(1 - \mu\nabla^2)\{M_{xx} \quad M_{yy} \quad M_{xy}\}^T = \mathbf{B}\varepsilon_1^0 + \mathbf{X}\varepsilon_1^1 \tag{2.40}$$

where

$$(\mathbf{A}, \mathbf{B}, \mathbf{X}) = \int_{-h/2}^{h/2} \mathbf{D}_b(1, z, z^2)dz; \quad \mathbf{A}^s = \frac{5}{6}\int_{-h/2}^{h/2} \mathbf{D}_s dz \tag{2.41}$$

Substituting internal forces from the equations (2.35), (2.37) and (2.39) into (2.30), (2.31), (2.32), (2.33), (2.34) and performing mathematical transformations, the equations of the system are expressed of Euler-Lagrange equations (by giving the corresponding values for the differential variables $\delta u, \delta v, \delta w, \delta\varphi_x, \delta\varphi_y$ equal to 0) of the following form:

$$\frac{\partial N_{xx}}{\partial x} + \frac{\partial N_{xy}}{\partial y} = (1 - \mu\nabla^2)(J_0\ddot{u}_0 + J_1\ddot{\varphi}_x) \tag{2.42}$$

$$\frac{\partial N_{xy}}{\partial x} + \frac{\partial N_{yy}}{\partial y} = (1 - \mu\nabla^2)(J_0\ddot{v}_0 + J_1\ddot{\varphi}_y) \tag{2.43}$$

$$\frac{\partial Q_{xz}}{\partial x} + \frac{\partial Q_{yz}}{\partial y} = (1 - \mu\nabla^2)(-k_1 w_0 + k_2\nabla^2 w_0 + F + J_0\ddot{w}_0) \tag{2.44}$$

$$\frac{\partial M_{xx}}{\partial x} + \frac{\partial M_{xy}}{\partial y} + Q_{xz} = (1 - \mu\nabla^2)(J_1\ddot{u}_0 + J_2\ddot{\varphi}_x) \tag{2.45}$$

$$\frac{\partial M_{xy}}{\partial x} + \frac{\partial M_{yy}}{\partial y} + Q_{yz} = (1 - \mu\nabla^2)(J_1\ddot{v}_0 + J_2\ddot{\varphi}_y) \tag{2.46}$$

The expanded form of equations (2.42), (2.43), (2.44), (2.45) and (2.46) are presented as follows:

$$A_{11}\frac{\partial^2 u_0}{\partial x^2} + A_{12}\frac{\partial^2 v_0}{\partial x^2} + B_{11}\frac{\partial^2 \varphi_x}{\partial x^2} + B_{12}\frac{\partial^2 \varphi_y}{\partial y\partial x}$$
$$+A_{66}\left(\frac{\partial^2 u_0}{\partial y^2} + \frac{\partial^2 v_0}{\partial x\partial y}\right) + B_{66}\left(\frac{\partial^2 \varphi_x}{\partial y^2} + \frac{\partial^2 \varphi_y}{\partial x\partial y}\right) = (1 - \mu\nabla^2)(J_0\ddot{u}_0 + J_1\ddot{\varphi}_x) \tag{2.47}$$

$$A_{66}\left(\frac{\partial^2 u_0}{\partial y\partial x} + \frac{\partial^2 v_0}{\partial x^2}\right) + B_{66}\left(\frac{\partial^2 \varphi_x}{\partial y\partial x} + \frac{\partial^2 \varphi_y}{\partial x^2}\right) +$$
$$A_{21}\frac{\partial^2 u_0}{\partial x\partial y} + A_{22}\frac{\partial^2 v_0}{\partial x\partial y} + B_{21}\frac{\partial^2 \varphi_x}{\partial x\partial y} + B_{22}\frac{\partial^2 \varphi_y}{\partial y^2} = (1 - \mu\nabla^2)(J_0\ddot{v}_0 + J_1\ddot{\varphi}_y) \tag{2.48}$$

$$A_{55}^s\left(\frac{\partial^2 w_0}{\partial x^2} + \frac{\partial \varphi_x}{\partial x}\right) + A_{44}^s\left(\frac{\partial^2 w_0}{\partial y^2} + \frac{\partial \varphi_y}{\partial y}\right)$$
$$= (1 - \mu\nabla^2)(-k_w w_0 + k_s\nabla^2 w_0 + F + J_0\ddot{w}_0) \tag{2.49}$$

$$B_{11}\frac{\partial^2 u_0}{\partial x^2} + B_{12}\frac{\partial^2 v_0}{\partial x^2} + X_{11}\frac{\partial^2 \varphi_x}{\partial x^2} + X_{12}\frac{\partial^2 \varphi_y}{\partial y\partial x} + B_{66}\left(\frac{\partial^2 u_0}{\partial y^2} + \frac{\partial^2 v_0}{\partial x\partial y}\right)$$
$$+X_{66}\left(\frac{\partial^2 \varphi_x}{\partial y^2} + \frac{\partial^2 \varphi_y}{\partial x\partial y}\right) + A_{55}^s\left(\frac{\partial w_0}{\partial x} + \varphi_x\right) = (1 - \mu\nabla^2)(J_1\ddot{u}_0 + J_2\ddot{\varphi}_x) \tag{2.50}$$

$$B_{66}\left(\frac{\partial^2 u_0}{\partial y\partial x} + \frac{\partial^2 v_0}{\partial x^2}\right) + X_{66}\left(\frac{\partial^2 \varphi_x}{\partial y\partial x} + \frac{\partial^2 \varphi_y}{\partial x^2}\right) + B_{21}\frac{\partial^2 u_0}{\partial x\partial y} + B_{22}\frac{\partial^2 v_0}{\partial x\partial y}$$
$$+X_{21}\frac{\partial^2 \varphi_x}{\partial x\partial y} + X_{22}\frac{\partial^2 \varphi_y}{\partial y^2} + A_{44}^s\left(\frac{\partial w_0}{\partial y} + \varphi_y\right) = (1 - \mu\nabla^2)(J_1\ddot{v}_0 + J_2\ddot{\varphi}_y) \tag{2.51}$$

Multiply equations (2.42), (2.43), (2.44), (2.45) and (2.46) by the differential variables δu_0, δv_0, δw_0, $\delta \varphi_x$, $\delta \varphi_y$, respectively, using the divergence theorem and ignoring the Neumann boundary, we get the following equation [71]:

$$\int_S \left|\begin{array}{l} \left[\left(\dfrac{\partial N_{xx}}{\partial x} + \dfrac{\partial N_{xy}}{\partial y}\right)\delta u_0 + \left(\dfrac{\partial N_{xy}}{\partial x} + \dfrac{\partial N_{yy}}{\partial y}\right)\delta v_0 \right. \\[3mm] \left(\dfrac{\partial Q_{xz}}{\partial x} + \dfrac{\partial Q_{yz}}{\partial y}\right)\delta w_0 + \left(\dfrac{\partial M_{xx}}{\partial x} + \dfrac{\partial M_{xy}}{\partial y} + Q_{xz}\right)\delta \varphi_x \\[3mm] \left(\dfrac{\partial M_{xy}}{\partial x} + \dfrac{\partial M_{yy}}{\partial y} + Q_{yz}\right)\delta \varphi_y \\[3mm] -(1 - \mu\nabla^2)\left[\begin{array}{l} (J_0\ddot{u}_0 + J_1\ddot{\varphi}_x)\delta u_0 + (J_0\ddot{v}_0 + J_1\ddot{\varphi}_y)\delta v_0 \\ +(-k_1 w_0 + k_2\nabla^2 w_0 + F + J_0\ddot{w}_0)\delta w_0 \\ +(J_1\ddot{u}_0 + J_2\ddot{\varphi}_x)\delta \varphi_x + (J_1\ddot{v}_0 + J_2\ddot{\varphi}_y)\delta \varphi_y \end{array}\right] \end{array}\right| dxdy = 0 \quad (2.52)$$

The expanded form of the equation (2.52) is expressed as follows:

$$\int_S \left\{ \begin{aligned} & \left[\begin{aligned} & A_{11}\frac{\partial^2 u_0}{\partial x^2} + A_{12}\frac{\partial^2 v_0}{\partial x^2} + B_{11}\frac{\partial^2 \varphi_x}{\partial x^2} + B_{12}\frac{\partial^2 \varphi_y}{\partial y \partial x} \\ & + A_{66}\left(\frac{\partial^2 u_0}{\partial y^2} + \frac{\partial^2 v_0}{\partial x \partial y} \right) + B_{66}\left(\frac{\partial^2 \varphi_x}{\partial y^2} + \frac{\partial^2 \varphi_y}{\partial x \partial y} \right) \end{aligned} \right] \delta u_0 \\ & + \left[\begin{aligned} & A_{66}\left(\frac{\partial^2 u_0}{\partial y \partial x} + \frac{\partial^2 v_0}{\partial x^2} \right) + B_{66}\left(\frac{\partial^2 \varphi_x}{\partial y \partial x} + \frac{\partial^2 \varphi_y}{\partial x^2} \right) + \\ & A_{21}\frac{\partial^2 u_0}{\partial x \partial y} + A_{22}\frac{\partial^2 v_0}{\partial x \partial y} + B_{21}\frac{\partial^2 \varphi_x}{\partial x \partial y} + B_{22}\frac{\partial^2 \varphi_y}{\partial y^2} \end{aligned} \right] \delta v_0 \\ & + \left[A_{55}^s\left(\frac{\partial^2 w_0}{\partial x^2} + \frac{\partial \varphi_x}{\partial x} \right) + A_{44}^s\left(\frac{\partial^2 w_0}{\partial y^2} + \frac{\partial \varphi_y}{\partial y} \right) \right] \delta w_0 \\ & + \left[\begin{aligned} & B_{11}\frac{\partial^2 u_0}{\partial x^2} + B_{12}\frac{\partial^2 v_0}{\partial x^2} + X_{11}\frac{\partial^2 \varphi_x}{\partial x^2} + X_{12}\frac{\partial^2 \varphi_y}{\partial y \partial x} \\ & + B_{66}\left(\frac{\partial^2 u_0}{\partial y^2} + \frac{\partial^2 v_0}{\partial x \partial y} \right) + X_{66}\left(\frac{\partial^2 \varphi_x}{\partial y^2} + \frac{\partial^2 \varphi_y}{\partial x \partial y} \right) \\ & + A_{55}^s\left(\frac{\partial w_0}{\partial x} + \varphi_x \right) \end{aligned} \right] \delta \varphi_x \\ & + \left[\begin{aligned} & B_{66}\left(\frac{\partial^2 u_0}{\partial y \partial x} + \frac{\partial^2 v_0}{\partial x^2} \right) + X_{66}\left(\frac{\partial^2 \varphi_x}{\partial y \partial x} + \frac{\partial^2 \varphi_y}{\partial x^2} \right) \\ & + B_{21}\frac{\partial^2 u_0}{\partial x \partial y} + B_{22}\frac{\partial^2 v_0}{\partial x \partial y} + X_{21}\frac{\partial^2 \varphi_x}{\partial x \partial y} \\ & + X_{22}\frac{\partial^2 \varphi_y}{\partial y^2} + A_{44}^s\left(\frac{\partial w_0}{\partial y} + \varphi_y \right) \end{aligned} \right] \delta \varphi_y \\ & - \dots \end{aligned} \right\} dS = 0$$

$$\int_S \left\{ - \left\{ \begin{aligned} & \left[J_0 \ddot{u}_0 \delta u_0 + \mu J_0 \left(\frac{\partial \ddot{u}_0}{\partial x} \frac{\partial \delta u_0}{\partial x} + \frac{\partial \ddot{u}_0}{\partial y} \frac{\partial \delta u_0}{\partial y} \right) \right. \\ & + J_1 \left[\ddot{\varphi}_x \delta u_0 + \mu \left(\frac{\partial \ddot{\varphi}_x}{\partial x} \frac{\partial \delta u_0}{\partial x} + \frac{\partial \ddot{\varphi}_x}{\partial y} \frac{\partial \delta u_0}{\partial y} \right) \right] \\ & + J_0 \left[\ddot{v}_0 \delta v_0 + \mu \left(\frac{\partial \ddot{v}_0}{\partial x} \frac{\partial \delta v_0}{\partial x} + \frac{\partial \ddot{v}_0}{\partial y} \frac{\partial \delta v_0}{\partial y} \right) \right] \\ & + J_1 \left[\ddot{\varphi}_y \delta v_0 + \mu \left(\frac{\partial \ddot{\varphi}_y}{\partial x} \frac{\partial \delta v_0}{\partial x} + \frac{\partial \ddot{\varphi}_y}{\partial y} \frac{\partial \delta v_0}{\partial y} \right) \right] \\ & - k_1 \left[w_0 \delta w_0 + \mu \left(\frac{\partial w_0}{\partial x} \frac{\partial \delta w_0}{\partial x} + \frac{\partial w_0}{\partial y} \frac{\partial \delta w_0}{\partial y} \right) \right] \\ & - k_2 \left[\begin{aligned} & \frac{\partial w_0}{\partial x} \frac{\partial \delta w_0}{\partial x} + \frac{\partial w_0}{\partial y} \frac{\partial \delta w_0}{\partial y} \\ & + \mu \left(\begin{aligned} & \frac{\partial^2 w_0}{\partial x^2} \frac{\partial^2 \delta w_0}{\partial x^2} + \frac{\partial^2 w_0}{\partial y^2} \frac{\partial^2 \delta w_0}{\partial y^2} \\ & + \frac{\partial^2 w_0}{\partial x^2} \frac{\partial^2 \delta w_0}{\partial y^2} + \frac{\partial^2 w_0}{\partial y^2} \frac{\partial^2 \delta w_0}{\partial x^2} \end{aligned} \right) \end{aligned} \right] \\ & + F \left[\delta w_0 - \mu \left(\frac{\partial^2 \delta w_0}{\partial x^2} + \frac{\partial^2 \delta w_0}{\partial y^2} \right) \right] \\ & + J_0 \left[\ddot{w}_0 \delta w_0 + \mu \left(\frac{\partial \ddot{w}_0}{\partial x} \frac{\partial \delta w_0}{\partial x} + \frac{\partial \ddot{w}_0}{\partial y} \frac{\partial \delta w_0}{\partial y} \right) \right] \\ & J_1 \ddot{u}_0 \delta \varphi_x + \mu J_1 \left(\frac{\partial \ddot{u}_0}{\partial x} \frac{\partial \delta \varphi_x}{\partial x} + \frac{\partial \ddot{u}_0}{\partial y} \frac{\partial \delta \varphi_x}{\partial y} \right) \\ & + J_2 \left[\ddot{\varphi}_x \delta \varphi_x + \mu \left(\frac{\partial \ddot{\varphi}_x}{\partial x} \frac{\partial \delta \varphi_x}{\partial x} + \frac{\partial \ddot{\varphi}_x}{\partial y} \frac{\partial \delta \varphi_x}{\partial y} \right) \right] \\ & + J_1 \left[\ddot{v}_0 \delta \varphi_y + \mu \left(\frac{\partial \ddot{v}_0}{\partial x} \frac{\partial \delta \varphi_y}{\partial x} + \frac{\partial \ddot{v}_0}{\partial y} \frac{\partial \delta \varphi_y}{\partial y} \right) \right] \\ & \left. + J_2 \left[\ddot{\varphi}_y \delta \varphi_y + \mu \left(\frac{\partial \ddot{\varphi}_y}{\partial x} \frac{\partial \delta \varphi_y}{\partial x} + \frac{\partial \ddot{\varphi}_y}{\partial y} \frac{\partial \delta \varphi_y}{\partial y} \right) \right] \right] \end{aligned} \right\} \right\} dS = 0$$

(2.53)

2.4. Finite element formulations

2.4.1. Finite element model

In this thesis, the eight-node rectangular element, which consisted of four nodes at the vertices of the quadrilateral and four nodes being the midpoints of the element's edge, is used. Each node has five degrees of freedom (DOFs) $\{u_0 \quad v_0 \quad w_0 \quad \varphi_x \quad \varphi_y\}$.
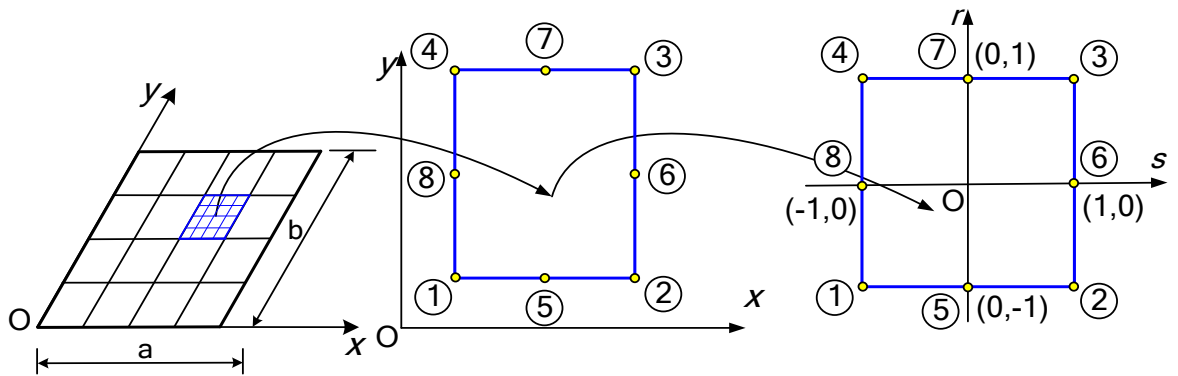
Figure 2.5. The eight-node rectangular element.

2.4.2. Element matrices and element vectors

2.4.2.1. Element displacement vector

The displacement vector of a point in the element is defined as follows:

$$\mathbf{u} = \{u \quad v \quad w\}^T \tag{2.54}$$

The displacement vector of any point on the mid-plane can be presented by

$$\mathbf{u}_0 = \{u_0 \quad v_0 \quad w_0 \quad \varphi_x \quad \varphi_y\}^T \tag{2.55}$$

From the equation (2.3), the relation between $\mathbf{u}$ and $\mathbf{u}_0$ as follows:

$$\mathbf{u} = \begin{bmatrix} 1 & 0 & 0 & z & 0 \\ 0 & 1 & 0 & 0 & z \\ 0 & 0 & 1 & 0 & 0 \end{bmatrix} \begin{bmatrix} u_0 \\ v_0 \\ w_0 \\ \varphi_x \\ \varphi_y \end{bmatrix} = \mathbf{L}_z \mathbf{u}_0 \qquad (2.56)$$

The node displacement vector is expressed by

$$\mathbf{q}_i = \{u_{0i} \quad v_{0i} \quad w_{0i} \quad \varphi_{xi} \quad \varphi_{yi}\}^T \qquad (2.57)$$
$$\text{5×1}$$

The element displacement vector is

$$\mathbf{q}_e = \begin{bmatrix} \mathbf{q}_1^T & \mathbf{q}_2^T & \mathbf{q}_3^T & \mathbf{q}_4^T & \mathbf{q}_5^T & \mathbf{q}_6^T & \mathbf{q}_7^T & \mathbf{q}_8^T \end{bmatrix}^T \qquad (2.58)$$
$$\text{40×1}$$

The author uses the Lagrange approximation function, which has forty coefficients according to the Pascal diagram.

The displacement vector at any point on the mid-plane is approximated by bilinear functions as follows:

$$\mathbf{u}_0 = \underbrace{\mathbf{P}(\mathrm{x},\ y)}_{\text{5×40}}\ \mathbf{a} \qquad (2.59)$$
$$\text{5×1} \qquad\qquad \text{40×1}$$

where

a: is the vector of approximate function coefficients.

P(x, y): is the matrix containing a polynomial approximation function.

Substituting the equation (2.59) into (2.57), the displacement at node i can be obtained by

$$\mathbf{q}_i = \mathbf{A}_i\ \mathbf{a} \qquad (2.60)$$
$$\text{5×1} \qquad \text{5×40} \quad \text{40×1}$$

where $\mathbf{A}_i$ is the matrix containing the coordinates of the node (x_i, y_i) in the element, defined as in appendices.

Substituting the equation (2.60) into (2.58), the element's node displacement vector is defined as follows:

$$\mathbf{q}_e = \mathbf{A}_n \, \mathbf{a}$$
$$\underset{40\times1}{} \quad \underset{40\times40}{} \underset{40\times1}{}$$

(2.61)

where $\mathbf{A}_n = [\mathbf{A}_1 \quad \mathbf{A}_2 \quad \mathbf{A}_3 \quad \mathbf{A}_4 \quad \mathbf{A}_5 \quad \mathbf{A}_6 \quad \mathbf{A}_7 \quad \mathbf{A}_8]^T$ is the matrix containing the coordinates of the element nodes (see Appendices).

From the equation (2.61), the approximate function coefficients vector can be expressed by

$$\mathbf{a} = \mathbf{A}^{-1}\mathbf{q}_e$$

(2.62)

Substituting the equation (2.62) into (2.59), the displacement vector of any point on the mid-plane can be defined as follows:

$$\mathbf{u}_{0e} = \mathbf{P}(r,s)\mathbf{A}_n^{-1}\mathbf{q}_e = \mathbf{N} \, \mathbf{q}_e$$
$$\underset{5\times1}{} \qquad\qquad\qquad \underset{5\times40}{} \underset{40\times1}{}$$

(2.63)

The shape function is defined by

$$\underset{5\times40}{\mathbf{N}} = \left[\underset{5\times5}{N_1 \mathbf{I}} \quad \underset{5\times5}{N_2 \mathbf{I}} \quad \underset{5\times5}{N_3 \mathbf{I}} \quad \underset{5\times5}{N_4 \mathbf{I}} \quad \underset{5\times5}{N_5 \mathbf{I}} \quad \underset{5\times5}{N_6 \mathbf{I}} \quad \underset{5\times5}{N_7 \mathbf{I}} \quad \underset{5\times5}{N_8 \mathbf{I}} \right]$$

(2.64)

where N_i is a polynomial in terms of r, s and the node coordinates $(\mathrm{r}_i, \mathrm{s}_i)$:

$$N_1 = \frac{1}{4}(1+rr_1)(1+ss_1)(rr_1 + ss_1 - 1); \; N_5 = \frac{1}{2}(1-r^2)(1+ss_5);$$

$$N_2 = \frac{1}{4}(1+rr_2)(1+ss_2)(rr_2 + ss_2 - 1); \; N_6 = \frac{1}{2}(1+rr_6)(1-s^2);$$

$$N_3 = \frac{1}{4}(1+rr_3)(1+ss_3)(rr_3 + ss_3 - 1); \; N_7 = \frac{1}{2}(1-r^2)(1+ss_7);$$

$$N_4 = \frac{1}{4}(1+rr_4)(1+ss_4)(rr_4 + ss_4 - 1); \; N_8 = \frac{1}{2}(1+rr_8)(1-s^2).$$

(2.65)

Substituting the node coordinates $M_1(-1,-1)$, $M_2(1,-1)$, $M_3(1,1)$, $M_4(-1,1)$, $M_5(0,-1)$, $M_6(1,0)$, $M_7(0,1)$, $M_8(-1,0)$ into equation (2.65), the shape functions in terms of the natural coordinates r, s are defined as follows:

$$N_1 = -\frac{1}{4}(1-r)(1-s)(1+r+s); \quad N_2 = \frac{1}{2}(1-r^2)(1-s);$$

$$N_3 = -\frac{1}{4}(1+r)(1-s)(1-r+s); \quad N_4 = \frac{1}{2}(1+r)(1-s^2);$$

$$N_5 = -\frac{1}{4}(1+r)(1+s)(1-r-s); \quad N_6 = \frac{1}{2}(1-r^2)(1+s);$$

$$N_7 = -\frac{1}{4}(1-r)(1+s)(1+r-s); \quad N_8 = \frac{1}{2}(1-r)(1-s^2).$$

(2.66)

2.4.2.2. The element stiffness matrix

The variation of strain energy is

$$\delta U_e = \int_{V_e} (1 - \mu \nabla^2) \boldsymbol{\sigma}^{nl}.\delta \boldsymbol{\varepsilon} dV \tag{2.67}$$

$$\delta U_e = \int_{V_e} \boldsymbol{\sigma}^l.\delta \boldsymbol{\varepsilon} dV \tag{2.68}$$

$$\delta U_e = \int_{V_e} \boldsymbol{\varepsilon}^T \mathbf{D} \delta \boldsymbol{\varepsilon} dV \tag{2.69}$$

$$\delta U_e = \int_{V_e} \left[\left(\boldsymbol{\varepsilon}_1^0 + z\boldsymbol{\varepsilon}_1^1 \right)^T \mathbf{D}_b \delta \left(\boldsymbol{\varepsilon}_1^0 + z\boldsymbol{\varepsilon}_1^1 \right) + \boldsymbol{\varepsilon}_2^{0\,T} \mathbf{D}_s \delta \boldsymbol{\varepsilon}_2^0 \right] dV \tag{2.70}$$

$$\delta U_e = \int_{V_e} \begin{bmatrix} \boldsymbol{\varepsilon}_1^{0\,T} \mathbf{D}_b \delta \boldsymbol{\varepsilon}_1^0 + \boldsymbol{\varepsilon}_1^{0\,T} z \mathbf{D}_b \delta \boldsymbol{\varepsilon}_1^1 + \boldsymbol{\varepsilon}_1^{1\,T} z \mathbf{D}_b \delta \boldsymbol{\varepsilon}_1^0 + \boldsymbol{\varepsilon}_1^{1\,T} z^2 \mathbf{D}_b \delta \boldsymbol{\varepsilon}_1^1 \\ + \boldsymbol{\varepsilon}_2^{0\,T} \mathbf{D}_s \delta \boldsymbol{\varepsilon}_2^0 \end{bmatrix} dV \tag{2.71}$$

$$\delta U_e = \int_{S_e} \begin{bmatrix} \boldsymbol{\varepsilon}_1^{0\,T} \mathbf{A} \delta \boldsymbol{\varepsilon}_1^0 + \boldsymbol{\varepsilon}_1^{0\,T} \mathbf{B} \delta \boldsymbol{\varepsilon}_1^1 + \boldsymbol{\varepsilon}_1^{1\,T} \mathbf{B} \delta \boldsymbol{\varepsilon}_1^0 + \boldsymbol{\varepsilon}_1^{1\,T} \mathbf{X} \delta \boldsymbol{\varepsilon}_1^1 \\ + \boldsymbol{\varepsilon}_2^{0\,T} \mathbf{A}^s \delta \boldsymbol{\varepsilon}_2^0 \end{bmatrix} dxdy \tag{2.72}$$

$$\delta U_e = \mathbf{q}_e^T \int_{S_e} \begin{bmatrix} \mathbf{B}_1^T \mathbf{A} \mathbf{B}_1 + \mathbf{B}_1^T \mathbf{B} \mathbf{B}_2 + \mathbf{B}_2^T \mathbf{B} \mathbf{B}_2 + \mathbf{B}_2^T \mathbf{X} \mathbf{B}_2 \\ + \mathbf{B}_3^T \mathbf{A}^s \mathbf{B}_3^T \end{bmatrix} dxdy \delta \mathbf{q}_e \tag{2.73}$$

From the equation (2.73), the element stiffness matrix is defined by

$$\mathbf{K}_e^b = \int_{S_e} \left(\begin{bmatrix} \mathbf{B}_1^T & \mathbf{B}_2^T \end{bmatrix} \begin{bmatrix} \mathbf{A} & \mathbf{B} \\ \mathbf{B} & \mathbf{X} \end{bmatrix} \begin{bmatrix} \mathbf{B}_1 \\ \mathbf{B}_2 \end{bmatrix} \right) dxdy \tag{2.74}$$

$$\mathbf{K}_e^s = \int_{S_e} \left(\mathbf{B}_3^T \mathbf{A}^s \mathbf{B}_3 \right) dxdy \tag{2.75}$$

The element stiffness matrix is written in the natural coordinate as follows:

$$\mathbf{K}_e^b = \int_{-1}^{1}\int_{-1}^{1} \left(\begin{bmatrix} \mathbf{B}_1^T & \mathbf{B}_2^T \end{bmatrix} \begin{bmatrix} \mathbf{A} & \mathbf{B} \\ \mathbf{B} & \mathbf{X} \end{bmatrix} \begin{bmatrix} \mathbf{B}_1 \\ \mathbf{B}_2 \end{bmatrix} \right) \det|J| drds \tag{2.76}$$

$$\mathbf{K}_e^s = \int_{-1}^{1}\int_{-1}^{1} \left(\mathbf{B}_3^T \mathbf{A}^s \mathbf{B}_3 \right) \det|J| drds \tag{2.77}$$

where

$\mathbf{K}_e^b$ and $\mathbf{K}_e^s$ are the bending stiffness matrix and the shear stiffness matrix, respectively

$$\mathbf{B}_1 = \begin{bmatrix} \dfrac{\partial \mathbf{N}_u}{\partial x} \\ \dfrac{\partial \mathbf{N}_v}{\partial y} \\ \dfrac{\partial \mathbf{N}_u}{\partial y} + \dfrac{\partial \mathbf{N}_v}{\partial x} \end{bmatrix} ; \mathbf{B}_2 = \begin{bmatrix} \dfrac{\partial \mathbf{N}_{\varphi x}}{\partial x} \\ \dfrac{\partial \mathbf{N}_{\varphi y}}{\partial y} \\ \dfrac{\partial \mathbf{N}_{\varphi x}}{\partial y} + \dfrac{\partial \mathbf{N}_{\varphi y}}{\partial x} \end{bmatrix} ; \mathbf{B}_3 = \begin{bmatrix} \dfrac{\partial \mathbf{N}_w}{\partial x} + \mathbf{N}_{\varphi x} \\ \dfrac{\partial \mathbf{N}_w}{\partial y} + \mathbf{N}_{\varphi y} \end{bmatrix} \tag{2.78}$$

From the equation (2.52), the elastic foundation stiffness matrix is determined as follows:

$$
\mathbf{K}_e^f = \int\limits_{S_e} \left\{ \begin{array}{l} k_1 \left[\mathbf{N}_w^T \mathbf{N}_w + \mu \left(\dfrac{\partial \mathbf{N}_w^T}{\partial x} \dfrac{\partial \mathbf{N}_w}{\partial x} + \dfrac{\partial \mathbf{N}_w^T}{\partial y} \dfrac{\partial \mathbf{N}_w}{\partial y} \right) \right] \\[4mm] +k_2 \left[\begin{array}{l} \left(\dfrac{\partial \mathbf{N}_w^T}{\partial x} \dfrac{\partial \mathbf{N}_w}{\partial x} + \dfrac{\partial \mathbf{N}_w^T}{\partial y} \dfrac{\partial \mathbf{N}_w}{\partial y} \right) \\[3mm] +\mu \left(\begin{array}{l} \dfrac{\partial^2 \mathbf{N}_w^T}{\partial x^2} \dfrac{\partial^2 \mathbf{N}_w}{\partial x^2} + \dfrac{\partial^2 \mathbf{N}_w^T}{\partial y^2} \dfrac{\partial^2 \mathbf{N}_w}{\partial y^2} \\[3mm] \dfrac{\partial^2 \mathbf{N}_w^T}{\partial x^2} \dfrac{\partial^2 \mathbf{N}_w}{\partial y^2} + \dfrac{\partial^2 \mathbf{N}_w^T}{\partial y^2} \dfrac{\partial^2 \mathbf{N}_w}{\partial x^2} \end{array} \right) \end{array} \right] \end{array} \right\} dxdy \qquad (2.79)
$$

The elastic foundation stiffness matrix is written in the natural coordinate as follows:

$$
\mathbf{K}_e^f = \int\limits_{-1}^{1}\int\limits_{-1}^{1} \left\{ \begin{array}{l} k_1 \left[\mathbf{N}_w^T \mathbf{N}_w + \mu \left(\dfrac{\partial \mathbf{N}_w^T}{\partial x} \dfrac{\partial \mathbf{N}_w}{\partial x} + \dfrac{\partial \mathbf{N}_w^T}{\partial y} \dfrac{\partial \mathbf{N}_w}{\partial y} \right) \right] \\[4mm] +k_2 \left[\begin{array}{l} \left(\dfrac{\partial \mathbf{N}_w^T}{\partial x} \dfrac{\partial \mathbf{N}_w}{\partial x} + \dfrac{\partial \mathbf{N}_w^T}{\partial y} \dfrac{\partial \mathbf{N}_w}{\partial y} \right) \\[3mm] +\mu \left(\begin{array}{l} \dfrac{\partial^2 \mathbf{N}_w^T}{\partial x^2} \dfrac{\partial^2 \mathbf{N}_w}{\partial x^2} + \dfrac{\partial^2 \mathbf{N}_w^T}{\partial y^2} \dfrac{\partial^2 \mathbf{N}_w}{\partial y^2} \\[3mm] \dfrac{\partial^2 \mathbf{N}_w^T}{\partial x^2} \dfrac{\partial^2 \mathbf{N}_w}{\partial y^2} + \dfrac{\partial^2 \mathbf{N}_w^T}{\partial y^2} \dfrac{\partial^2 \mathbf{N}_w}{\partial x^2} \end{array} \right) \end{array} \right] \end{array} \right\} \det|J| drds \qquad (2.80)
$$

2.4.2.3. The element mass matrix

The variation of kinetic energy is written by

$$
\delta T_e = \int\limits_{V_e} \rho(z)\left(1 - \mu\nabla^2\right)\left(\dot{u}\delta\dot{u} + \dot{v}\delta\dot{v} + \dot{w}\delta\dot{w}\right) dV \qquad (2.81)
$$

$$
\delta T_e = \int\limits_{V_e} \rho(z)\left(1 - \mu\nabla^2\right)\left[\begin{array}{l} \left(\dot{u}_0 + z\dot{\varphi}_x\right)\delta\left(\dot{u}_0 + z\dot{\varphi}_x\right) \\ +\left(\dot{v}_0 + z\dot{\varphi}_y\right)\delta\left(\dot{v}_0 + z\dot{\varphi}_y\right) + \dot{w}_0\delta\dot{w}_0 \end{array} \right] dV \qquad (2.82)
$$

$$\delta T_e = \int_{V_e} \rho(z)\left(1-\mu\nabla^2\right)\begin{pmatrix} \dot{u}_0\delta\dot{u}_0 + z\dot{u}_0\delta\dot{\varphi}_x + z\dot{\varphi}_x\delta\dot{u}_0 + z^2\dot{\varphi}_x\delta\dot{\varphi}_x \\ + \dot{v}_0\delta\dot{v}_0 + z\dot{v}_0\delta\dot{\varphi}_y + z\dot{\varphi}_y\delta\dot{v}_0 + z^2\dot{\varphi}_y\delta\dot{\varphi}_y \\ + \dot{w}_0\delta\dot{w}_0 \end{pmatrix} dV \quad (2.83)$$

$$\delta T_e = \ddot{\mathbf{q}}_e^T \int_{S_e} \left(1-\mu\nabla^2\right)\begin{pmatrix} \mathbf{N}_u^T J_0 \mathbf{N}_u + \mathbf{N}_u^T J_1 \mathbf{N}_{\varphi x} + \mathbf{N}_{\varphi x}^T J_1 \mathbf{N}_u + \mathbf{N}_{\varphi x}^T J_2 \mathbf{N}_{\varphi x} \\ + \mathbf{N}_v^T J_0 \mathbf{N}_v + \mathbf{N}_v^T J_1 \mathbf{N}_{\varphi y} + \mathbf{N}_{\varphi y}^T J_1 \mathbf{N}_v + \mathbf{N}_{\varphi y}^T J_2 \mathbf{N}_{\varphi y} \\ + \mathbf{N}_w^T J_0 \mathbf{N}_w \end{pmatrix} dxdy\,\delta\mathbf{q}_e$$

$$(2.84)$$

From the equation (2.84), the element mass matrix is :

$$\mathbf{M}_e = \int_{S_e} \left[\mathbf{N}^T \mathbf{D}_m \mathbf{N} + \mu\left(\frac{\partial\mathbf{N}^T}{\partial x}\mathbf{D}_m\frac{\partial\mathbf{N}}{\partial x} + \frac{\partial\mathbf{N}^T}{\partial y}\mathbf{D}_m\frac{\partial\mathbf{N}}{\partial y} \right) \right] dxdy \quad (2.85)$$

The element mass matrix is written in the natural coordinate as follows:

$$\mathbf{M}_e = \int_{-1}^{1}\int_{-1}^{1} \left[\mathbf{N}^T \mathbf{D}_m \mathbf{N} + \mu\left(\frac{\partial\mathbf{N}^T}{\partial x}\mathbf{D}_m\frac{\partial\mathbf{N}}{\partial x} + \frac{\partial\mathbf{N}^T}{\partial y}\mathbf{D}_m\frac{\partial\mathbf{N}}{\partial y} \right) \right] \det|J|drds \quad (2.86)$$

where

$$\mathbf{N} = \begin{bmatrix} \mathbf{N}_u^T & \mathbf{N}_v^T & \mathbf{N}_w^T & \mathbf{N}_{\varphi x}^T & \mathbf{N}_{\varphi y}^T \end{bmatrix}^T \quad (2.87)$$

$$\mathbf{D}_m = \begin{bmatrix} J_0 & 0 & 0 & J_1 & 0 \\ & J_0 & 0 & 0 & J_1 \\ & & J_0 & 0 & 0 \\ & & & J_2 & 0 \\ sym & & & & J_2 \end{bmatrix} \quad (2.88)$$

2.4.2.4. The element load vector

The element load vector is defined by

$$\mathbf{F}_e = \int_{S_e} (1-\mu\nabla^2)\mathbf{N}_w^T F dxdy \quad (2.89)$$

$$\mathbf{F}_e = \int\limits_{S_e} \left\{ \mathbf{N}_w^T F - \mu \left[F\left(\frac{\partial^2 \mathbf{N}_w^T}{\partial x^2} + \frac{\partial^2 \mathbf{N}_w^T}{\partial y^2} \right) + \mathbf{N}_w^T \left(\frac{\partial^2 F}{\partial x^2} + \frac{\partial^2 F}{\partial y^2} \right) \right] \right\} dxdy \quad (2.90)$$

The element load vector is written in the natural coordinate as follows:

$$\mathbf{F}_e = \int\limits_{-1}^{1}\int\limits_{-1}^{1} \left\{ \mathbf{N}_w^T F - \mu \left[F\left(\frac{\partial^2 \mathbf{N}_w^T}{\partial x^2} + \frac{\partial^2 \mathbf{N}_w^T}{\partial y^2} \right) + \mathbf{N}_w^T \left(\frac{\partial^2 F}{\partial x^2} + \frac{\partial^2 F}{\partial y^2} \right) \right] \right\} \det|J| drds \quad (2.91)$$

All integrations in equations (2.76), (2.77), (2.80), (2.86), and (2.91) are calculated using full Gauss integration with three integral points.

From equation (2.14), the real state of the plate corresponding to the minimum of H_e leads to:

$$\frac{\partial U_e}{\partial q_e} + \frac{\partial V_e}{\partial q_e} - \frac{\partial W_e}{\partial q_e} - \left(-\frac{d}{dt}\frac{\partial T_e}{\partial \dot{q}_e} \right) = 0 \qquad (2.92)$$

The equation (2.92) is rewritten as:

$$\frac{d}{dt}\left(-\frac{\partial T_e}{\partial \dot{q}_e} \right) + \frac{\partial\left(U_e + V_e\right)}{\partial q_e} = \frac{\partial W_e}{\partial q_e} \qquad (2.93)$$

From the equation (2.93), the governing equation of motion of the plate element without resistance has the form:

$$\mathbf{M}_e.\ddot{\mathbf{q}}_e + \mathbf{K}_e.\mathbf{q}_e = \mathbf{F}_e \qquad (2.94)$$

where $\mathbf{M}_e, \mathbf{K}_e, \mathbf{F}_e$ are the element mass matrix, the element stiffness matrix, and the element load vector, respectively.

After gathering the element mass matrix, element stiffness matrix, and element node force vector, the governing equation of motion of the plate without resistance as follows:

$$\mathbf{M}.\ddot{\mathbf{q}} + \mathbf{K}.\mathbf{q} = \mathbf{F} \qquad (2.95)$$

where $\mathbf{M}, \mathbf{K}, \mathbf{F}$ are the global mass matrix, the global stiffness matrix, and global load vector, respectively.

2.5. Boundary conditions

Considering plates with different bonding conditions such as simply supported, clamped supported. Boundary conditions for each specific case are as follows:

2.5.1. Rectangular nanoplate

2.5.1.1. Completely simply supported (CSS)

At $x = 0, x = a : v_{0i} = w_i = \varphi_{yi} = 0$.

At $y = 0, y = b : u_{0i} = w_i = \varphi_{xi} = 0$.

2.5.1.2. Completely clamped supported (CCS)

At $x = 0, x = a : u_{0i} = v_{0i} = w_i = \varphi_{xi} = \varphi_{yi} = 0$.

At $x = 0, x = a : u_{0i} = v_{0i} = w_i = \varphi_{xi} = \varphi_{yi} = 0$.

2.5.2. L-shape nanoplate

2.5.2.1. Completely simply supported

At $x = 0; \ x = \dfrac{a}{2}, y = 0 \div \dfrac{b}{2}; \ x = a, y = \dfrac{b}{2} \div b : v_{0i} = w_i = \varphi_{yi} = 0$.

At $y = 0; \ y = \dfrac{b}{2}, x = 0 \div \dfrac{a}{2}; \ y = b, x = \dfrac{a}{2} \div a : u_{0i} = w_i = \varphi_{xi} = 0$.

2.5.2.2. Completely clamped supported

At $x = 0; \ x = \dfrac{a}{2}, y = 0 \div \dfrac{b}{2}; \ x = a, y = \dfrac{b}{2} \div b : u_{0i} = v_{0i} = w_i = \varphi_{xi} = \varphi_{yi} = 0$.

At $y = 0; \ y = \dfrac{b}{2}, x = 0 \div \dfrac{a}{2}; \ y = b, x = \dfrac{a}{2} \div a : u_{0i} = v_{0i} = w_i = \varphi_{xi} = \varphi_{yi} = 0$.

2.5.3. Annular nanoplate

2.5.3.1. Simply supported

- Simply supported at the inner border: At $r_i = r_1$: $w_i = 0$.

- Simply supported at the outer border: At $r_i = R$: $w_i = 0$.

- Completely simply supported: At $r_i = r_1, r_i = R$: $w_i = 0$.

2.5.3.2. Clamped supported

- Clamped at the inner border: At $r_i = r_1$: $u_{0i} = v_{0i} = w_i = \varphi_{xi} = \varphi_{yi} = 0$.

- Clamped at the outer border: At $r_i = R$: $u_{0i} = v_{0i} = w_i = \varphi_{xi} = \varphi_{yi} = 0$.

- Completely clamped: At $r_i = r_1, r_i = R$: $u_{0i} = v_{0i} = w_i = \varphi_{xi} = \varphi_{yi} = 0$.

2.5.4. Half-annular nanoplate

2.5.4.1. Simply supported

- Simply supported at the inner border: At $r_i = r_1$: $w_i = 0$.

- Simply supported at the outer border: At $r_i = R$: $w_i = 0$.

- Completely simply supported: At $r_i = r_1, r_i = R$: $w_i = 0$.

2.5.4.2. Clamped supported

- Clamped at the inner border: At $r_i = r_1$: $u_{0i} = v_{0i} = w_i = \varphi_{xi} = \varphi_{yi} = 0$.

- Clamped at the outer border: At $r_i = R$: $u_{0i} = v_{0i} = w_i = \varphi_{xi} = \varphi_{yi} = 0$.

- Completely clamped: At $r_i = r_1, r_i = R$: $u_{0i} = v_{0i} = w_i = \varphi_{xi} = \varphi_{yi} = 0$.

2.6. Summary of Chapter 2

Using the finite element method based on first-order shear deformation theory and nonlocal elasticity theory, the author has built a stiffness matrix, mass matrix, and load vector. From there, based on Hamilton's principle, the motion equation is established for calculating FGP nanoplates with different shapes resting on elastic foundation.

Defining specific boundary conditions for different shapes nanoplates.

The formulations in this chapter are the scientific basis for building algorithms and calculation programs to solve the static problem in chapter 3, the free vibration problem, and forced vibration in chapter 4.

The expanded expressions in this chapter are used for calculations in the next studies.

Chapter 3 STATIC ANALYSIS OF FGM POROUS NANOPLATES RESTING ON ELASTIC FOUNDATION

In this chapter, the author establishes the static equilibrium equation and a program to solve the static bending problem. Simultaneously, the influence of some parameters on the static response of nanoplates such as nonlocal factor, material characteristics, and elastic foundation, are investigated.

3.1. Problem formulation

Consider the FGP nanoplates resting on an elastic foundation subjected to static loads, as shown in Figure 3.1. Geometric parameters are presented specifically in each model. With the flexible imposition of boundary conditions, the finite element method allows the analysis of complex structures that are difficult or even impossible to perform with analytical methods.

a) Rectangular nanoplate

b) L-shape nanoplate

c) Annular nanoplate

d) Half-annular nanoplate
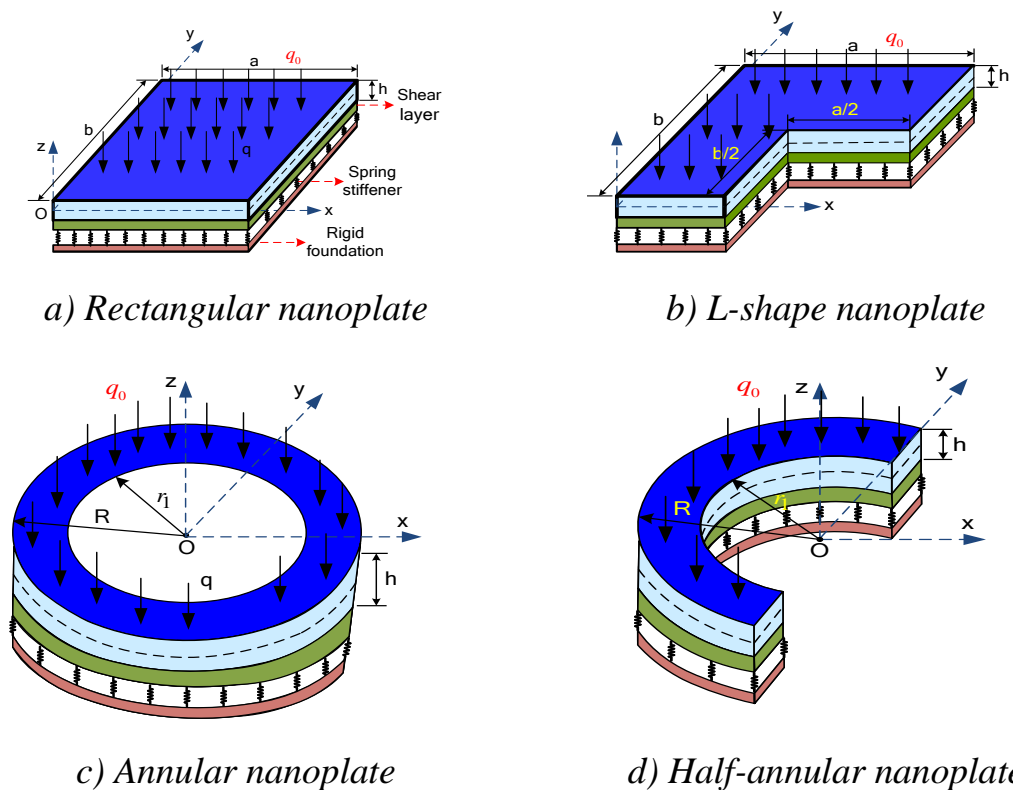
Figure 3.1. The model of FGP nanoplates subjected to static load.

3.2. Finite element algorithm and calculation programs

The equilibrium equation of nanoplates subjected to static loads is:

$$\mathbf{K}.\mathbf{q} = \mathbf{F} \tag{3.1}$$

in which $\mathbf{K}, \mathbf{q}, \mathbf{F}$ are the global stiffness matrix, the global force vector, and the global displacement vector. They are gathered from the element stiffness matrix, the element force vector, and the element displacement vector.

From the equation (3.1), the global node displacement vector is calculated according to the following formulation:

$$\mathbf{q} = \mathbf{K}^{-1}\mathbf{F} \tag{3.2}$$

Algorithm diagram for solving FGP nanoplates subjected to static load as shown in Figure 3.2.
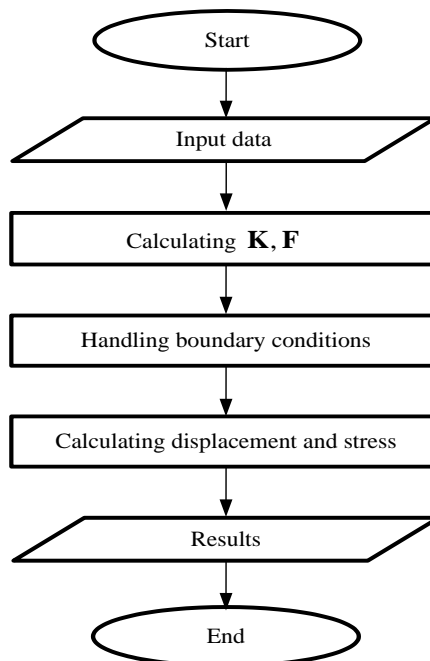
Figure 3.2. Algorithm diagram for solving FGP nanoplates subjected to the static load.

Based on the above algorithm presented, the calculation program FGP_Nanoplates_FSDT_Nonlocal_Static_2022 (FNFNS_2022) is built in

Matlab software to analyze the static behavior of the FGP nanoplates resting on the elastic foundation. The program consists of the following main modules:

- The module for input data and meshing elements.

- The module solves the static behavior for FGP nanoplate resting on the elastic foundation.

- The module outputs the results.

The program FGP_Nanoplates_FSDT_Nonlocal_Static_2022 can solve the static behavior of FGP nanoplates resting on an elastic foundation and investigate the influence of factors such as boundary conditions, material properties, elastic foundation characteristics on the static behavior of the nanoplates.

3.3. Verification study

Considering completely simply supported FGM square nanoplates. Material properties of the individual materials as shown in Table 3.1, and geometry parameters as $a=b=10\ nm$, $h=a/10$, $k = 0$, $K_2 = 0$.

The dimensionless quantities are introduced by

$$w^* = \frac{100E_2h^3}{q_0a^4}w, \sigma_{xx}^* = \frac{10h}{q_0a}\sigma_{xx}, \sigma_{xy}^* = \frac{10h}{q_0a}\sigma_{xy},$$

$$K_1 = \frac{k_wa^4}{H}, K_2 = \frac{k_sa^2}{H}, H = \frac{E_2h^3}{12(1-v^2)}$$

(3.3)

Table 3.1. Material properties

Materials	E (GPa)	v	ρ (kg/m^3)
Al$_2$O$_3$ (ceramic)	380	0.3	3800
Al (metal)	70	0.3	2707

As exhibited in Table 3.2 the present results are in good agreement with an analytical method of Sobhy [73]. It means that the present method is highly reliable.

Table 3.2. The displacement and stress of square nanoplates.

Method	K_1	$\mu = 0$		$\mu = 4$	
		$w^*\left(\dfrac{a}{2};\dfrac{b}{2};0\right)$	$\sigma_{xx}^*\left(\dfrac{a}{2};\dfrac{b}{2};\dfrac{h}{2}\right)$	$w^*\left(\dfrac{a}{2};\dfrac{b}{2};0\right)$	$\sigma_{xx}^*\left(\dfrac{a}{2};\dfrac{b}{2};\dfrac{h}{2}\right)$
[73]	0	2.9603	19.9550	5.2977	35.7108
	100	2.3290	15.6991	3.5671	24.0455
Thesis	0	2.9600 *(0.01%)*	19.8990 *(0.28%)*	5.2971 *(0.01%)*	35.6106 *(0.28%)*
	100	2.3288 *(0.01%)*	15.6555 *(4.36%)*	3.5669 *(0.01%)*	23.9791 *(0.28%)*

3.4. Numerical results and discussion

Based on the calculation program, in this section, the author analyzes the static bending of FGP nanoplates with different shapes, geometrical parameters, material properties, boundary conditions, and elastic stiffness. The static load is evenly distributed in the direction perpendicular to the plate surface.

3.4.1. Rectangular nanoplate

Considering the completely simply supported FGP square nanoplates as in Figure 3.1 a. Geometric dimensions $a = b = 10nm; h = a/10$. Material properties of the individual materials as shown in Table 3.1, power-law index $k=1$, porosity factor $\xi = 0.1$, nonlocal factor $\mu = 2$, the stiffness of foundation:

K_1=50, K_2=10. The plate is subjected to uniform load q_0 in perpendicular directions. The deformation and stress of the square nanoplate with various mesh sizes are shown in Table 3.3. It can be seen that the results converge at a mesh size of 8×8.

Table 3.3. The deformation and stress of the square nanoplate with various mesh sizes.

	Mesh size	2×2	4×4	6×6	8×8	10×10
Even porosity	Max (w^*)	10.9205	10.9174	10.9150	10.9135	10.9135
	$\sigma_{xx}^*(\frac{a}{2};\frac{b}{2};0)$	-6.3154	-6.3010	-6.2841	-6.2831	-6.2831
Uneven porosity	Max (w^*)	10.0801	10.0785	10.0777	10.0772	10.0772
	$\sigma_{xx}^*(\frac{a}{2};\frac{b}{2};0)$	-5.4740	-5.4732	-5.4726	-5.4722	-5.4722

The deformation field of the nanoplate is shown in Figure 3.3 a, b. The stresses at the midpoint of the plate according to plate thickness are presented in Figure 3.3 c, d. It can be seen that the law of stress distribution according to the thickness of the plate at a point is consistent with the law of effective mechanical properties of FGP materials. In addition, in the case of a square plate, with completely simply supported, the maximum displacement will be at the center of the plate, and the strain field varies uniformly from this point to the surrounding.

a) The deformation field

b) The top view deformation field

c) The stress σ_{xx}^{*} at the midpoint

d) The stress σ_{xy}^{*} at the midpoint
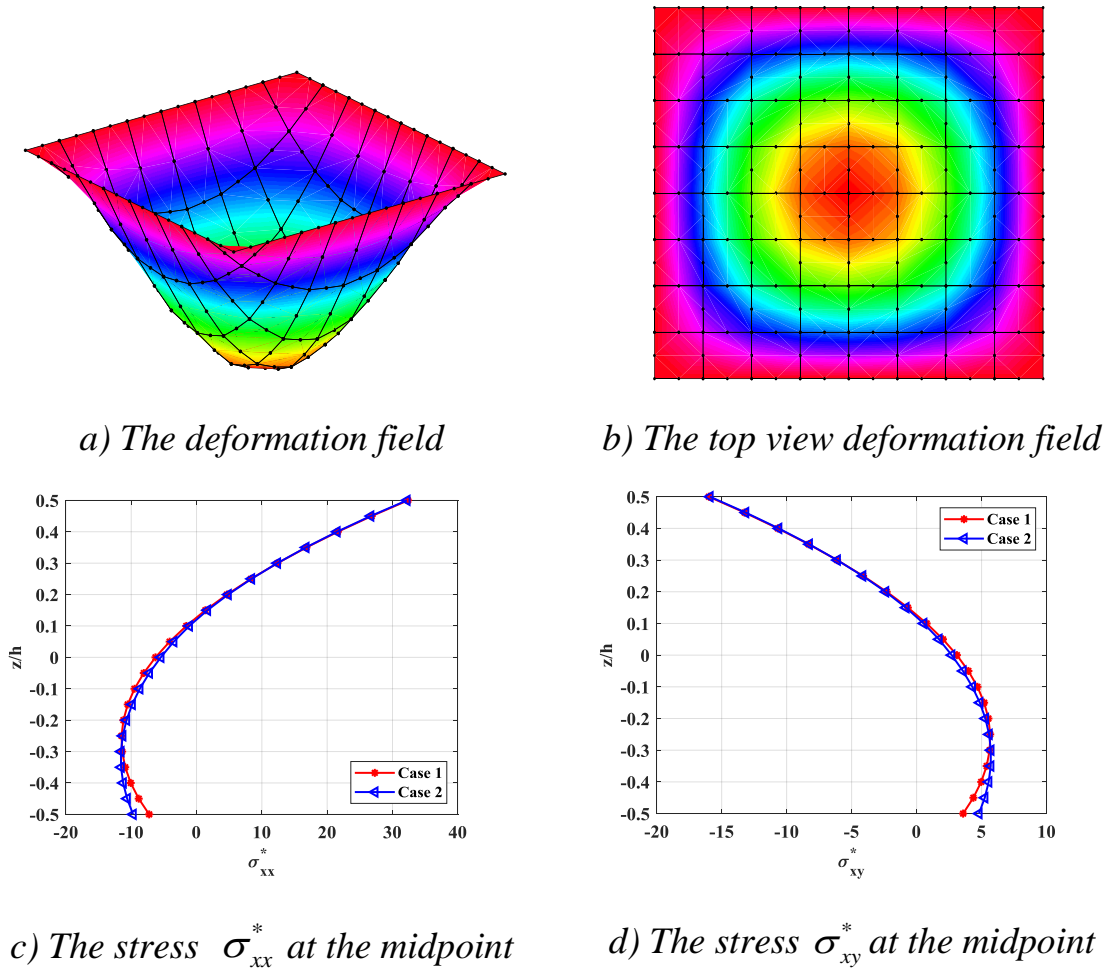
Figure 3.3. The deformation and stresses of the completely simply supported square nanoplate (Case 1: Even porosity, Case 2: Uneven porosity).

3.4.2. L-shape nanoplate

Considering the completely simply supported FGP L-shape nanoplates as in Figure 3.1 b. Geometric dimensions $a = b = 10$ nm, $h = 1$ nm. Material properties of the individual materials as shown in Table 3.1, power-law index $k=5$, porosity factor $\xi = 0.2$, nonlocal factor $\mu = 4$, the foundation stiffness: $K_1 = 100$, $K_2 = 10$. The FGP nanoplate is subjected to uniformly load q_0 in perpendicular directions. The deformation and stress of the L-shape nanoplate

with various mesh sizes are listed in Table 3.4. It can be seen that the results converge at a mesh size of 48 elements.

The deformation field of the nanoplate is shown in Figure 3.4 a, b. The stresses at the A-point of the nanoplate are presented in Figure 3.4 c, d. From the deformation field can be seen that the vicinity of the L-angle is most susceptible to failure due to stress concentration because of the sudden change in shape at the L-angle.

a) The deformation field

b) The top view deformation field

c) The stress σ_{xx}^* at A-point

d) The stress σ_{xy}^* at A-point
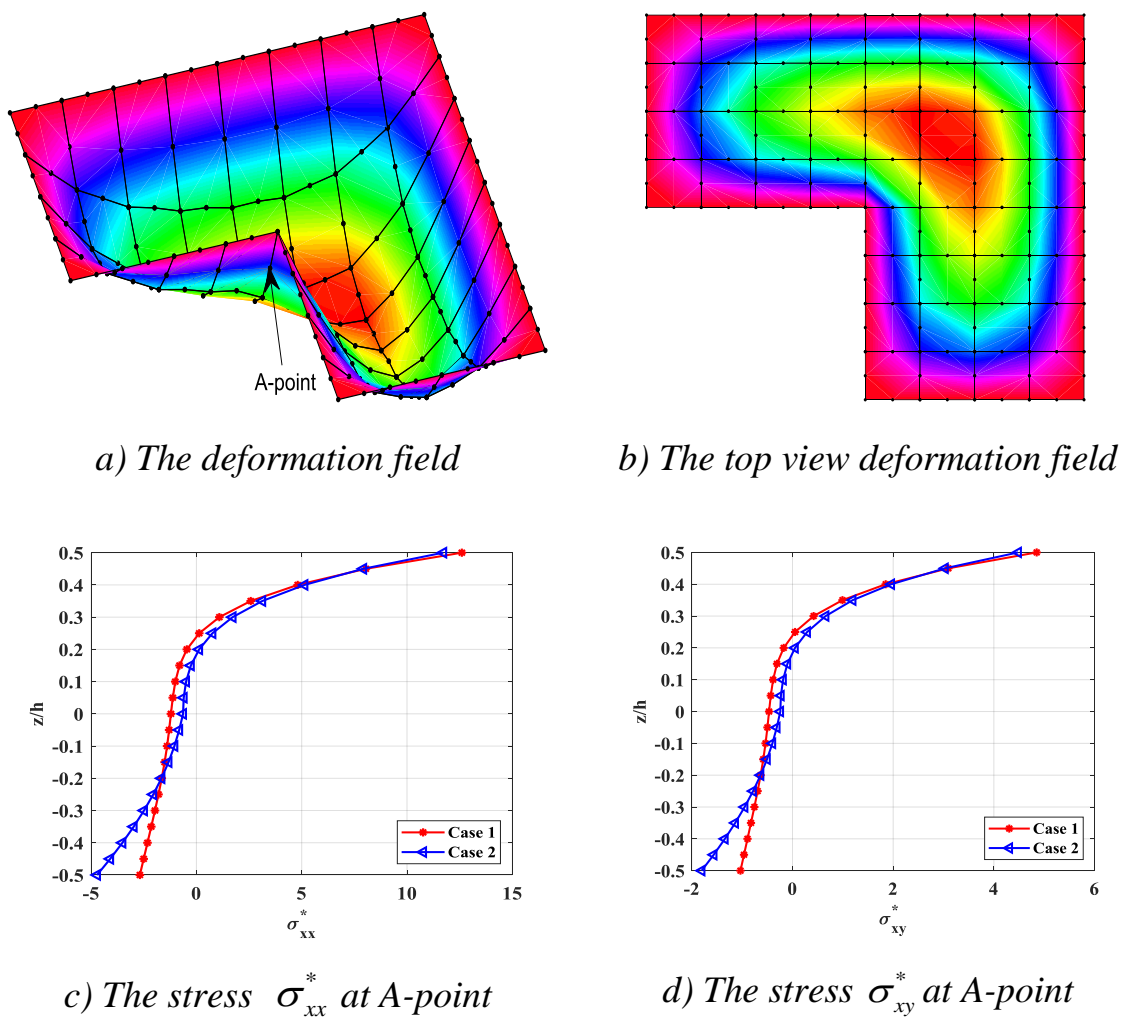
Figure 3.4. The deformation and stresses of the completely simply supported L-shape nanoplate (Case 1: Even porosity, Case 2: Uneven porosity).

Table 3.4. The deformation and stress of the L-shape nanoplate with various mesh sizes.

	Mesh size	12	24	32	48	96
Even porosity	Max $\left(w^*\right)$	6.1217	6.1202	6.1198	6.1193	6.1192
	$\sigma_{xx}^*(5;5.625;0)$	-1.2134	-1.2123	-1.2117	-1.2113	-1.2112
Uneven porosity	Max $\left(w^*\right)$	4.2618	4.2609	4.2601	4.2598	4.2597
	$\sigma_{xx}^*(5;5.625;0)$	-0.6362	-0.6353	-0.6348	-0.6343	-0.6342

3.4.3. Annular nanoplate

Consider the FGP annular nanoplates as in Figure 3.1c with clamped supported at the outer border. Material properties of the individual materials are listed in Table 3.1 with geometric dimensions $R = 5$ nm, $r_1 = 2.5$ nm, $h = 1$ nm, power-law index $k=2$, porosity factor $\xi = 0.3$, nonlocal factor $\mu = 1$, the stiffness of foundation: $K_1 = 50$, $K_2 = 50$. The FGP annular nanoplate is subjected to uniformly load q_0 in perpendicular directions. The deformation and stress of the annular nanoplate with various mesh sizes are shown in Table 3.5. It can be seen that the results converge at a mesh size of 64 elements.

Table 3.5. The deformation and stress of the annular nanoplate with various mesh sizes.

	Mesh size	8	16	32	64	128
Even porosity	Max $\left(w^*\right)$	1.5192	1.5185	1.5180	1.5177	1.5176
	$\sigma_{xx}^*(0;2.8125;0)$	-0.0386	-0.0381	-0.0377	-0.0370	-0.0370
Uneven porosity	Max $\left(w^*\right)$	1.0142	1.0137	1.0131	1.0128	1.0127
	$\sigma_{xx}^*(0;2.8125;0)$	-0.0236	-0.0230	-0.0226	-0.0221	-0.0220

The deformation field of the FGP annular nanoplate is indicated in Figure 3.5 a, b. The stresses of the A-point through the thickness of the FGP annular nanoplate are presented in Figure 3.5 c, d. It can be seen that with the annular shape, the displacement and deformation fields are symmetric to the center of the plate.

a) The deformation field

b) The top view deformation field

c) The stress σ_{xx}^* at the A-point

d) The stress σ_{xy}^* at the A-point
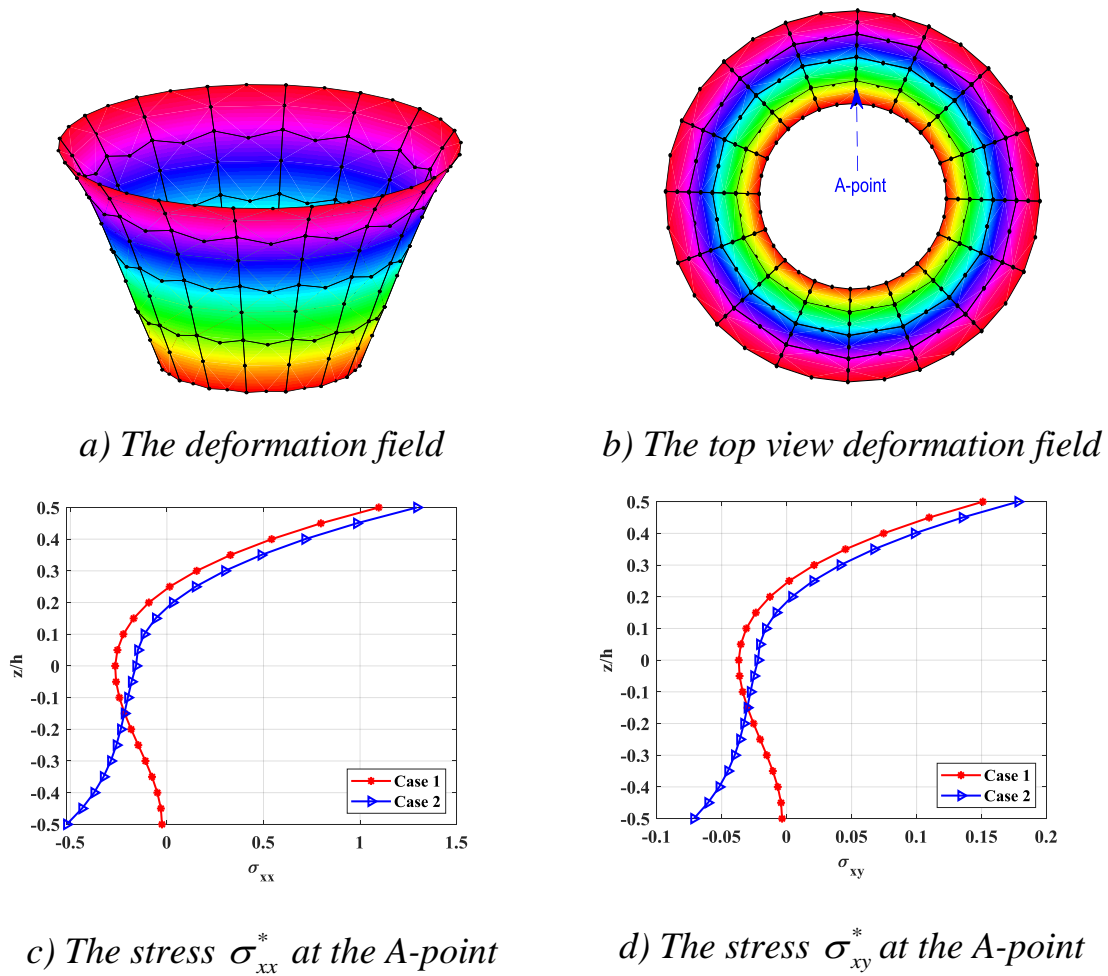
Figure 3.5. The deformation and stresses of the clamped supported at the outer border FGP annular nanoplate (Case 1: Even porosity, Case 2: Uneven porosity).

3.4.4. Half-annular nanoplate

Considering the FGP annular nanoplates as in Figure 3.1c with clamped supported at the outer border. Material properties of the individual materials as

shown in Table 3.1 and geometric dimensions $R = 5$ nm, $r_1 = 2.5$ nm, $h = 1$ nm, power-law index $k=5$, porosity factor $\xi = 0.3$, nonlocal factor $\mu = 3$, the foundation stiffness: $K_1 = 75$, $K_2 = 25$. The deformation and stress of the L-shape nanoplate with various mesh sizes are displayed in Table 3.6. It can be seen that the results converge at a mesh size of 32 elements.

Table 3.6. The deformation and stress of the half-annular nanoplate with various mesh sizes.

	Mesh size	4	8	24	32	64
Even porosity	Max $\left(w^* \right)$	1.0325	1.0318	1.0312	1.0306	1.0305
	$\sigma_{xx}^*(2.8125;0;0)$	0.3210	0.3200	0.3194	0.3189	0.3188
Uneven porosity	Max $\left(w^* \right)$	0.2983	0.2988	0.2982	0.2977	0.2976
	$\sigma_{xx}^*(2.8125;0;0)$	-0.4674	-0.4668	-0.4662	-0.4656	-0.4655

The FGP plate is subjected to uniformly load q_0 in perpendicular directions. The deformation field of the FGP annular nanoplate is indicated in Figure 3.6a, b. The stresses at the A-point through the thickness of the FGP annular nanoplate are presented in Figure 3.6 c, d. It can be seen that the displacement and deformation fields of the plate are symmetric to the x-axis.

a) The deformation field

b) The top view deformation field

c) The stress σ_{xx}^* at the A-point

d) The stress σ_{xy}^* at the A-point
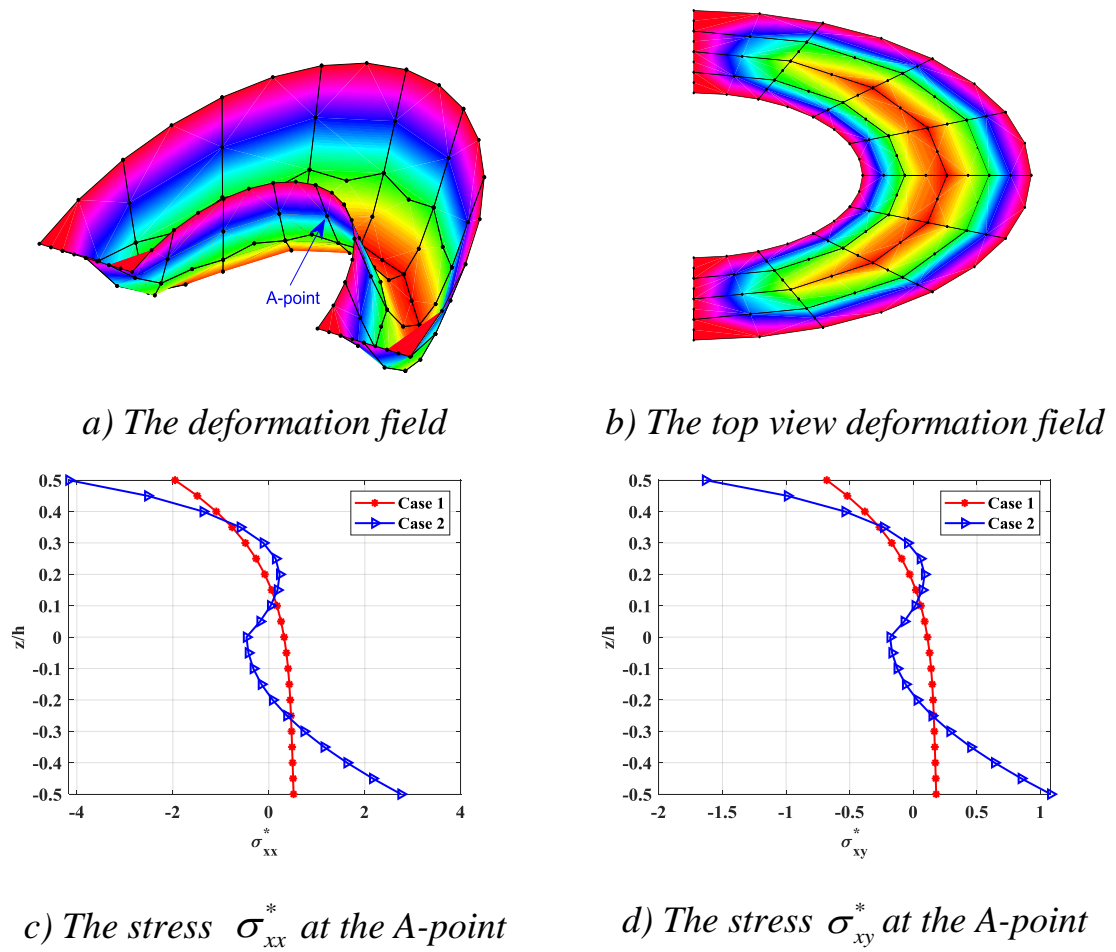
Figure 3.6. The deformation and stresses of the clamped supported at outer border FGP half-annular nanoplate (Case 1: Even porosity, Case 2: Uneven porosity).

3.5. The influence of some factors on the static response of FGP nanoplates

The main objective of this section is to investigate the influence of geometrical parameters, material properties, and boundary conditions on the static behavior of FGP nanoplates. The mechanical properties of the component materials are shown in Table 3.1.

3.5.1. Influence of the nonlocal factor

To investigate the effect of the nonlocal factor on the static bending of nanoplate, in this survey, authors choose the nonlocal factor in range $\mu = 0 \div 4$

with $\mu = 0$ is the classical plate. Porosity volume fraction $\xi = 0.1$, power-law index $k=1$. The foundation stiffness: $K_1 = 100$, $K_2 = 10$. It can be found that nonlocal factor increases make the displacement increase due to the increase of nonlocal factor leading to reduce the FGP nanoplate stiffness.

Table 3.7. Displacement and stress of FGP nanoplates versus the nonlocal factor.

		μ	0	1	2	3	4
Square nanoplate	w^*	Case 1	7.964	9.147	10.2936	11.4065	12.488
		Case 2	7.3465	8.464	9.5466	10.5978	11.6201
	σ^*_{xx}	Case 1	25.1153	28.7036	32.1849	35.5692	38.8635
		Case 2	24.9304	28.5908	32.1379	35.585	38.9413
L-shape nanoplate	w^*	Case 1	1.7263	2.0036	2.2776	2.551	2.8203
		Case 2	1.5809	1.8395	2.0931	2.347	2.5976
	σ^*_{xx}	Case 1	8.7668	10.2498	11.7086	13.1449	14.5598
		Case 2	8.6256	10.1046	11.5593	12.9919	14.4038
Annular nanoplate	w^*	Case 1	0.8996	1.0571	1.2138	1.369	1.5225
		Case 2	0.8199	0.9653	1.1098	1.2531	1.3948
	σ^*_{xx}	Case 1	5.2235	6.108	6.9973	7.8844	8.7663
		Case 2	5.0972	5.9732	6.8516	7.7272	8.5977
Half-annular nanoplate	w^*	Case 1	0.0717	0.0855	0.0996	0.1137	0.1277
		Case 2	0.0667	0.0795	0.0928	0.1059	0.119
	σ^*_{xx}	Case 1	0.3825	0.4505	0.5196	0.589	0.6585
		Case 2	0.4995	0.5891	0.6799	0.771	0.8622
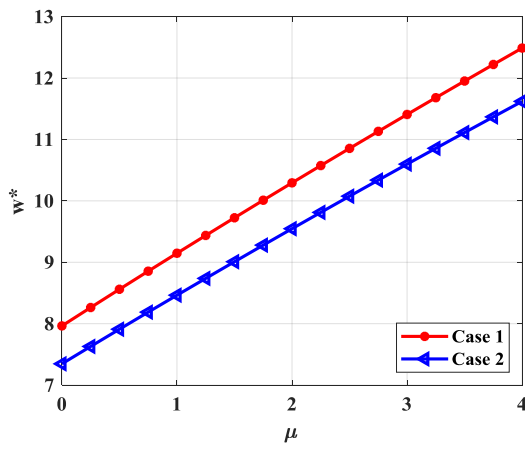
a) The maximum displacement of completely simply supported square nanoplate
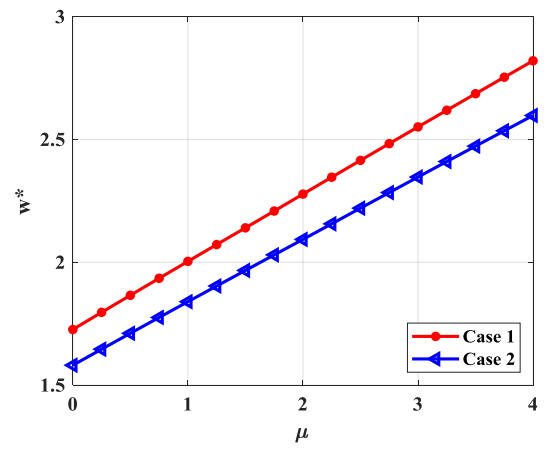
b) The maximum displacement of completely simply supported L-shape nanoplate
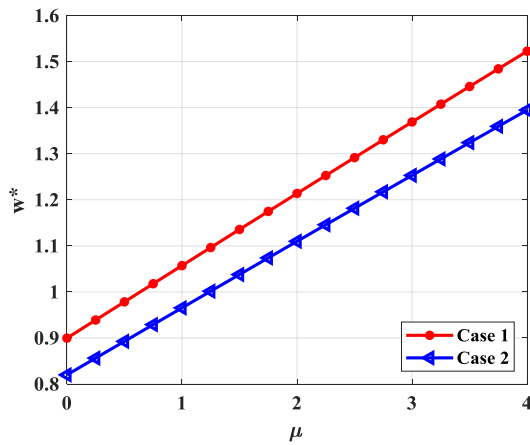
c) The maximum displacement of clamped supported at outer border annular nanoplate

d) The maximum displacement of clamped supported at outer border half-annular nanoplate

Figure 3.7. Effect of nonlocal factor on displacement of FGP nanoplates.
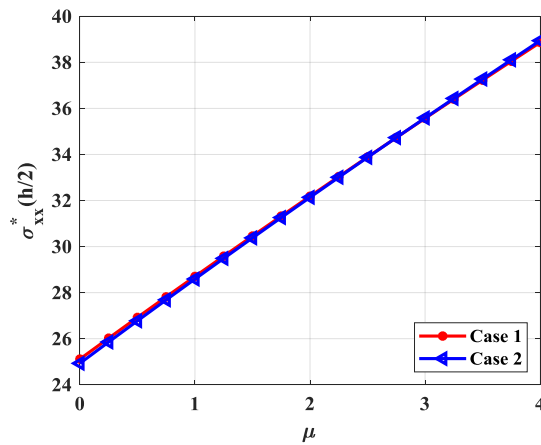
*a) Stress at middle-point of square
completely simply supported
nanoplate*
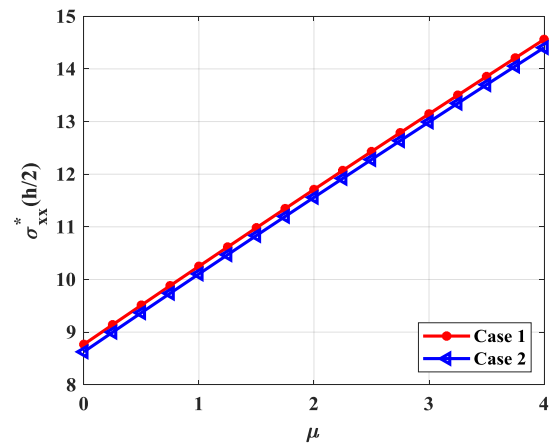
*b) Stress at A-point of L-shape
completely simply supported
nanoplate*
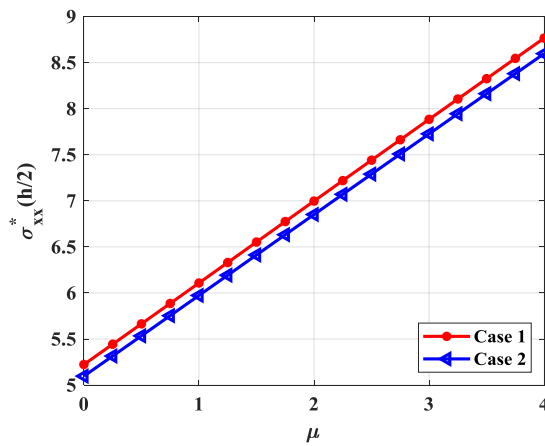
*c) Stress at A-point of annular
clamped outer border nanoplate*
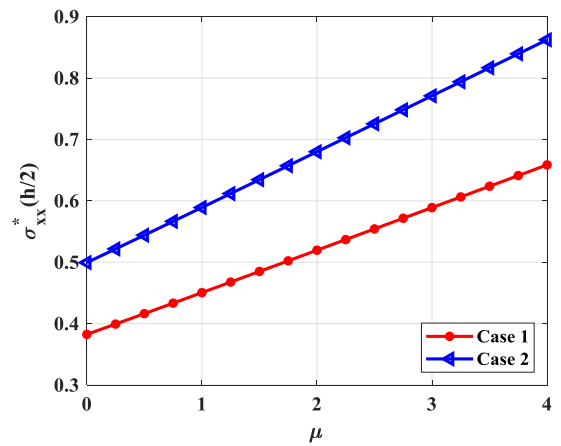
*d) Stress at A-point of half-annular
clamped outer border nanoplate*

Figure 3.8. Effect of nonlocal factor on stresses of FGP nanoplates.

3.5.2. Influence of the volume fraction index

Considering nanoplate with porosity factor $\xi = 0.1$, nonlocal factor $\mu = 2$, the foundation stiffness: $K_1 = 100$, $K_2 = 10$. The power-law index k gets a value from 0 to 100. From Figure 3.9 and Figure 3.10 it can be concluded that when k increases lead to displacement increase due to the nanoplate stiffness decrease. The displacement of the nanoplate decreases rapidly when k

increases from 0 to 10. We also find that the FGP annular nanoplates with porosity distribution case 2 are harder than case 1. Note that, k is larger the nanoplate becomes metal-rich and thus the nanoplate stiffness decreases.

Table 3.8. Displacement and stress of FGP nanoplates according to the power-law index.

		k	0	1	2	5	10
Square nanoplate	w^*	Case 1	5.6955	10.2936	12.7027	14.6521	15.5987
		Case 2	5.4854	9.5466	11.4985	13.0441	13.8905
	σ_{xx}^*	Case 1	23.3473	32.1849	35.4019	38.9136	45.2147
		Case 2	23.8698	32.1379	34.9899	38.5843	44.7592
L-shape nanoplate	w^*	Case 1	1.1807	2.2776	2.9696	3.6934	4.1212
		Case 2	1.1352	2.0931	2.6419	3.1997	3.5522
	σ_{xx}^*	Case 1	7.879	11.7086	13.5162	15.6399	18.6602
		Case 2	8.0319	11.5593	13.0982	15.0667	17.8879
Annular nanoplate	w^*	Case 1	0.6113	1.2138	1.5995	1.9967	2.2332
		Case 2	0.5869	1.1098	1.412	1.7143	1.9072
	σ_{xx}^*	Case 1	4.5272	6.9973	8.2189	9.5334	11.3514
		Case 2	4.6058	6.8516	7.8547	9.0219	10.6917
Half-annular nanoplate	w^*	Case 1	0.053	0.0996	0.1341	0.1898	0.2349
		Case 2	0.0512	0.0928	0.1215	0.1666	0.2021
	σ_{xx}^*	Case 1	1.4395	2.3207	2.7894	3.2739	3.9042
		Case 2	1.4618	2.2538	2.6269	3.0351	3.600
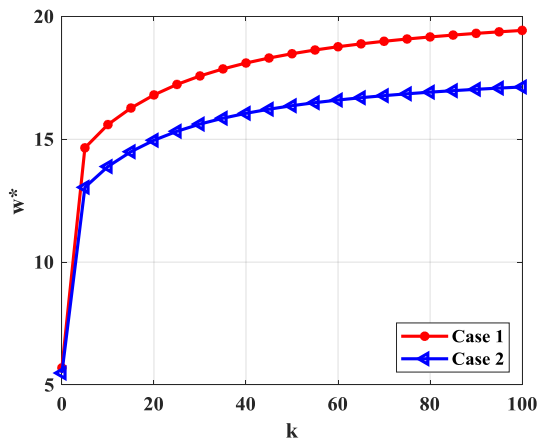
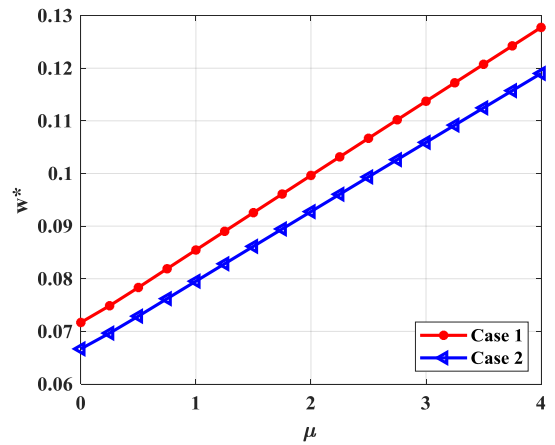*a) The maximum displacement of completely simply supported square nanoplate*
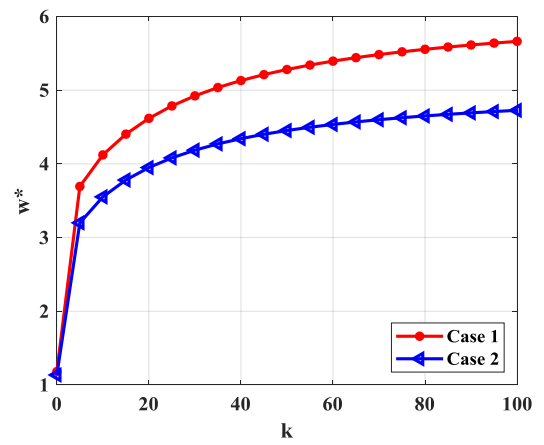
b) The maximum displacement of completely simply supported L-shape nanoplate
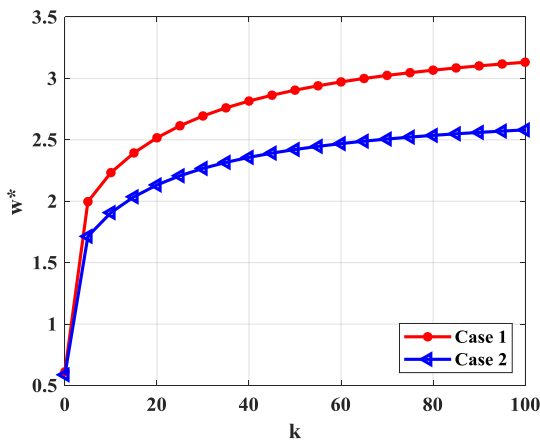
*c) The maximum displacement of clamped supported at outer border annular nanoplate*
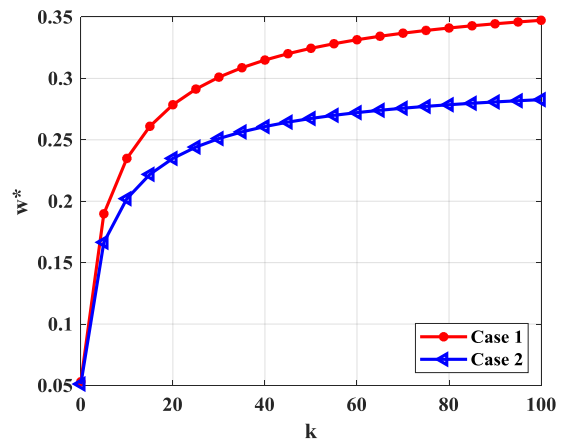
d) The maximum displacement of clamped supported at outer border half-annular nanoplate

Figure 3.9. Effect of power-law index on stresses of FGP nanoplates.
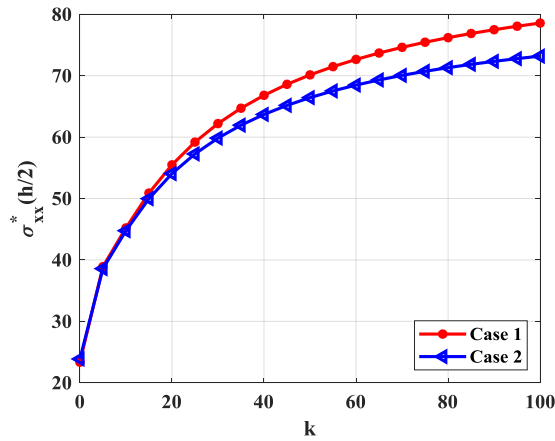
a) Stress at the middle-point of completely simply supported square nanoplate

b) Stress at the A-point of completely simply supported L-shape nanoplate
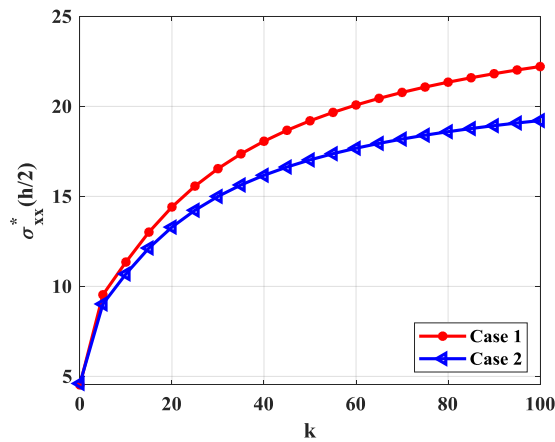
c) Stress at the A-point of clamped supported at outer border annular nanoplate
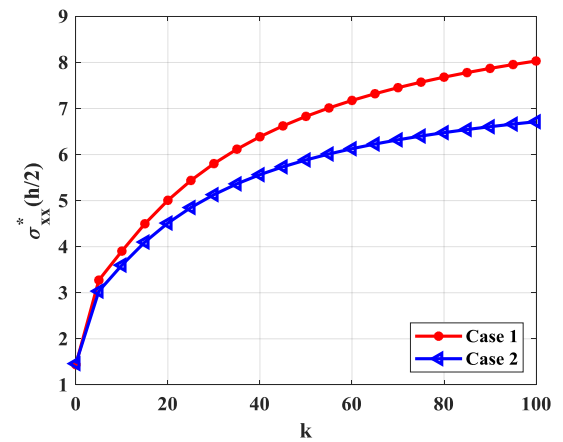
d) Stress at the A-point of clamped supported at outer border half-annular nanoplate

Figure 3.10. Effect of power-law index on stresses of FGP nanoplates.

3.5.3. Influence of the porosity factor

To investigate the effect of the porosity factor, in this section, nanoplate with power-law index $k=1$, nonlocal factor $\mu = 2$. The foundation stiffness: $K_1=100$, $K_2=10$ is considered. The porosity factor ξ gets a value from 0 to 0.4.

From Figure 3.11 and Figure 3.12 it can be concluded that when the porosity factor increases lead to displacement increase due to the nanoplate stiffness decrease.

Table 3.9. Displacement and stress of FGP nanoplates versus the porosity factor

		ξ	0	0.1	0.2	0.3	0.4
Square nanoplate	w^*	Case 1	9.2687	10.2936	11.6287	13.4685	16.2327
		Case 2	9.2687	9.5466	9.8499	10.1834	10.5536
	σ_{xx}^*	Case 1	31.6889	32.1849	32.8621	33.8554	35.4906
		Case 2	31.6889	32.1379	32.586	33.0294	33.4624
L-shape nanoplate	w^*	Case 1	2.016	2.2776	2.6322	3.1478	3.9925
		Case 2	2.016	2.0931	2.1781	2.2726	2.3789
	σ_{xx}^*	Case 1	11.3265	11.7086	12.2346	13.0183	14.3474
		Case 2	11.3265	11.5593	11.8001	12.049	12.3057
Annular nanoplate	w^*	Case 1	1.0682	1.2138	1.4136	1.7103	2.2131
		Case 2	1.0682	1.1098	1.156	1.2075	1.2656
	σ_{xx}^*	Case 1	6.7078	6.9973	7.4066	8.0393	9.1761
		Case 2	6.7078	6.8516	7.0019	7.1591	7.3237
Half-annular nanoplate	w^*	Case 1	0.0885	0.0996	0.1144	0.1352	0.1685
		Case 2	0.0885	0.0928	0.0975	0.1028	0.1088
	σ_{xx}^*	Case 1	0.1482	0.1583	0.1727	0.1959	0.2428
		Case 2	0.1482	0.1542	0.1606	0.1675	0.1749
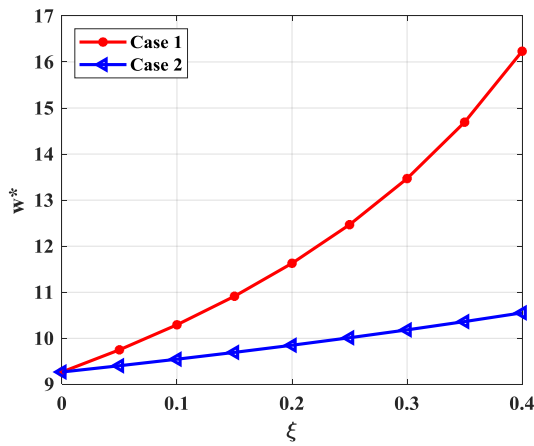
a) The maximum displacement of completely simply supported square nanoplate
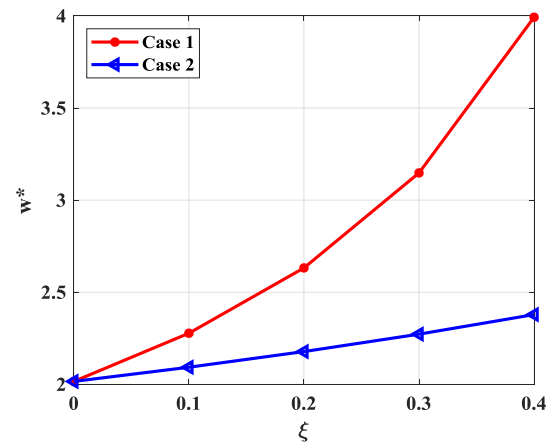
b) The maximum displacement of completely simply supported L-shape nanoplate
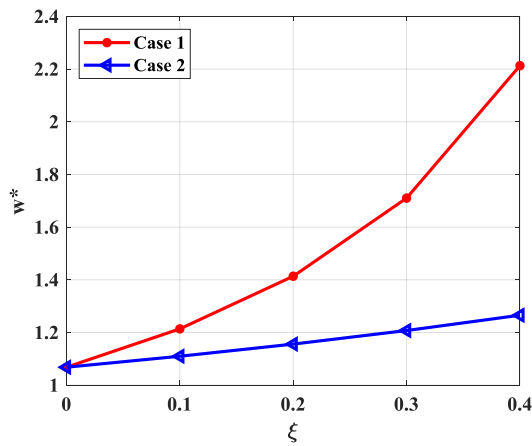
c) The maximum displacement of clamped supported at outer border annular nanoplate
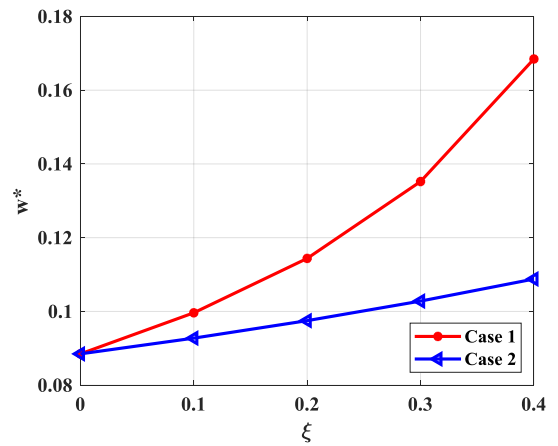
d) The maximum displacement of clamped supported at outer border half-annular nanoplate

Figure 3.11. Effect of porosity factor on the displacement of FGP nanoplates.
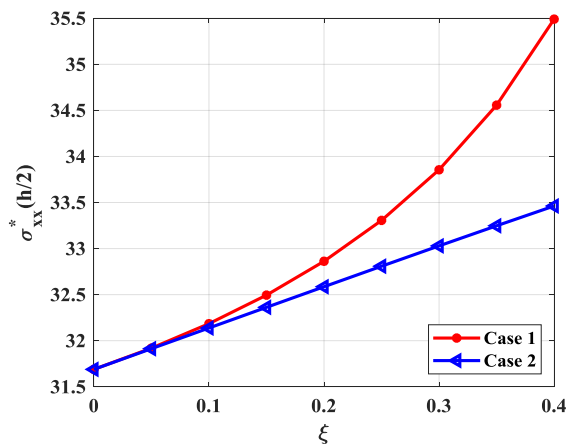
a) Stress at middle-point of completely simply supported square nanoplate
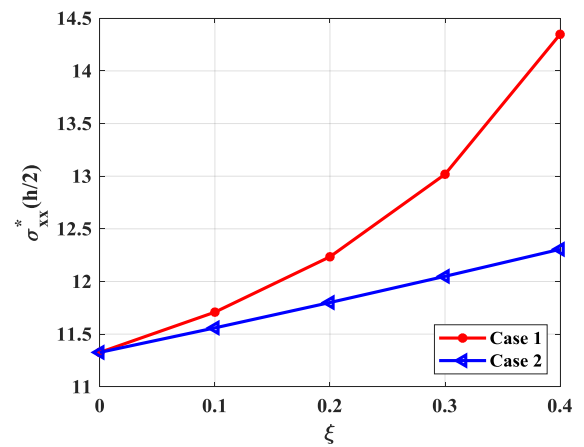
b) Stress at A-point of completely simply supported L-shape nanoplate
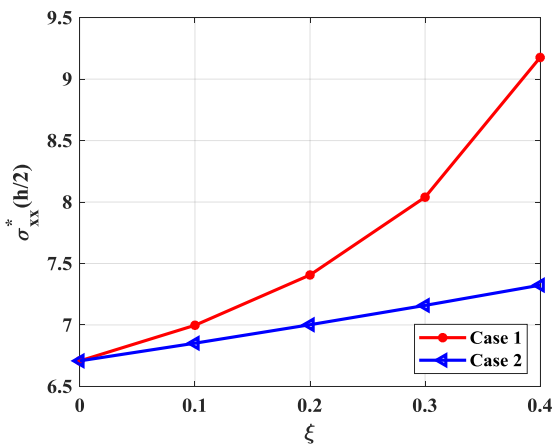
c) Stress at A-point of clamped supported at outer border annular nanoplate
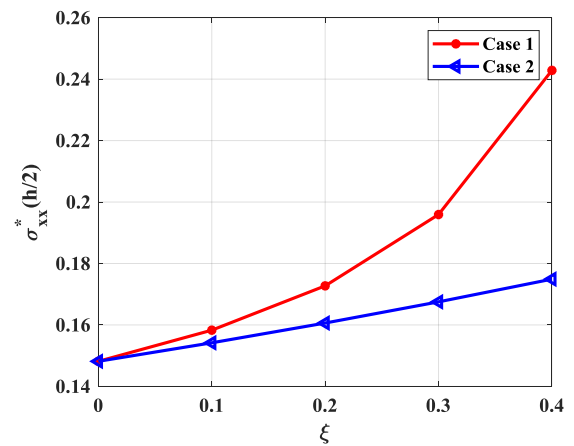
d) Stress at A-point of clamped supported at outer border half-annular nanoplate

Figure 3.12. Effect of porosity factor on stresses of FGP nanoplates.

3.5.4. Influence of the plate thickness

To investigate the effect of plate thickness, in this example, nanoplate with power-law index $k=1$, porosity factor $\xi = 0.1$, nonlocal factor $\mu = 2$. The stiffness foundation: $K_1=100$, $K_2=10$ is considered. The plate thickness a/h gets a value from 10 to 80 (a is const). From Figure 3.11 and Figure 3.12, it can be

concluded that plate thickness increases lead to displacement decrease because the thicker plate has a greater stiffness. This is consistent with mechanical law. In this study, *a/h*=10 corresponds to the thick plate, and *a/h*=80 corresponds to the thin plates.

Table 3.10. Displacement and stress of FGP nanoplates versus the porosity factor

|		*a/h*	10	20	40	60	80
Square nanoplate	w^*	Case 1	0.0103	0.0796	0.6305	2.1228	5.0261
		Case 2	0.0095	0.0738	0.5842	1.9668	4.6569
	σ_{xx}^*	Case 1	3.2185	12.8818	51.3564	115.2453	204.4133
		Case 2	3.2138	12.8725	51.3349	115.2084	204.3636
L-shape nanoplate	w^*	Case 1	0.0023	0.0145	0.0957	0.2945	0.6621
		Case 2	0.0021	0.0133	0.0876	0.2691	0.6044
	σ_{xx}^*	Case 1	1.1709	4.0637	13.3425	26.9615	44.7016
		Case 2	1.1559	4.0228	13.2182	26.6863	44.229
Annular nanoplate	w^*	Case 1	0.0012	0.0085	0.0645	0.2129	0.4937
		Case 2	0.0011	0.0077	0.0587	0.1937	0.4495
	σ_{xx}^*	Case 1	0.6997	2.7536	10.5875	22.8657	39.0835
		Case 2	0.6852	2.701	10.4087	22.5108	38.517
Half-annular nanoplate	w^*	Case 1	0.0001	0.0004	0.0023	0.0068	0.0149
		Case 2	0.0001	0.0004	0.0021	0.0062	0.0135
	σ_{xx}^*	Case 1	0.052	0.2061	0.7252	1.3987	2.1675
		Case 2	0.068	0.2708	0.9594	1.8588	2.8866
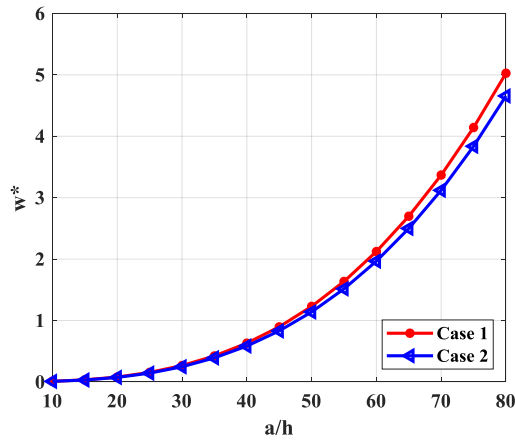
a) The maximum displacement of completely simply supported square nanoplate
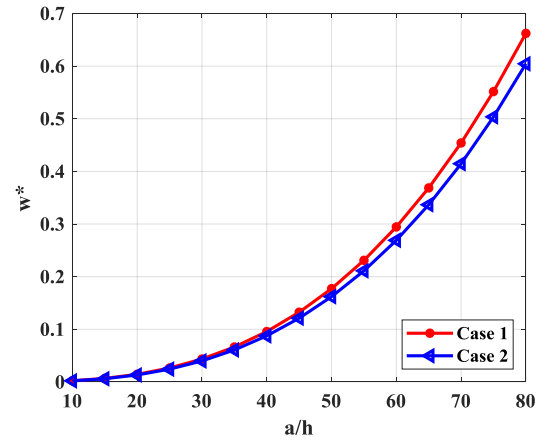
*b) The maximum displacement of completely simply supported L-shape nanoplate*
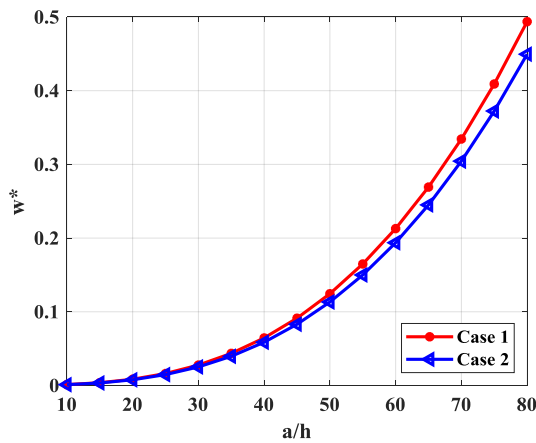
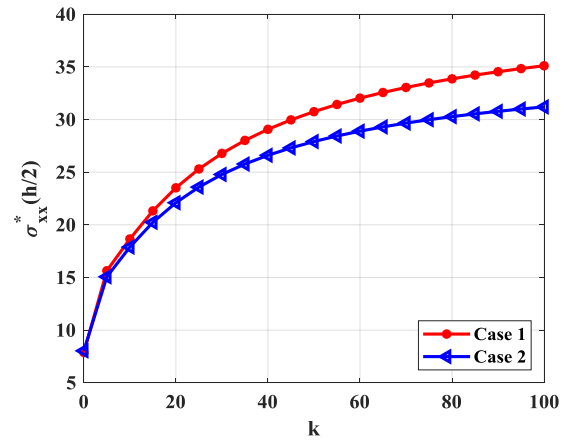*c) The maximum displacement of clamped supported at the outer border annular nanoplate*
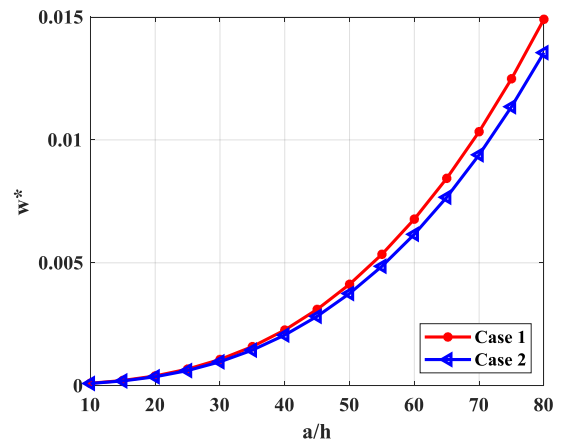
*d) The maximum displacement of clamped supported at the outer border half-annular nanoplate*

Figure 3.13. Effect of plate thickness on the displacement of FGP nanoplates.
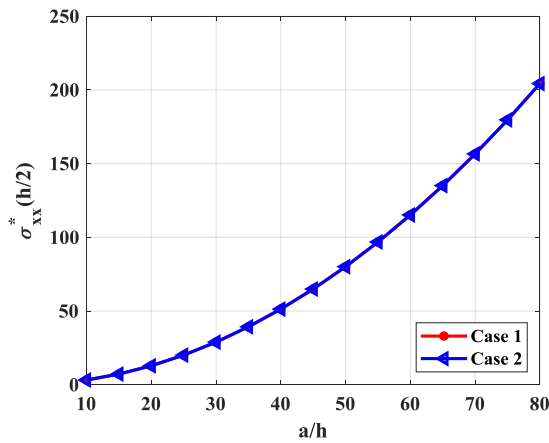
a) Stress at the middle-point of completely simply supported square nanoplate
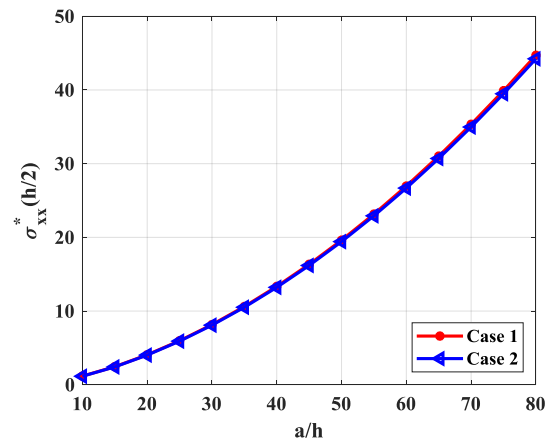
b) Stress at the A-point of completely simply supported L-shape nanoplate
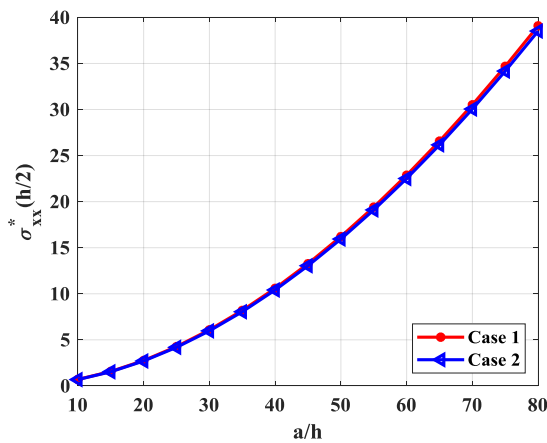
c) Stress at the A-point of clamped supported at the outer border annular nanoplate
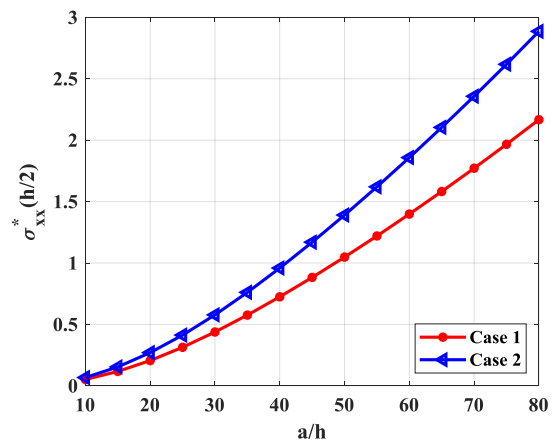
d) Stress at the A-point of clamped supported at the outer border half-annular nanoplate

Figure 3.14. Effect of plate thickness on stresses of FGP nanoplates.

3.5.5. Influence of the parameters of the elastic foundation

Finally, consider the influences of the stiffness of the foundation on the static bending of the FGP nanoplate. The author changed K_1 from 0 to 100 and K_2 from 0 to 10 with plate thickness $h=a/10$, power-law index $k = 1$, porosity factor $\xi = 0.1$, and nonlocal factor $\mu = 2$. From the numerical results shown in

Figure 3.15, it can be concluded that when increasing K_1 and K_2 leads to the displacement of nanoplates decrease. This is perfectly reasonable because when the foundation stiffness increases, the stiffness of the plate increase. Furthermore, the Pasternak foundation supports more strongly than the Winkler foundation. In other words, the shear layer of the foundation provides better support than the spring layer.
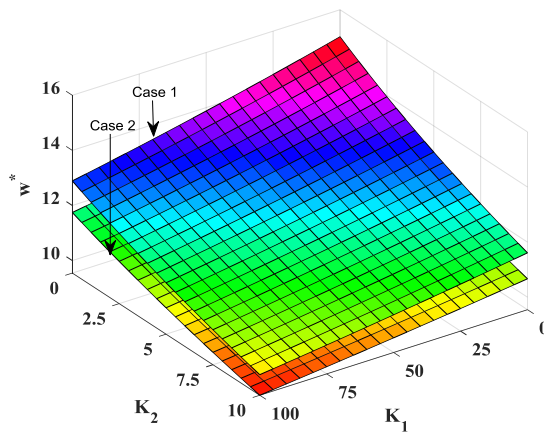
a) Completely simply supported square nanoplate
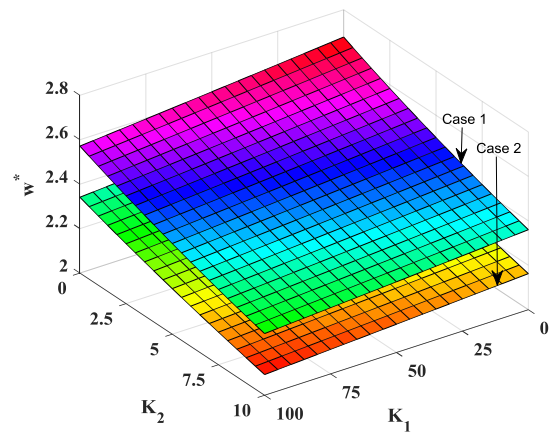
b) Completely simply supported L-shape nanoplate
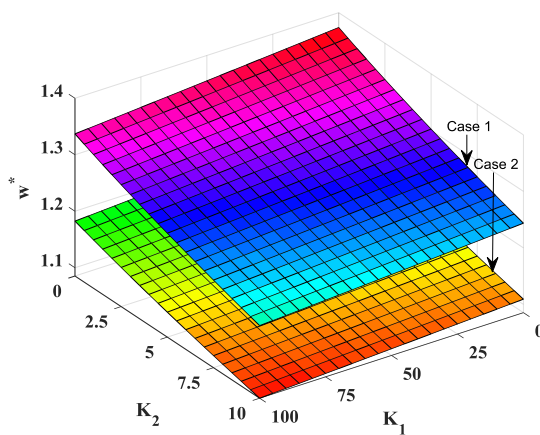
c) Clamped supported at outer border annular nanoplate
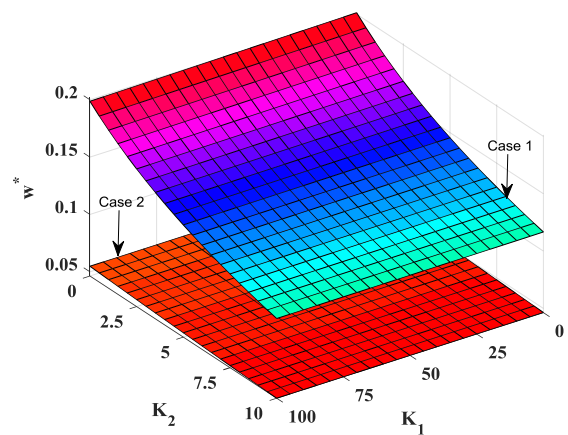
d) Clamped supported at outer border half-annular nanoplate

Figure 3.15. Effect of K_1 and K_2 on the displacement of FGP nanoplates.

3.6. Summary of Chapter 3

In this chapter, the author presents the algorithm to analyze the FGP nanoplates with different shapes resting on an elastic foundation subjected to static loads. From the proposed formulation and the numerical results, the author can withdraw some following points:

The author has built an algorithm and a calculation program FGP_Nanoplates_FSDT_Nonlocal_Static_2022 (FNFNS_2022) to calculate the FGP nanoplates resting on an elastic foundation under static load. The calculation results of the program are compared with other published results showing accuracy and reliability.

The survey results show that there are many factors affecting the static response of FGP nanoplates resting on the elastic foundation. However, there are significant influencing factors, such as the nonlocal factor, the parameters of FGP, and the foundation stiffness. Therefore, when designing nanoplates for special requirements, engineers must attention to the above issues for the structure to operate at high efficiency.

The obtained results in this chapter have been shown in paper number 2 and number 4 (List of publications).

Chapter 4 DYNAMIC ANALYSIS OF FGM POROUS NANOPLATES RESTING ON ELASTIC FOUNDATION

In this chapter, the author established the equations, an algorithm, and a calculation program algorithms to calculate the free vibration and forced vibration of the FGP nanoplates. Simultaneously, the influence of some parameters on plate vibrations, such as nonlocal factor, material characteristics, elastic foundation, and boundary conditions, are investigated.

4.1. Free vibration

4.1.1. Finite element algorithm and calculation programs

From the equation of motion (2.95), in case of the external load is zero, the free vibration equation of the plate is as follows:

$$\mathbf{M\ddot{q}} + \mathbf{Kq} = \mathbf{0} \tag{4.1}$$

Assuming that the oscillations are harmonic with amplitude $\mathbf{q}_0$ and frequency ω, then the solution of the equation (4.1) has form $\mathbf{q} = \mathbf{q}_0 \sin(\omega t)$. From there, the free vibration equation (4.1) leads to:

$$\left(\mathbf{K} - \mathbf{M}\omega^2\right)\mathbf{q}_0 = \mathbf{0} \tag{4.2}$$

The equations (4.2) are homogeneous linear equations. It has a non-trivial solution $\mathbf{q}_0 \neq \mathbf{0}$ if and only if:

$$\left\|\left(\mathbf{K} - \mathbf{M}\omega^2\right)\right\| = 0 \tag{4.3}$$

The equation (4.3) is a polynomial equation of order N. Solving this equation give N values of natural frequencies ω_i. Substituting natural frequencies ω_i into the equation (4.2) we find the corresponding eigenvector.

The algorithm diagram to solve the free vibration problem of FGP nanoplates is shown in Figure 4.1.

Based on the calculation algorithm, the program FGP_Nanoplates_FSDT_Nonlocal_Freevibration_2022 (FNFNF_2022) is developed in Matlab software to analyze the free vibrations of FGP nanoplates resting on an elastic foundation. The program consists of the following main modules:

- The module for input data and meshing elements.

- The module solves the free vibration for FGP nanoplate resting on an elastic foundation.

- The module outputs the results.

The program FGP_Nanoplates_FSDT_Nonlocal_Freevibration_2022 can analyze the free vibration of FGP nanoplates resting on an elastic foundation. In addition, it is also able to investigate the influence of factors such as boundary conditions, material properties, and elastic foundation characteristics on the free vibration of nanoplates.
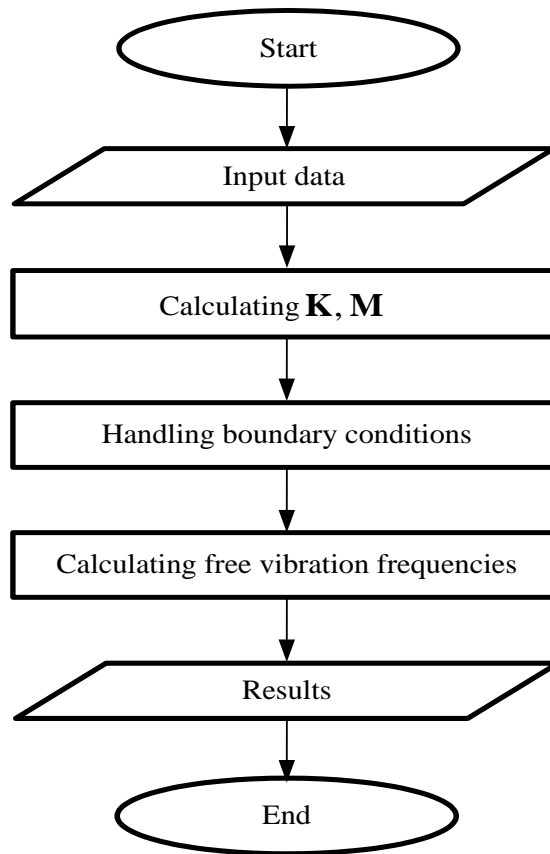
Figure 4.1. Algorithm diagram to solve the free vibration problem of FGP nanoplates.

4.1.2. Convergence and verification study

To verify the accuracy and convergence of the present work, the numerical results of the free vibration of the nanoplate are compared with the other published results.

Example 1: Considering a completely simply supported FGM square nanoplate without a nonlocal factor $(\mu = 0)$. The material properties are presented in Table 4.1.

Table 4.1. Material properties

Materials	E (GPa)	ν	ρ (kg/m^3)
Al$_2$O$_3$ (ceramic)	380	0.3	3800
Al (metal)	70	0.3	2707

For comparison convenience, the author uses the dimensionless frequencies of FGP nanoplates as follows [74]:

$$\Omega = 10\omega h\sqrt{\frac{\rho_m}{E_m}}; K_1 = \frac{k_w a^2}{D_m}; K_2 = \frac{k_s a^4}{D_m}; D_m = \frac{E_m h^3}{12(1-v^2)} \qquad (4.4)$$

The numerical results with various mesh sizes compared with the AM in [74] are listed in Table 4.2 and presented in Figure 4.2. It can be seen that using the Q8 element converges faster and more accurately than using the mixed interpolation of tensorial components (MITC) for the four-node quadrilateral element (MITC4) and the 4-node quadrilateral (Q4) element. Specifically, using the Q8 element with mesh 4×4 is exactly as MITC4 element with mesh 12×12 and more exactly the Q4 element with mesh 12×12. For the free vibration problem, with mesh 8×8, numerical results are obtained as accurately as those in the published work of Thai et al. [74]. Therefore, the thesis uses mesh 8×8 to investigate the free vibration of FGP nanoplates.

Table 4.2. The convergence of the natural frequency Ω_1 of the completely simply supported FGM nanoplate ($a/h = 10$).

k	Mesh	4×4	6×6	8×8	10×10	12×12	[74]
	Q4	0.0727	0.0617	0.0603	0.0591	0.0588	
0	MITC4	0.0617	0.0587	0.0584	0.0580	0.0580	0.0577
	Q8	0.0580	0.0578	0.0578	0.0578	0.0577	
	Q4	0.0572	0.0477	0.0465	0.0454	0.0451	
1	MITC4	0.0473	0.0449	0.0447	0.0444	0.0444	0.0442
	Q8	0.0444	0.0443	0.0442	0.0442	0.0442	

	Q4	0.0484	0.0409	0.040	0.0391	0.0389	
4	MITC4	0.0409	0.0389	0.0387	0.0384	0.0384	0.0381
	Q8	0.0384	0.0383	0.0383	0.0383	0.0383	
	Q4	0.0451	0.0388	0.0380	0.0373	0.0372	
10	MITC4	0.0391	0.0372	0.0370	0.0368	0.0368	0.0364
	Q8	0.0367	0.0366	0.0366	0.0366	0.0366	
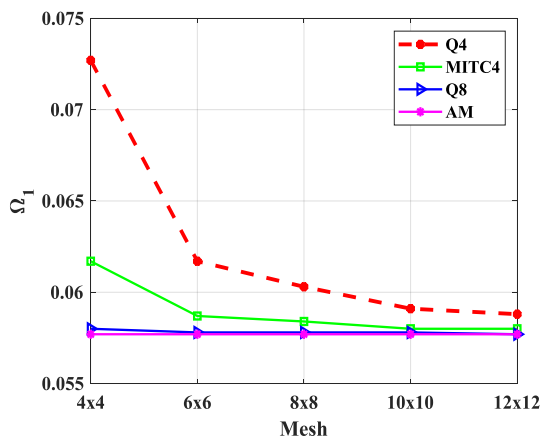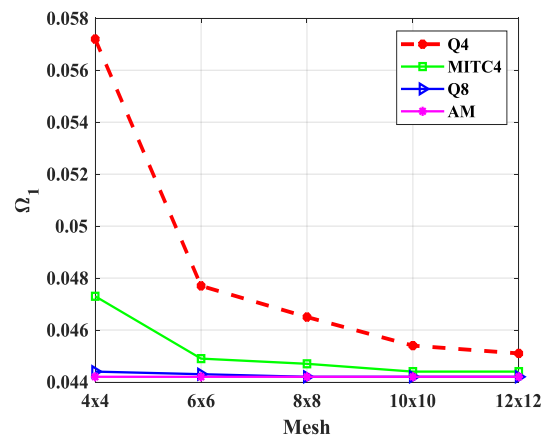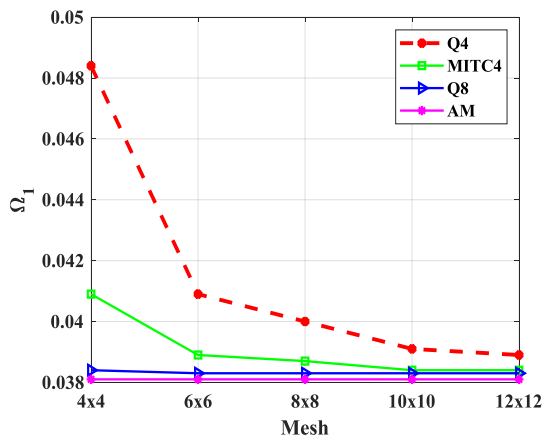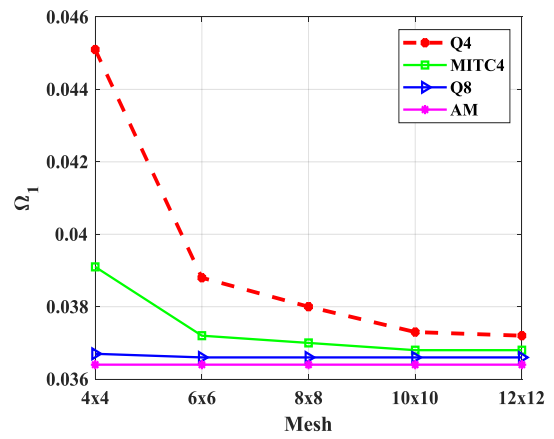
a) k = 0 *b) k = 1* *c) k = 4* *d) k = 10*

Figure 4.2. The convergence of element mesh to the dimensionless frequency of the FGM nanoplate.

Example 2: The completely clamped supported L-shape isotropic plate with $h = a / 10$ (a is fixed), $v = 0.3$ is considered. The first four dimensionless natural frequencies $\bar{\omega} = \omega a \sqrt{\dfrac{2(1+v)\rho}{E}}$ of the plate are listed in Table 4.2. It can be concluded that the results of the proposed method are in good agreement with those of Roque et al. [75] using the finite-difference technique (FDT) and results of Thai et al. [76] using IGA based on the HSDT. The error between the results of our work and those of references is less than 3%, which is perfectly acceptable.

Table 4.3. Dimensionless natural frequencies $\bar{\omega}$ of the completely clamped isotropic L-shape plates.

Method	Parameters	$\bar{\omega}_1$	$\bar{\omega}_2$	$\bar{\omega}_3$	$\bar{\omega}_4$
FDT [75]	$\bar{\omega}$	1.8832	2.3450	2.7698	3.5714
	Er (%)	*1.64*	*0.37*	*2.82*	*1.19*
IGA [76]	$\bar{\omega}$	1.8395	2.3735	2.7507	3.6030
	Er (%)	*0.70*	*0.83*	*2.14*	*2.06*
Thesis	$\bar{\omega}$	1.8524	2.3537	2.6918	3.5288

Example 3: The completely simply supported homogeneous square nanoplate with geometrical parameters $a = b = 10$ *nm*, $h = a/10$ and material properties: $E = 30MPa$, $v = 0.3$ is studied. The dimensionless natural frequencies $\omega^* = \omega h \sqrt{\rho / G}$ are listed in Table 4.4. It can be seen that the obtained results in the thesis are closed to those of Belkorissat et al. [77] based on hyperbolic refined plate theory (the maximum error is 1.18 %) and results of Aghababaei et al. [78] using Navier solution based on the first-order shear deformation theory and the third-order shear deformation theory (the maximum error is less than 1%). Numerical results also indicate that the obtained frequencies based on the classical plate theory are significantly greater than the

obtained results using other theories, the maximum error is 3 % in the case of moderately thick plates. Overall, the results of the thesis method are more reliable than those of the classical plate theory.

Table 4.4. The first dimensionless natural frequency ω^* of homogeneous square nanoplates.

a/h	μ	HSDT [77]		CPT [78]		FSDT [78]		TSDT [78]		Thesis
		ω_1^*	Er	ω_1^*	Er	ω_1^*	Er	ω_1^*	Er	
10	0	0.0930	0.32	0.0936	0.32	0.0930	0.32	0.0935	0.21	0.0933
	1	0.0850	0.35	0.0880	3.07	0.0850	0.35	0.0854	0.12	0.0853
	2	0.0787	0.51	0.0816	3.06	0.0788	0.38	0.0791	0.00	0.0791
	3	0.0737	0.14	0.0763	3.28	0.0737	0.14	0.0741	0.40	0.0738
	4	0.0695	0.29	0.0720	3.19	0.0696	0.14	0.0699	0.29	0.0697
	5	0.0659	0.30	0.0683	3.22	0.0660	0.15	0.0663	0.30	0.0661
20	0	0.0238	0.00	0.0239	0.42	0.0239	0.42	0.0238	0.00	0.0238
	1	0.0218	0.00	0.0220	0.91	0.0218	0.00	0.0218	0.00	0.0218
	2	0.0202	0.50	0.0204	0.49	0.0202	0.50	0.0202	0.50	0.0203
	3	0.0189	0.53	0.0191	0.52	0.0189	0.53	0.0189	0.53	0.0190
	4	0.0178	0.56	0.0180	0.56	0.0179	0.00	0.0179	0.00	0.0179
	5	0.0169	1.18	0.0171	0.00	0.0170	0.59	0.0170	0.59	0.0171

4.1.3. Numerical results and discussion

For this problem, consider the FGP nanoplate resting on the elastic foundation. Figure 4.3 and Figure 4.4 show the first four mode shapes of FGP square nanoplate, which has geometric dimensions $a = b = 10$ nm, $h = a/10$, $K_1 = 100$, $K_2 = 10$, $k = 1$, $\mu = 2$, $\xi = 0.2$. It can be observed that the second dimensionless frequency is equal to the third dimensionless frequency. This is

suitable for symmetrical nanoplates under the same supported conditions. With the L-shape nanoplate, the first four mode shapes are shown in Figure 4.5 and Figure 4.6. It can be seen that the L-shape nanoplate has higher dimensionless frequencies due to limited boundary conditions.

4.1.3.1. Square nanoplate
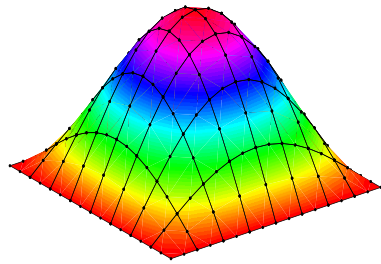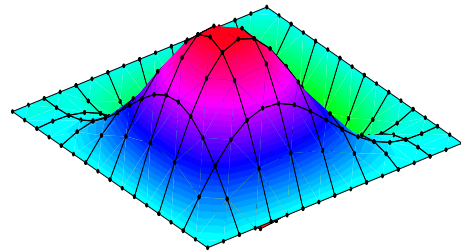
a) 1st mode, $\Omega_1 = 0.8442$ b) 2nd mode, $\Omega_2 = 1.5156$
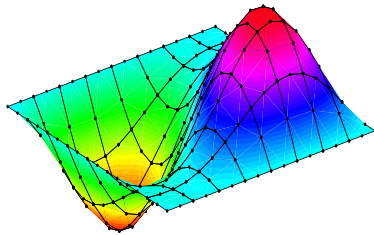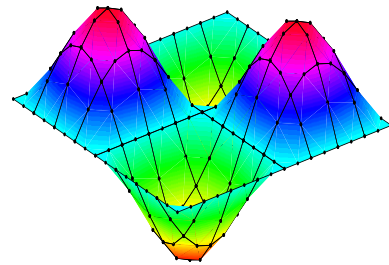
c) 3rd mode, $\Omega_3 = 1.5156$ d) 4th mode, $\Omega_4 = 1.9983$

Figure 4.3. The first four mode shapes of the completely simply supported FGP square nanoplate with even porosity.

Figure 4.7 and Figure 4.8 show the first four-mode shapes of the annular and half-annular FGP nanoplates with geometric dimensions $R = 5$ nm, $r_1 = 2.5$ nm, $h = a/10$. For asymmetric and complex structures, such as L-shape and half-annular with different boundary conditions, the numerical method proves its great efficiency compared to the analytical method.
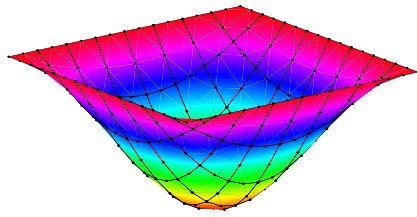
a) 1st mode, $\Omega_1 = 0.8682$
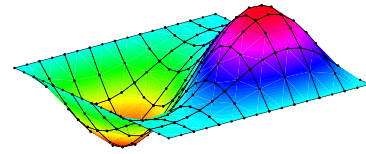
b) 2nd mode, $\Omega_2 = 1.5853$
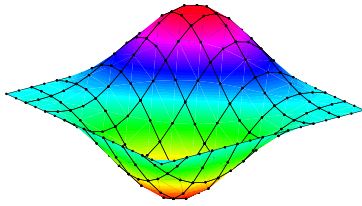
c) 3rd mode, $\Omega_3 = 1.5853$
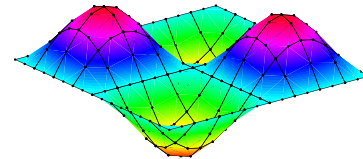
d) 4th mode, $\Omega_4 = 2.091$

Figure 4.4. The first four mode shapes of the completely simply supported FGP square nanoplate with uneven porosity.

4.1.3.2. L-shape nanoplate
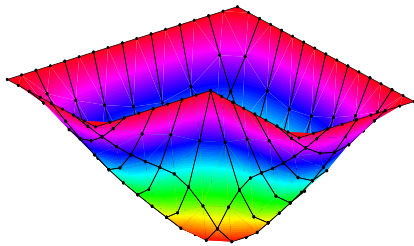
a) 1st mode, $\Omega_1 = 1.5102$
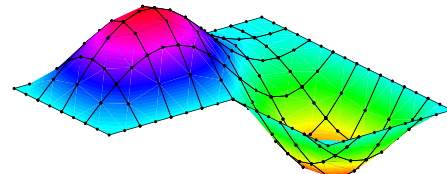
b) 2nd mode, $\Omega_2 = 1.7367$
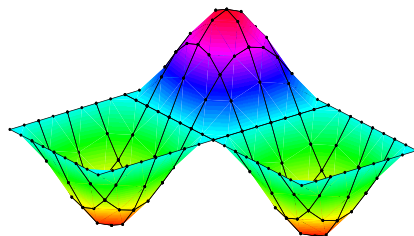
c) 3rd mode, $\Omega_3 = 1.9983$
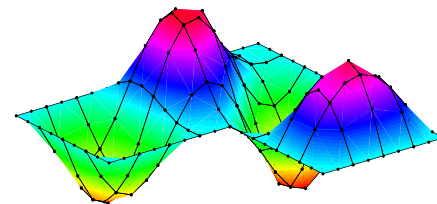
d) 4th mode, $\Omega_4 = 2.4818$

Figure 4.5. The first four mode shapes of the completely simply supported FGP L-shape nanoplate with even porosity.
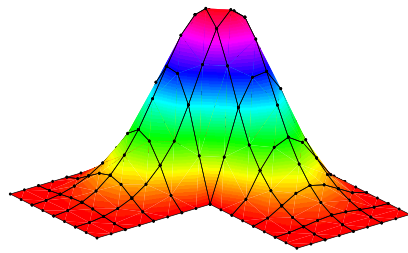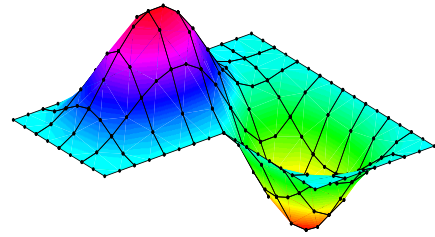
a) *1st mode,* $\Omega_1 = 2.1559$ b) *2nd mode,* $\Omega_2 = 2.4591$
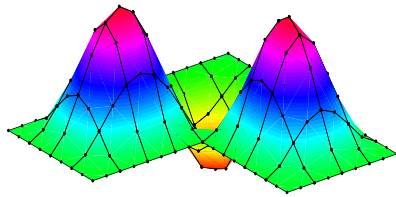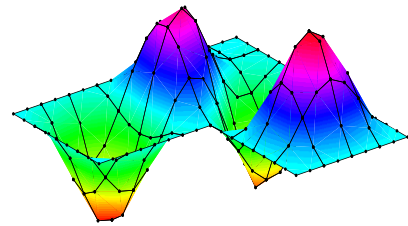
c) *3rd mode,* $\Omega_3 = 2.6306$ d) *4th mode,* $\Omega_4 = 2.9559$

Figure 4.6. The first four mode shapes of the completely clamped supported
FGP L-shape nanoplate with even porosity.

4.1.3.3. Annular nanoplate
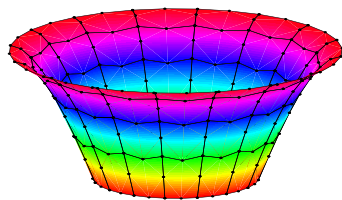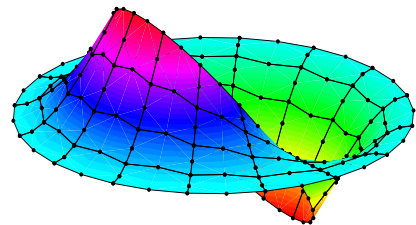
a) *1st mode,* $\Omega_1 = 1.7710$ b) *2nd mode,* $\Omega_2 = 1.9901$
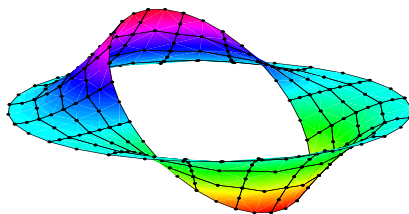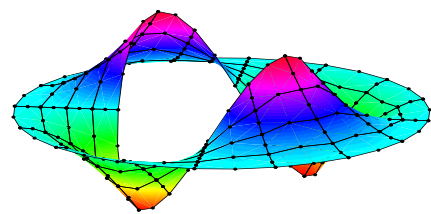
c) *3rd mode,* $\Omega_3 = 1.9901$ d) *4th mode,* $\Omega_4 = 2.4671$

Figure 4.7. The first four mode shapes of the completely clamped supported
FGP annular nanoplate with even porosity.

4.1.3.4. Half-annular nanoplate

a) 1ˢᵗ mode, $\Omega_1 = 0.6367$ *b) 2ⁿᵈ mode, $\Omega_2 = 1.0892$*

c)3ʳᵈ mode, $\Omega_3 = 1.3944$ *d) 4ᵗʰ mode, $\Omega_4 = 1.6566$*
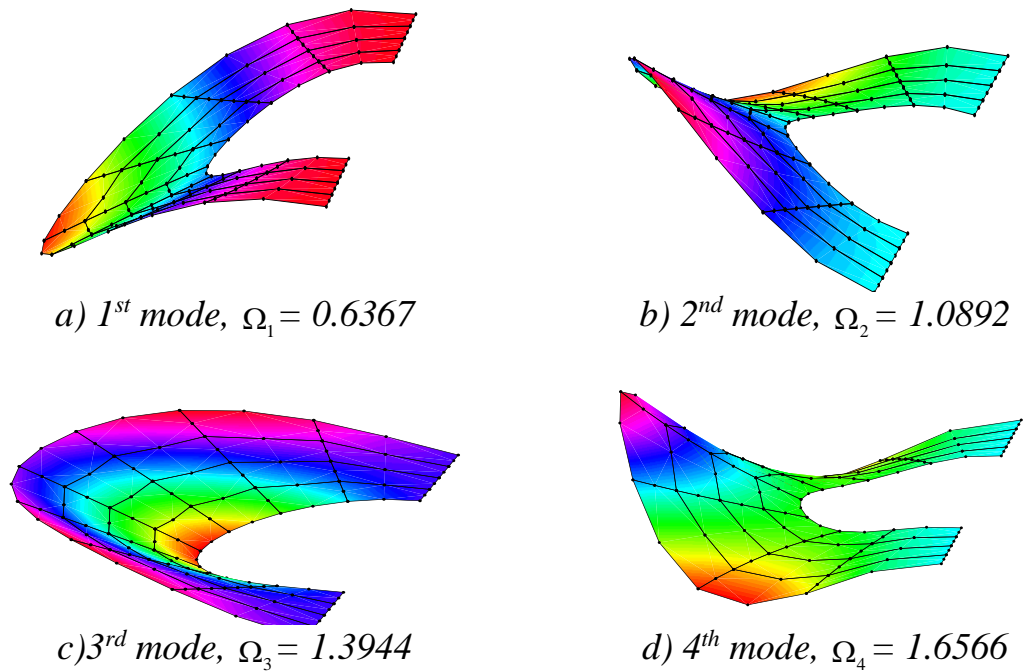
Figure 4.8. The first four mode shapes of the completely clamped supported
FGP half-annular nanoplate with even porosity.

4.1.4. Influence of some factors on the natural frequency of FGP nanoplate

4.1.4.1. Influence of the elastic foundation

Firstly, in order to consider the influences of dimensionless parameters of elastic foundation stiffness on free vibration of the FGP square nanoplate, change K_1 from 100 to 1000 and K_2 from 10 to 100 with respect to $k = 1$, $\xi = 0.2$ and nonlocal factor gets values $\mu = 0, 1, 2, 4$. The first natural frequencies of the FGP nanoplate with two cases of porosity distribution are presented in Table 4.5, Table 4.6, Table 4.7, Table 4.8 and shown in Figure 4.9. It can be found that when increasing K_1 and K_2 lead to the natural frequency of nanoplates also increase. Furthermore, the effects of the Pasternak foundation are stronger than the Winkler foundation for all cases of porosity distributions.

Specifically, with the same geometry parameters and material properties (see Table 4.5 with nonlocal factor $\mu = 1$), when $K_2 = 100$ and K_1 increases from 100 to 1000, the first non-dimensional natural frequency increases from 1.4841 to 1.7447 (17.6 %), but when $K_1 = 100$ and K_2 only increase from 10 to 100, the first non-dimensional natural frequency fast increases from 0.9026 to 1.4841 (64,4%). In addition, the frequencies of the completely clamped FGP nanoplate are greater than the completely simply supported FGP nanoplate. The results are quite reasonable because the simply supported boundary condition is more flexible than the clamped boundary condition.

Table 4.5. Natural frequencies of the completely simply supported FGP square nanoplate with even porosity versus K_1 and K_2.

Nonlocal factor (μ)	K_1 / K_2	100	250	500	750	1000
0	10	0.9783	1.0476	1.1538	1.2510	1.3412
	25	1.1109	1.1723	1.2681	1.3572	1.4408
	50	1.3022	1.3550	1.4387	1.5177	1.5929
	75	1.4687	1.5157	1.5910	1.6628	1.7317
	100	1.6182	1.6610	1.7300	1.7963	1.8602
1	10	0.9026	0.9773	1.0904	1.1928	1.2871
	25	1.0228	1.0892	1.1917	1.2861	1.3740
	50	1.1965	1.2537	1.3437	1.4281	1.5077
	75	1.3479	1.3990	1.4802	1.5572	1.6305
	100	1.4841	1.5306	1.6051	1.6764	1.7447
2	10	0.8442	0.9236	1.0425	1.1492	1.2468
	25	0.9546	1.0254	1.1337	1.2325	1.3240
	50	1.1145	1.1758	1.2713	1.3602	1.4436
	75	1.2542	1.3089	1.3954	1.4768	1.5539
	100	1.3798	1.4298	1.5093	1.5849	1.6570
4	10	0.7590	0.8464	0.9748	1.0881	1.1907
	25	0.8549	0.9333	1.0512	1.1571	1.2540
	50	0.9944	1.0626	1.1674	1.2636	1.3529
	75	1.1165	1.1777	1.2731	1.3618	1.4451
	100	1.2266	1.2825	1.3706	1.4534	1.5317

Table 4.6. Natural frequencies of the completely clamped supported FGP square nanoplate with even porosity versus K_1 and K_2.

Nonlocal factor (μ)	K_1 / K_2	100	250	500	750	1000
0	10	1.5338	1.5788	1.6512	1.7205	1.7872
	25	1.6350	1.6774	1.7457	1.8114	1.8748
	50	1.7894	1.8282	1.8911	1.9519	2.0109
	75	1.9299	1.9659	2.0245	2.0815	2.1369
	100	2.0595	2.0933	2.1484	2.2022	2.2547
1	10	1.3857	1.4352	1.5141	1.5891	1.6607
	25	1.4775	1.5241	1.5986	1.6698	1.7381
	50	1.6179	1.6605	1.7291	1.7952	1.8589
	75	1.7457	1.7853	1.8494	1.9113	1.9712
	100	1.8639	1.9010	1.9613	2.0198	2.0766
2	10	1.2744	1.3279	1.4126	1.4925	1.5683
	25	1.3588	1.4092	1.4892	1.5652	1.6376
	50	1.4881	1.5341	1.6080	1.6786	1.7464
	75	1.6060	1.6488	1.7177	1.7840	1.8479
	100	1.7151	1.7552	1.8202	1.8828	1.9435
4	10	1.1167	1.1772	1.2716	1.3594	1.4419
	25	1.1901	1.2470	1.3365	1.4203	1.4995
	50	1.3027	1.3549	1.4376	1.5159	1.5903
	75	1.4057	1.4542	1.5317	1.6053	1.6758
	100	1.5013	1.5468	1.6198	1.6896	1.7567

Table 4.7. Natural frequencies of the completely simply supported FGP with uneven porosity square nanoplate versus K_1 and K_2.

Nonlocal factor (μ)	K_2 \ K_1	100	250	500	750	1000
0	10	1.0092	1.0692	1.1623	1.2485	1.3291
	25	1.1245	1.1787	1.2637	1.3434	1.4187
	50	1.2941	1.3414	1.4167	1.4883	1.5565
	75	1.4439	1.4865	1.5548	1.6202	1.6831
	100	1.5796	1.6185	1.6815	1.7422	1.8008
1	10	0.9297	0.9945	1.0940	1.1851	1.2698
	25	1.0343	1.0929	1.1842	1.2689	1.3483
	50	1.1884	1.2398	1.3209	1.3973	1.4698
	75	1.3247	1.3710	1.4447	1.5149	1.5820
	100	1.4482	1.4907	1.5588	1.6241	1.6868
2	10	0.8682	0.9372	1.0422	1.1375	1.2255
	25	0.9645	1.0271	1.1237	1.2126	1.2954
	50	1.1064	1.1614	1.2477	1.3283	1.4043
	75	1.2322	1.2818	1.3604	1.4347	1.5054
	100	1.3462	1.3918	1.4645	1.5338	1.6001
4	10	0.7783	0.8547	0.9686	1.0705	1.1635
	25	0.8621	0.9316	1.0372	1.1329	1.2212
	50	0.9861	1.0475	1.1423	1.2299	1.3117
	75	1.0962	1.1517	1.2386	1.3198	1.3963
	100	1.1962	1.2472	1.3279	1.4039	1.4760

Table 4.8. Natural frequencies of the completely clamped supported FGP square nanoplate with uneven porosity versus K_1 and K_2.

Nonlocal factor (μ)	K_1 / K_2	100	250	500	750	1000
0	10	1.6016	1.6400	1.7022	1.7622	1.8202
	25	1.6880	1.7245	1.7838	1.8411	1.8967
	50	1.8218	1.8557	1.9109	1.9645	2.0167
	75	1.9451	1.9769	2.0288	2.0794	2.1288
	100	2.0601	2.0901	2.1393	2.1874	2.2344
1	10	1.4462	1.4885	1.5564	1.6215	1.6841
	25	1.5247	1.5649	1.6296	1.6919	1.7520
	50	1.6464	1.6837	1.7440	1.8024	1.8589
	75	1.7587	1.7937	1.8505	1.9056	1.9591
	100	1.8636	1.8966	1.9504	2.0028	2.0538
2	10	1.3293	1.3750	1.4481	1.5176	1.5841
	25	1.4015	1.4450	1.5147	1.5813	1.6452
	50	1.5136	1.5540	1.6190	1.6815	1.7417
	75	1.6173	1.6551	1.7163	1.7754	1.8326
	100	1.7141	1.7499	1.8079	1.8640	1.9186
4	10	1.1631	1.2149	1.2967	1.3737	1.4465
	25	1.2260	1.2753	1.3534	1.4273	1.4976
	50	1.3238	1.3696	1.4427	1.5122	1.5787
	75	1.4145	1.4574	1.5263	1.5922	1.6555
	100	1.4993	1.5399	1.6052	1.6680	1.7285
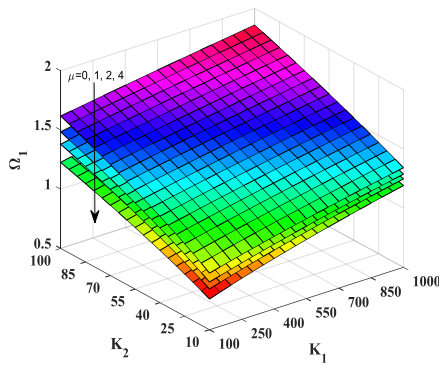
a) The completely simply supported FGP nanoplate with even porosity
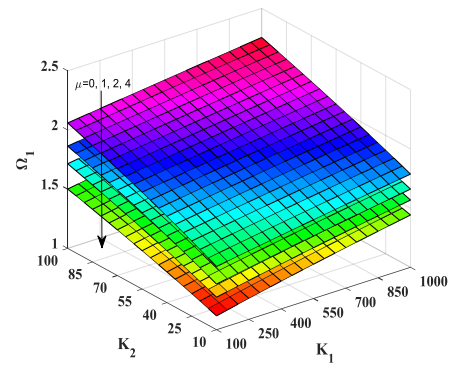
b) The completely clamped supported FGP nanoplate with even porosity
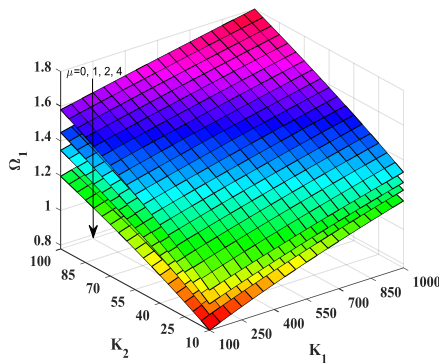
c) The completely simply supported FGP nanoplate with uneven porosity
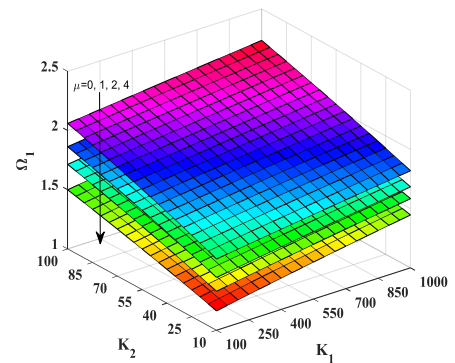
d) The completely clamped supported FGP nanoplate with uneven porosity

Figure 4.9. Natural frequencies of FGP square nanoplate versus K_1 and K_2.

4.1.4.2. Influence of material properties

Secondly, let's consider the effect of material properties on the free vibration of the FGP square nanoplate. The power-law index k gets values from 0 to 10, and the porosity factor ξ changes from 0 to 0.3, the foundation stiffness $K_1 = 100, K_2 = 10,$ and nonlocal factor $\mu = 0, 1, 2, 4.$ The authors only choose the power-law index k in the range from 0 to 10 for investigation because many published works show that when k is greater than 10, the natural frequency of FGP structures does not change much and the recommended value of porosity volume fraction ξ is in the range (0-0.3).

The natural frequencies of FGP nanoplate with different boundary conditions are listed in Table 4.9, Table 4.10, Table 4.11, and Table 4.12 and are shown in Figure 4.10 and Figure 4.11. It can be seen that when k increases, the stiffness of the FGP nanoplate decreases (nanoplate is metal-rich), and hence natural frequencies decrease. We also found that when the increase of nonlocal factor μ leads to natural frequencies of FGP nanoplates decrease. The results are quite reasonable because the increase of the nonlocal factor reduces the stiffness of structures in the nonlocal elastic theory. Specifically, with nonlocal factor $\mu = 0$ (classical elastic theory), the natural frequencies of FGP nanoplates are maximum.

From Figure 4.11, we can see that with the power-law index, $k = 0$ when the porosity volume fraction ξ increases, the natural frequencies of FGP nanoplates increase for both cases of porosity distribution. This is because porosity affects both the stiffness and the mass of nanoshells. This simultaneous interaction causes the natural frequency to increase. Besides, the natural frequencies of the FGP nanoplate with porosity distribution of case 1 are larger than the FGP nanoplate with porosity distribution of case 2. For the case of $k > 2$ when ξ increases from 0 to 0.3, the natural frequencies of FGP nanoplates with even porosity decrease. However, the natural frequencies of FGP nanoplates with uneven porosity are less change and larger than the natural frequencies of FGP nanoplates with even porosity. Basically, the pore appearance in the material reduces the stiffness of the structure. It can also be concluded that the rule of the porosity distribution largely affects the free vibration of FGP nanoplates.

Table 4.9. Natural frequencies of the completely simply supported FGP square nanoplate with even porosity versus k and ξ.

Nonlocal factor (μ)	ξ \ k	0	2	4	6	8	10
0	0	1.2171	0.9272	0.9018	0.8944	0.8878	0.8811
	0.06	1.2301	0.9166	0.8873	0.8804	0.8747	0.8688
	0.12	1.2445	0.9025	0.8669	0.8602	0.8558	0.8511
	0.18	1.2604	0.8830	0.8370	0.8297	0.8268	0.8238
	0.24	1.2781	0.8552	0.7904	0.7793	0.7772	0.7764
	0.30	1.2980	0.8140	0.7101	0.6829	0.6747	0.6723
1	0	1.1170	0.8550	0.8324	0.8259	0.8200	0.8141
	0.06	1.1291	0.8460	0.8199	0.8138	0.8088	0.8036
	0.12	1.1425	0.8337	0.8021	0.7964	0.7925	0.7884
	0.18	1.1573	0.8168	0.7760	0.7697	0.7673	0.7647
	0.24	1.1737	0.7926	0.7350	0.7254	0.7238	0.7232
	0.30	1.1922	0.7566	0.6644	0.6405	0.6335	0.6316
2	0	1.0393	0.7992	0.7788	0.7730	0.7678	0.7624
	0.06	1.0507	0.7914	0.7679	0.7625	0.7581	0.7533
	0.12	1.0633	0.7808	0.7522	0.7472	0.7438	0.7402
	0.18	1.0773	0.7659	0.7291	0.7236	0.7216	0.7194
	0.24	1.0928	0.7445	0.6926	0.6842	0.6829	0.6825
	0.30	1.1102	0.7126	0.6296	0.6084	0.6022	0.6006
4	0	0.9252	0.7179	0.7008	0.6961	0.6917	0.6871
	0.06	0.9357	0.7119	0.6922	0.6879	0.6843	0.6804
	0.12	0.9471	0.7036	0.6798	0.6759	0.6732	0.6702
	0.18	0.9598	0.6919	0.6611	0.6569	0.6554	0.6538
	0.24	0.9739	0.6748	0.6314	0.6248	0.6240	0.6239
	0.30	0.9898	0.6490	0.5797	0.5624	0.5577	0.5566

Table 4.10. Natural frequencies of the completely clamped supported FGP square nanoplate with even porosity versus k and ξ.

| Nonlocal factor (μ)	ξ \ k	0	2	4	6	8	10
0	0	1.9954	1.4548	1.3900	1.3658	1.3473	1.3310
	0.06	2.0139	1.4273	1.3534	1.3286	1.3107	1.2949
	0.12	2.0344	1.3915	1.3038	1.2781	1.2611	1.2465
	0.18	2.0572	1.3434	1.2329	1.2046	1.1892	1.1765
	0.24	2.0825	1.2758	1.1229	1.0856	1.0709	1.0615
	0.30	2.1110	1.1746	0.9226	0.8422	0.8123	0.7996
1	0	1.7996	1.3144	1.2574	1.2363	1.2202	1.2060
	0.06	1.8165	1.2900	1.2247	1.2034	1.1879	1.1741
	0.12	1.8351	1.2581	1.1805	1.1584	1.1439	1.1313
	0.18	1.8558	1.2152	1.1173	1.0929	1.0799	1.0692
	0.24	1.8788	1.1550	1.0192	0.9867	0.9744	0.9667
	0.30	1.9047	1.0650	0.8414	0.7708	0.7448	0.7339
2	0	1.6518	1.2088	1.1574	1.1388	1.1244	1.1116
	0.06	1.6673	1.1867	1.1280	1.1090	1.0953	1.0830
	0.12	1.6846	1.1579	1.0880	1.0684	1.0557	1.0445
	0.18	1.7037	1.1192	1.0308	1.0092	0.9978	0.9885
	0.24	1.7250	1.0647	0.9419	0.9130	0.9024	0.8958
	0.30	1.7489	0.9834	0.7815	0.7184	0.6953	0.6858
4	0	1.4407	1.0589	1.0155	1.0000	0.9880	0.9772
	0.06	1.4545	1.0403	0.9907	0.9751	0.9637	0.9535
	0.12	1.4697	1.0161	0.9569	0.9409	0.9305	0.9212
	0.18	1.4866	0.9834	0.9086	0.8909	0.8818	0.8742
	0.24	1.5054	0.9375	0.8334	0.8096	0.8012	0.7961
	0.30	1.5266	0.8689	0.6985	0.6460	0.6271	0.6194

Table 4.11. Natural frequencies of the completely simply supported FGP square nanoplate with uneven porosity versus k and ξ.

| Nonlocal factor (μ)	ξ \ k	0	2	4	6	8	10
0	0	1.2171	0.9272	0.9018	0.8944	0.8878	0.8811
	0.06	1.2279	0.9298	0.9032	0.8962	0.8901	0.8839
	0.12	1.2392	0.9322	0.9040	0.8974	0.8919	0.8862
	0.18	1.2509	0.9343	0.9041	0.8979	0.8931	0.8880
	0.24	1.2632	0.9361	0.9033	0.8974	0.8933	0.8890
	0.30	1.2761	0.9374	0.9013	0.8955	0.8922	0.8887
1	0	1.1170	0.8550	0.8324	0.8259	0.8200	0.8141
	0.06	1.1270	0.8576	0.8339	0.8278	0.8224	0.8168
	0.12	1.1373	0.8600	0.8349	0.8292	0.8244	0.8193
	0.18	1.1482	0.8622	0.8354	0.8300	0.8258	0.8213
	0.24	1.1595	0.8641	0.8350	0.8299	0.8264	0.8225
	0.30	1.1714	0.8656	0.8336	0.8286	0.8258	0.8227
2	0	1.0393	0.7992	0.7788	0.7730	0.7678	0.7624
	0.06	1.0486	0.8018	0.7805	0.7750	0.7702	0.7652
	0.12	1.0583	0.8043	0.7817	0.7766	0.7723	0.7677
	0.18	1.0684	0.8066	0.7824	0.7776	0.7739	0.7699
	0.24	1.0790	0.8086	0.7824	0.7779	0.7748	0.7714
	0.30	1.0901	0.8103	0.7814	0.7770	0.7746	0.7719
4	0	0.9252	0.7179	0.7008	0.6961	0.6917	0.6871
	0.06	0.9336	0.7205	0.7026	0.6982	0.6943	0.6900
	0.12	0.9423	0.7231	0.7042	0.7001	0.6966	0.6928
	0.18	0.9514	0.7255	0.7053	0.7015	0.6985	0.6952
	0.24	0.9609	0.7277	0.7058	0.7023	0.6999	0.6971
	0.30	0.9708	0.7297	0.7055	0.7022	0.7003	0.6981

Table 4.12. Natural frequencies of the completely clamped supported FGP square nanoplate with uneven porosity versus k and ξ.

Nonlocal factor (μ)	ξ \ k	0	2	4	6	8	10
0	0	1.9954	1.4548	1.3900	1.3658	1.3473	1.3310
	0.06	2.0114	1.4546	1.3865	1.3621	1.3439	1.3280
	0.12	2.0280	1.4538	1.3816	1.3570	1.3392	1.3236
	0.18	2.0455	1.4522	1.3751	1.3502	1.3327	1.3176
	0.24	2.0637	1.4496	1.3665	1.3410	1.3240	1.3094
	0.30	2.0828	1.4458	1.3553	1.3288	1.3121	1.2981
1	0	1.7996	1.3144	1.2574	1.2363	1.2202	1.2060
	0.06	1.8141	1.3144	1.2543	1.2333	1.2175	1.2036
	0.12	1.8292	1.3138	1.2502	1.2290	1.2136	1.2001
	0.18	1.8450	1.3125	1.2446	1.2232	1.2082	1.1951
	0.24	1.8615	1.3104	1.2371	1.2152	1.2007	1.1881
	0.30	1.8788	1.3071	1.2272	1.2045	1.1904	1.1784
2	0	1.6518	1.2088	1.1574	1.1388	1.1244	1.1116
	0.06	1.6651	1.2090	1.1549	1.1362	1.1221	1.1097
	0.12	1.6790	1.2086	1.1513	1.1325	1.1189	1.1068
	0.18	1.6935	1.2075	1.1463	1.1274	1.1142	1.1025
	0.24	1.7087	1.2057	1.1397	1.1204	1.1076	1.0965
	0.30	1.7247	1.2029	1.1308	1.1109	1.0986	1.0880
4	0	1.4407	1.0589	1.0155	1.0000	0.9880	0.9772
	0.06	1.4524	1.0592	1.0136	0.9981	0.9865	0.9760
	0.12	1.4646	1.0592	1.0108	0.9954	0.9841	0.9740
	0.18	1.4773	1.0586	1.0069	0.9914	0.9805	0.9709
	0.24	1.4906	1.0573	1.0015	0.9858	0.9754	0.9662
	0.30	1.5046	1.0552	0.9943	0.9780	0.9681	0.9595
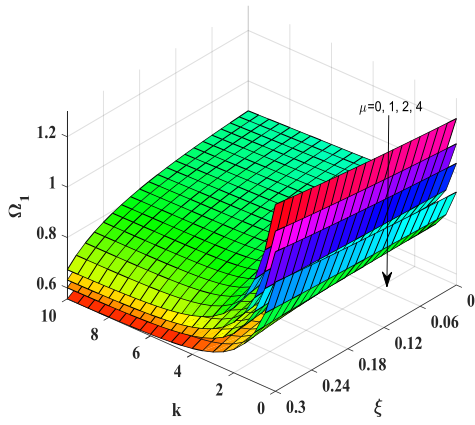
a) *The completely simply supported FGP nanoplate even porosity*
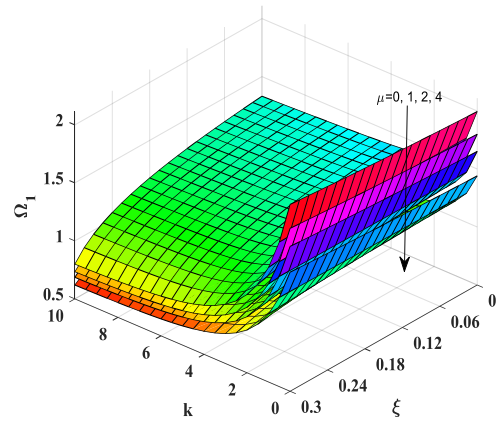
b) *The completely clamped supported FGP nanoplate even porosity*
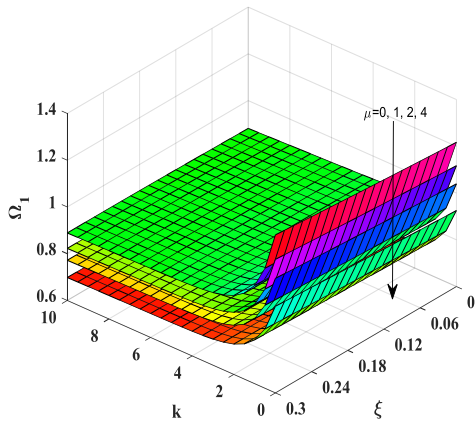
c) *The completely simply supported FGP nanoplate uneven porosity*
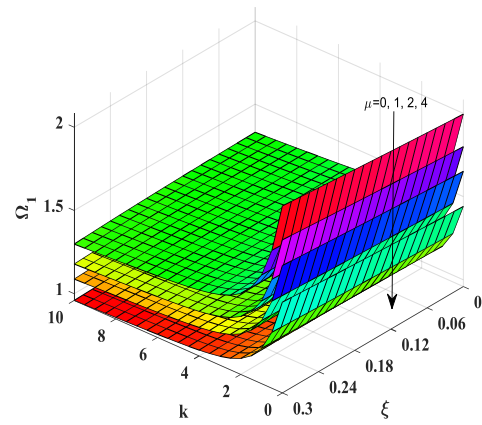
d) *The completely clamped supported FGP nanoplate with uneven porosity*

Figure 4.10. Natural frequencies of FGP square nanoplate versus k and ξ .
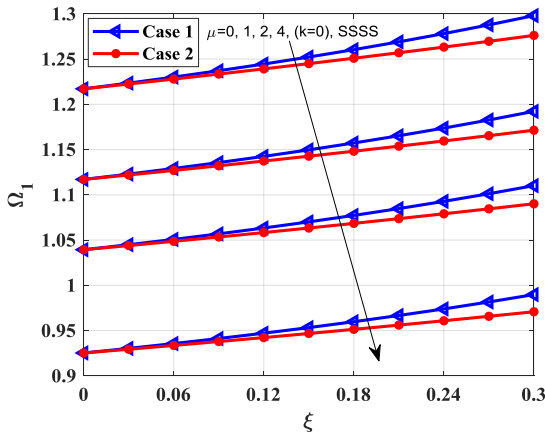
a) *The CSS FGP nanoplate, k = 0*
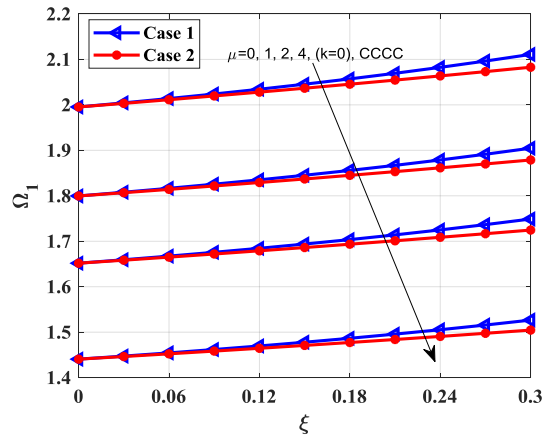
b) *The CCS FGP nanoplate, k = 0*
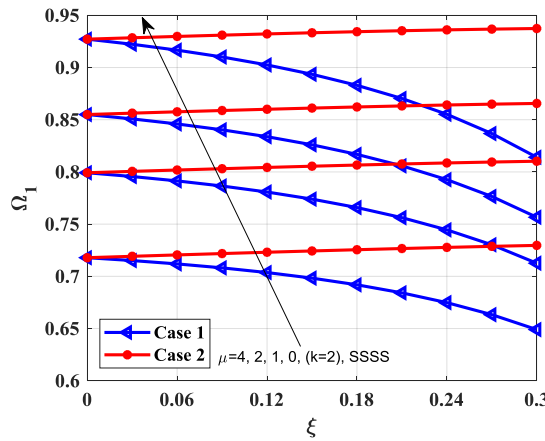
c) *The CSS FGP nanoplate, k = 2*
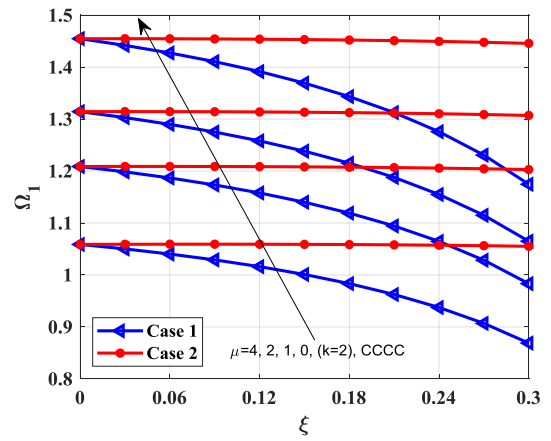
d) *The CCS FGP nanoplate, k = 2*
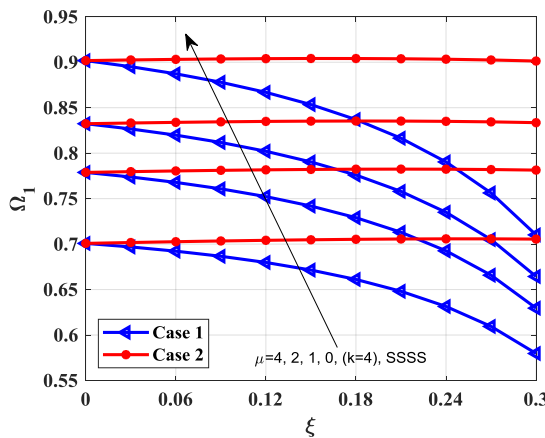
e) *The CSS FGP nanoplate, k = 4*
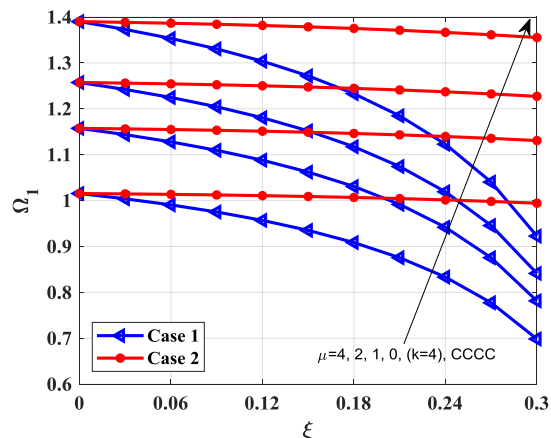
f) *The CCS FGP nanoplate, k = 4*

Figure 4.11. Natural frequencies of the FGP square nanoplate versus ξ.

4.2. Forced vibration

4.2.1. Problem formulation

Consider functionally graded porous nanoplates with different shapes resting on an elastic foundation subjected to dynamic load, as shown in Figure 4.12.

a) Rectangular nanoplate

b) L-shape nanoplate

c) Annular nanoplate

d) Half-annular nanoplate
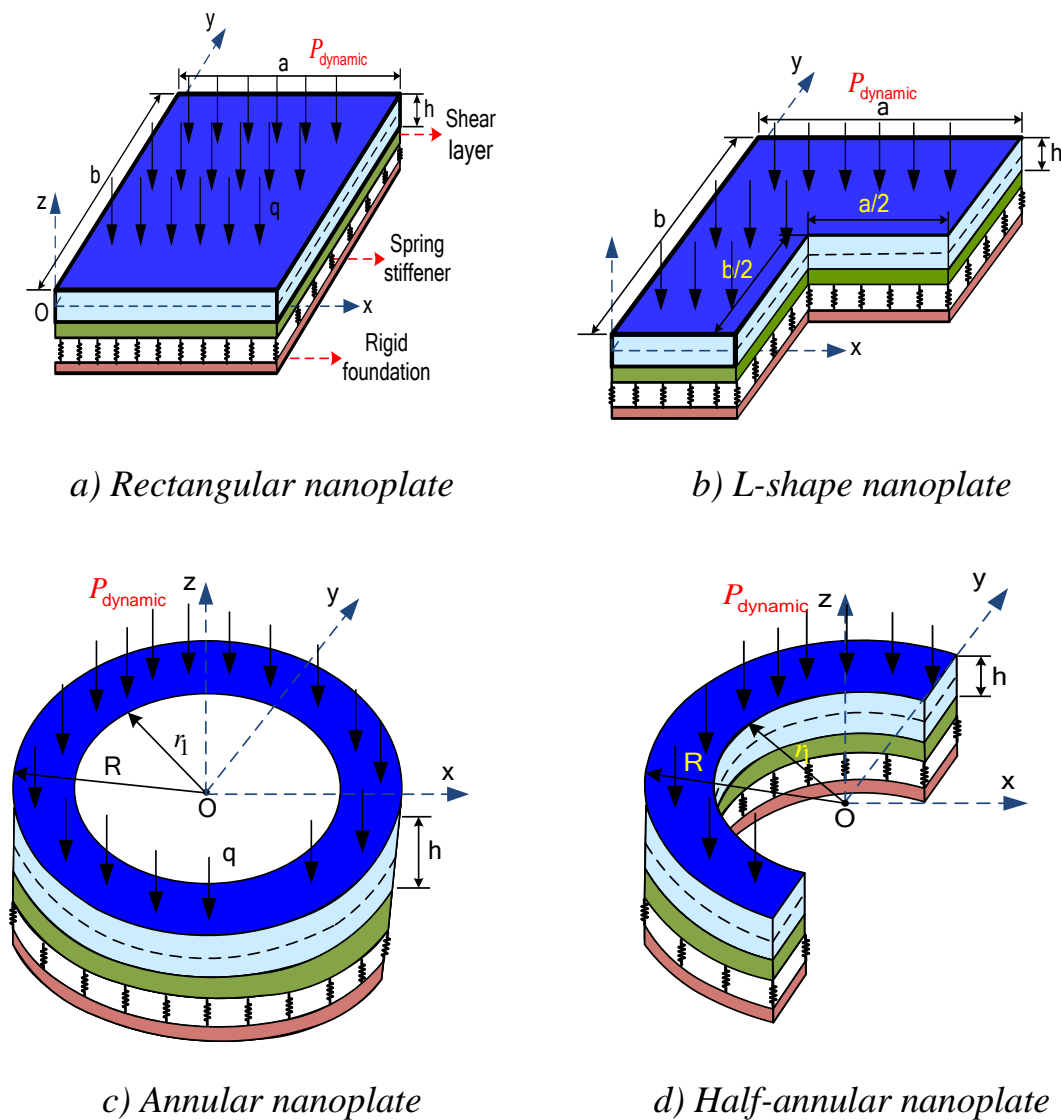
Figure 4.12. The model of FGP nanoplates subjected to dynamic load.

4.2.2. Finite element algorithm and calculation programs

Considering the drag coefficient, which is linearly dependent on velocity, the governing equations of motion for forced vibration of the plate have the following form [71]:

$$\mathbf{M\ddot{q} + C\dot{q} + Kq = F} \tag{4.5}$$

in which $\mathbf{M, K, F, q}$ are the global mass matrix, the global stiffness matrix, the global force vector, and the global displacement vector

Due to the difficulties in computing the exact values of the drag coefficient, it was essential to use Rayleigh's theory of drag. After this stage, the mass matrix and element stiffness matrix are linearly blended to give the drag matrix [71]:

$$\mathbf{C} = \alpha\mathbf{M} + \beta\mathbf{K} \tag{4.6}$$

where α and β are the Rayleigh constant based on the natural frequency and the drag coefficient ς. Normally, the drag coefficient is determined mostly by the first two modes of vibrations corresponding to the two lowest natural frequencies. Assuming the drag coefficient ratio ς is constant, one obtains:

$$\beta = \frac{2\varsigma}{\omega_1 + \omega_2}, \alpha = \omega_1\omega_2\beta \tag{4.7}$$

The equations (4.5) are linear differential equations of second order with constant coefficients. There are two primary methods for solving the system (4.5), which are direct integration and the mode superposition method.

- Among the direct integration techniques are the Newmark method, the central difference method, the Houblt method, and the Wilson method θ, among others; nevertheless, the Newmark method is the one that is used most often.

- Mode superposition method: This method is often used to solve equations involving forced vibration. Utilizing eigenforms, which is another way of saying taking use of the outcomes of the eigen-oscillation issue, is very useful in this regard (modes).

To solve the system of differential equations (4.5), the thesis uses the Newmark method of direct integration. The following is a synopsis of the procedure.

To begin, let's assume that the equation of motion for the structure takes the following form:

$$\mathbf{M\ddot{q}} + \mathbf{C\dot{q}} + \mathbf{Kq} = \mathbf{F} \tag{4.8}$$

When the obtained solution of (4.8) at time t is the sth step. Find the solution at time $t+\Delta t$ which is the $(s + 1)^{th}$ step as follows:

$$\mathbf{M}_{s+1}\ddot{\mathbf{q}}_{s+1} + \mathbf{C}_{s+1}\dot{\mathbf{q}}_{s+1} + \mathbf{K}_{s+1}\mathbf{q}_{s+1} = \mathbf{F}_{s+1} \tag{4.9}$$

Step 1: Determine the initial conditions:

$$\mathbf{q}(0) = \mathbf{q}_0; \dot{\mathbf{q}}(0) = \dot{\mathbf{q}}_0; \ddot{\mathbf{q}}(0) = \mathbf{M}_0^{-1}\left(\mathbf{F}_0 - \mathbf{K}_0\mathbf{q}_0 - \mathbf{C}_0\dot{\mathbf{q}}_0\right) \tag{4.10}$$

Calculation time step: $\Delta t = \dfrac{t_{tol}}{n}$

The coefficients:

$$a_0 = \frac{2}{\gamma\Delta t^2}; a_1 = \frac{2\alpha}{\gamma\Delta t}; a_2 = \frac{2}{\gamma\Delta t}; a_3 = \frac{1}{\gamma} - 1; a_4 = \frac{2\alpha}{\gamma} - 1;$$
$$a_5 = \left(\frac{\alpha}{\gamma} - 1\right)\Delta t; a_6 = (1-\alpha)\Delta t; a_7 = \alpha\Delta t. \tag{4.11}$$

in which α and γ are selected according to the linear law for the varying acceleration:

$$\ddot{\mathbf{q}}(\tau) = \ddot{\mathbf{q}}_s + \frac{\tau}{\Delta t}\left(\ddot{\mathbf{q}}_{s+1} - \ddot{\mathbf{q}}_s\right) \text{ with } t_s \leq \tau \leq t_{s+1} \text{ and } t_{s+1} = t_s + \Delta t .$$

To ensure solution accuracy, choose $\alpha = \dfrac{1}{2}; \gamma = \dfrac{1}{3}$.

Step 2: Compute the efficiency stiffness matrix and the efficiency nodal force vector:

$$\mathbf{K}^* = \mathbf{K} + a_0\mathbf{M} + a_1\mathbf{C} \tag{4.12}$$

$$\mathbf{F}^* = \mathbf{F}_{s+1} + \mathbf{M}\left(a_0\mathbf{q}_i + a_2\dot{\mathbf{q}}_i + a_3\ddot{\mathbf{q}}_i\right) + \mathbf{C}\left(a_1\mathbf{q}_i + a_4\dot{\mathbf{q}}_i + a_5\ddot{\mathbf{q}}_i\right) \tag{4.13}$$

Step 3: Determine the required quantities.

- Vector $\mathbf{q}_{s+1}$ according to the equation:

$$\mathbf{K}^*_{s+1}.\mathbf{q}_{s+1} = \mathbf{F}^*_{s+1} \tag{4.14}$$

- Vectors $\ddot{\mathbf{q}}_{s+1}, \dot{\mathbf{q}}_{s+1}$ according to the equations:

$$\ddot{\mathbf{q}}_{s+1} = a_0\left(\mathbf{q}_{s+1} - \mathbf{q}_s\right) - a_2\dot{\mathbf{q}}_s - a_3\ddot{\mathbf{q}}_s \tag{4.15}$$

$$\dot{\mathbf{q}}_{s+1} = \dot{\mathbf{q}}_s + a_6\ddot{\mathbf{q}}_s + a_7\ddot{\mathbf{q}}_{s+1} \tag{4.16}$$

and then repeat the loop until the time runs out.

A flowchart of Newmark's method for solving the dynamic response of nanoplate is shown in Figure 4.13.

Based on the algorithm, the calculation program FGP_Nanoplates_FSDT_Nonlocal_Dynamic_2022 (FNFNS_2022) is built in Matlab software to analyze the dynamic behavior of the FGP nanoplate resting on an elastic foundation. The program consists of the following main modules:

- The module for input data and meshing elements.

- The module solves the dynamic behavior for FGP nanoplate resting on an elastic foundation.

- The module outputs the results.

The program FGP_Nanoplates_FSDT_Nonlocal_Dynamic_2022 can solve the dynamic behavior of FGP nanoplate resting on an elastic foundation

and investigate the influence of factors such as boundary conditions, material properties, elastic foundation stiffness on the dynamic behavior of the nanoplates.

Start

Input data

Calculating
$\mathbf{K}, \mathbf{M}, \mathbf{C}, \Delta t, \alpha, \delta, ...$
$\mathbf{q_o}, \dot{\mathbf{q}}_o, \ddot{\mathbf{q}}_o, \mathbf{K}^*, \mathrm{n} = t_{cal} / \Delta t$

$t = t + \Delta t$

Calculating $\mathbf{F}^*_{t+\Delta t}$

Calculating $\mathbf{q}_{t+\Delta t} = \mathbf{K}^{*-1} \mathbf{F}^*_{t+\Delta t}$

Calculating $\dot{\mathbf{q}}_{t+\Delta t}, \ddot{\mathbf{q}}_{t+\Delta t}$

Calculating $\boldsymbol{\sigma}_{t+\Delta t}, \boldsymbol{\varepsilon}_{t+\Delta t}, \mathbf{F}_{t+\Delta t}$

No j < n

Yes j = n

Results

End
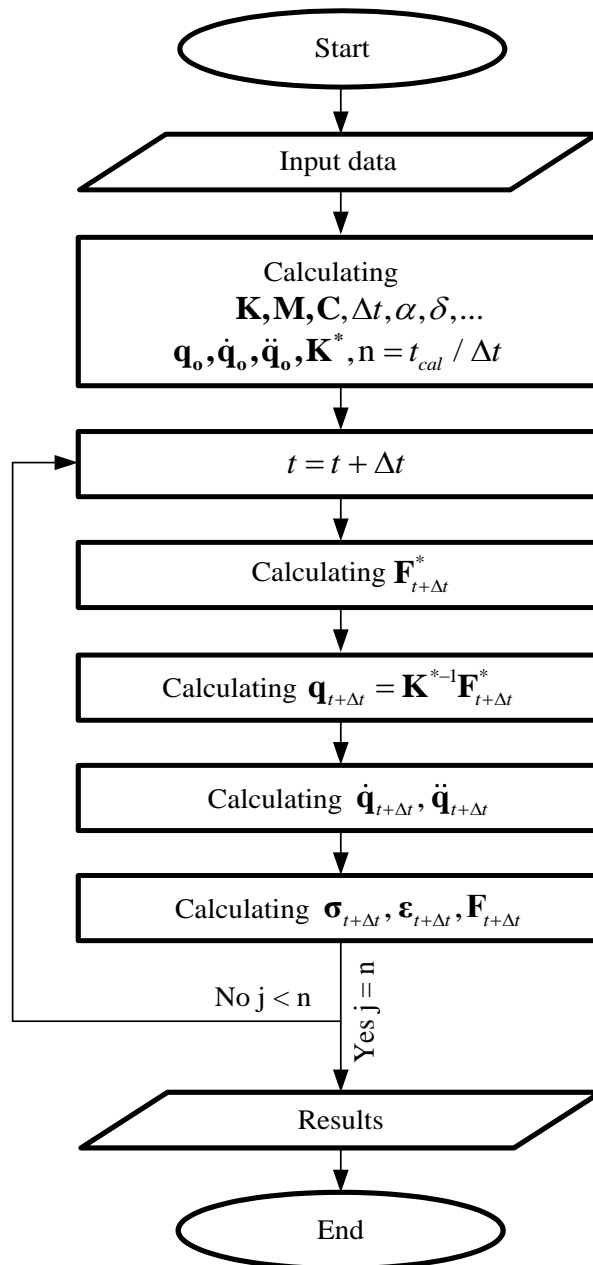
Figure 4.13. Flowchart of Newmark's method for solving the dynamic response of FGP nanoplates.

4.2.3. Verification study

The completely clamped supported homogeneous square plate with parameters $a = b = 1m$, $h = a / 10$, $E = 30GPa$, $\rho = 2800 \, kg / m^3$ and $v = 0.3$ is considered. The plate is subjected to a sudden distribution load $p_0 = 10 \, kPa$. The non-dimensional deflection is given by the formula $w^* = \dfrac{100Eh^3}{12p_0a^4(1-v^2)} w$.

The deflection response of the midpoint of the plate is shown in Figure 4.14, (integral time is *5ms*, and acting time of load is *2ms*). Observing this figure, it can be seen that the center deflection response of plates is similar in both shape and value with Ref. [79] using Meshless Petrov-Galerkin (MLPG) method. From the above examples, it can be concluded that the author's formula and program ensure accuracy and reliability.
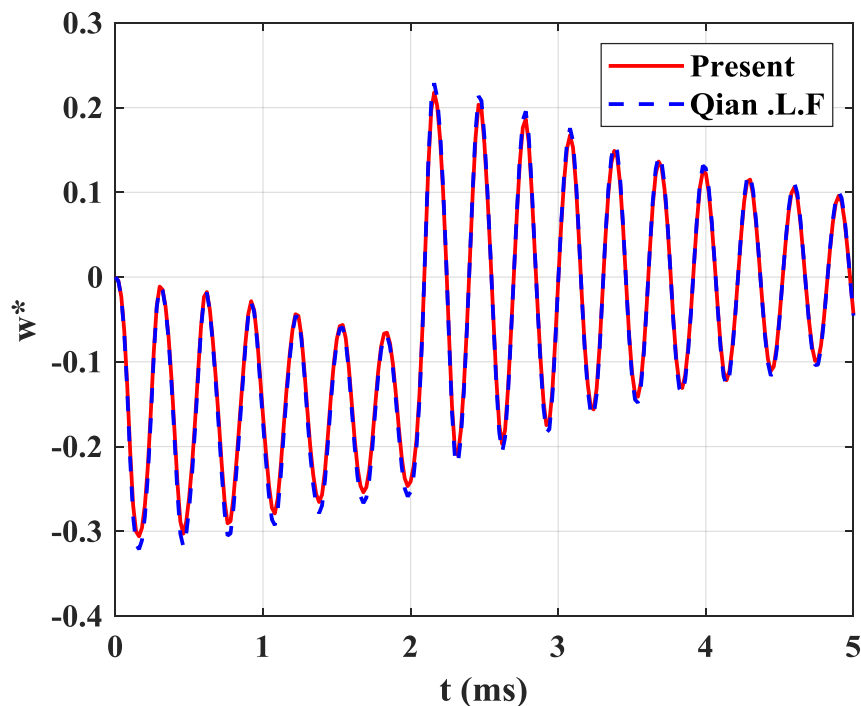
Figure 4.14. The deflection response of the center square plate over time.

4.2.4. Numerical results and discussion

4.2.4.1. Square nanoplate

Considering FGP (Al$_2$O$_3$/Al) square nanoplate with geometric dimensions $a = 10$ *nm*, $h = 1$ *nm.* The plate is subjected to a load $p(t)$ over time as follows:

$$p(t) = q_0 . F(t); \quad F(t) = \begin{cases} 1 - \dfrac{t}{\tau_{hd}} & (0 \le t \le \tau_{hd}) \\ 0 & otherwise \end{cases} \tag{4.17}$$

with q_0 is uniformly distributed load.

a) Influence of the nonlocal factor

Figure 4.15 presents the effect of nonlocal factor μ on the displacement response of the completely clamped supported FGP nanoplate with even porosity, porosity factor $\xi = 0.5$, power-law index $k = 1$, time step $\Delta t = 0.08$. The stiffness of foundation: K_1=100, K_2=10. It can be seen that the vibration is damped after the application time of the load and nonlocal factor reduce stiffness of nanoplate hence displacement increase.
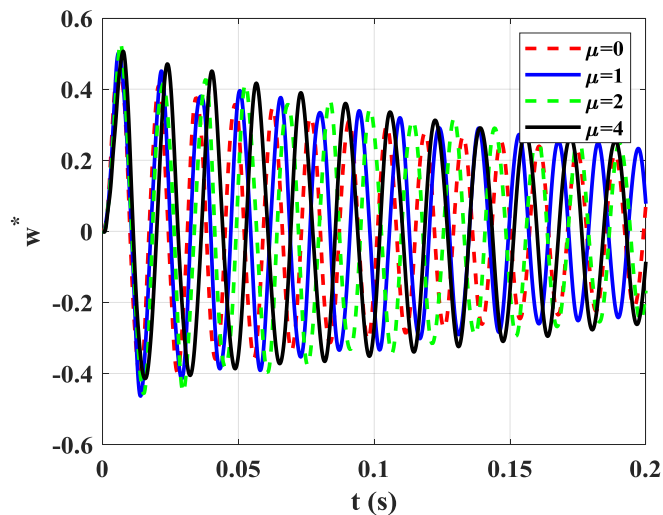
Figure 4.15. The displacement response of the completely clamped supported FGP square nanoplate with even porosity.

b) Influence of the power-law index

Furthermore, Figure 4.16 displays the influence of the power-law index k on the displacement response of the completely clamped supported FGP nanoplate with uneven porosity, porosity factor $\xi = 0.2$, and nonlocal factor $\mu = 1$. The stiffness of foundation: K_1=150, K_2=50. It can be observed that the power-law index k increase, and the stiffness of nanoplate gets stronger. This leads to the displacement increase. Besides, rich-metal nanoplate's stiffness is smaller than rich-ceramic nanoplate's stiffness. In this example, the damping ratio $\zeta = 0.008$ is used.
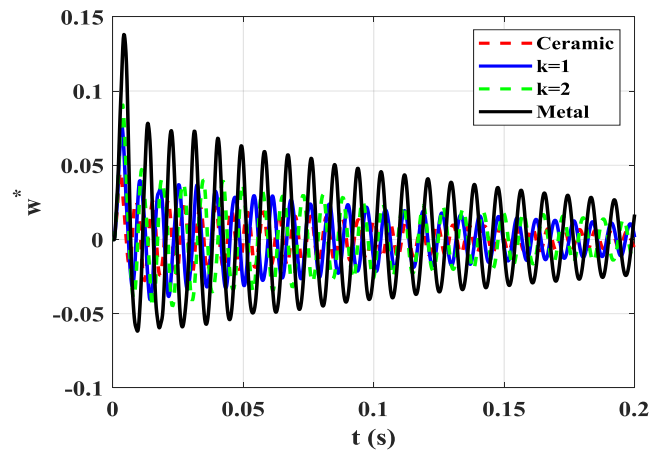
Figure 4.16. The displacement response of the completely clamped supported FGP square nanoplate with uneven porosity.

4.2.4.2. L-shape nanoplate

Consider FGP (Al$_2$O$_3$/Al) nanoplate with geometric dimensions $a = b = 10$ nm. The FGP nanoplate is subjected to a load $p(t)$ over time as follows the formula (4.17).

a) Influence of the nonlocal factor

Figure 4.17 - Figure 4.19 present the effect of the nonlocal factor μ on the displacement and stress response of the completely simply supported FGP L-shape nanoplate with uneven porosity at A-point has coordinates (3.75, 6.25)

with the thickness $h = a/20$, the porosity volume fraction $\xi = 0.3$, the power-law index $k = 4$ in two cases: without damping ratio $\zeta = 0$ and include damping ratio $\zeta = 0.1$. The foundation stiffness: $K_1 = 200, K_2 = 20$. It can be seen that the vibration is damped after the application time of the load, and the nonlocal factor reduces the stiffness of nanoplates; hence displacement and stress increase. In general, structural resistance always exists, and after a period of application of the load, the nanoplate oscillates and then fades away (displacement and stress equal to 0).

a) The damping ratio $\zeta = 0$ b) The damping ratio $\zeta = 0.1$
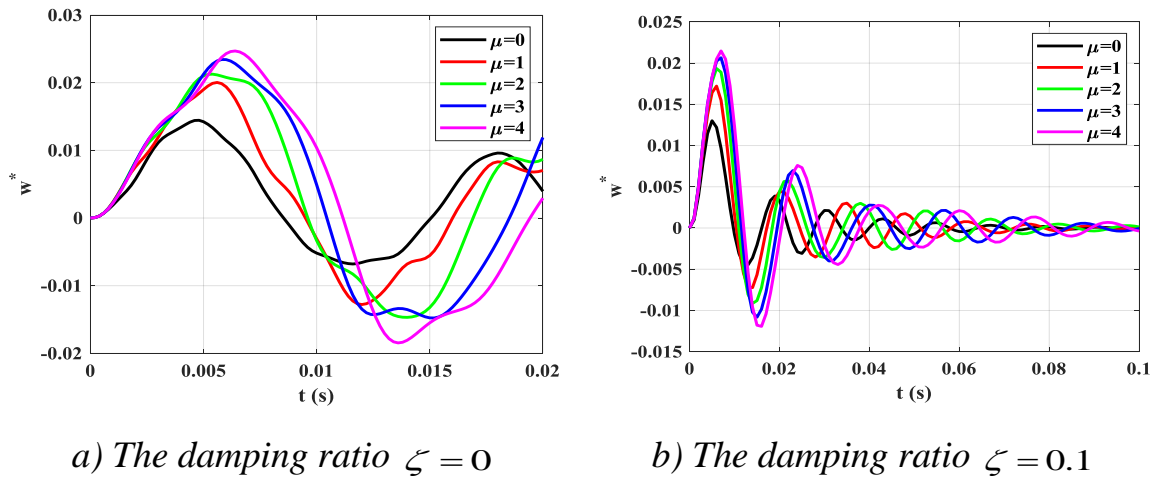
Figure 4.17. The deflection response of the A-point over time t.

a) The damping ratio $\zeta = 0$ b) The damping ratio $\zeta = 0.1$
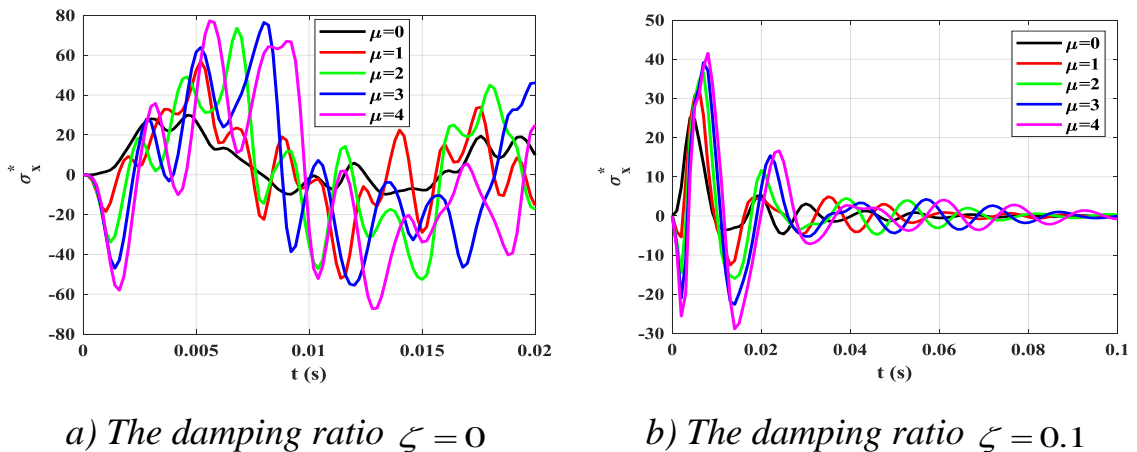
Figure 4.18. The stress response σ_{xx}^{*} of the A-point over time t at $z = h/2$.
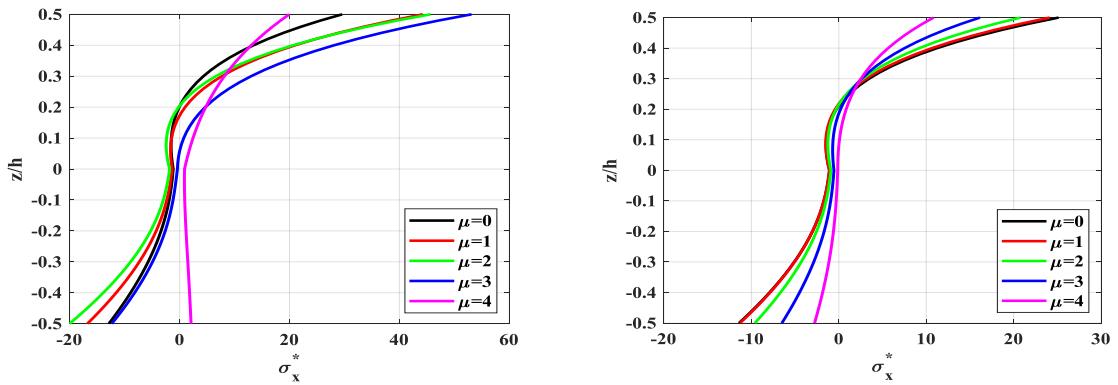
a) The damping ratio $\zeta = 0$ *b) The damping ratio $\zeta = 0.1$*

Figure 4.19. The stress σ^*_{xx} of the A-point of nanoplates along thickness at $t = 0.005s$.

b) Influence of the power-law index

Figure 4.20 - Figure 4.22 display the influence of the power-law index k on the displacement and stress response of completely clamped supported FGP L-shape nanoplates at A-point with porosity volume fraction $\xi = 0.2$, the plate thickness $h = a / 50$, nonlocal factor $\mu = 1$, the foundation stiffness $K_1 = 100$, $K_2 = 10$ in two cases: without the damping ratio $\zeta = 0$ and include the damping ratio $\zeta = 0.1$. It can be observed that the power-law index k increase and the stiffness of nanoplate obtains higher. As a result, the displacement increase. Besides, rich-metal nanoplate stiffness is smaller than rich-ceramic nanoplate stiffness.
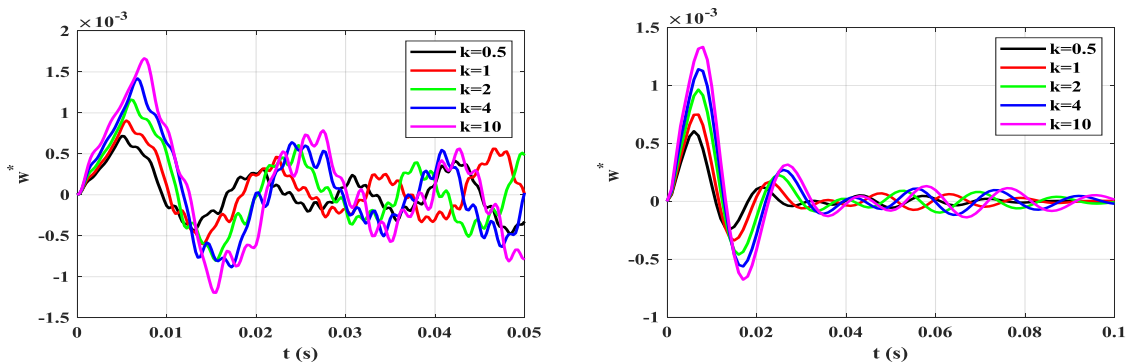
a) The damping ratio $\zeta = 0$ *b) The damping ratio $\zeta = 0.1$*

Figure 4.20. The deflection response of the A-point over time t.

a) The damping ratio $\zeta = 0$ *b) The damping ratio $\zeta = 0.1$*
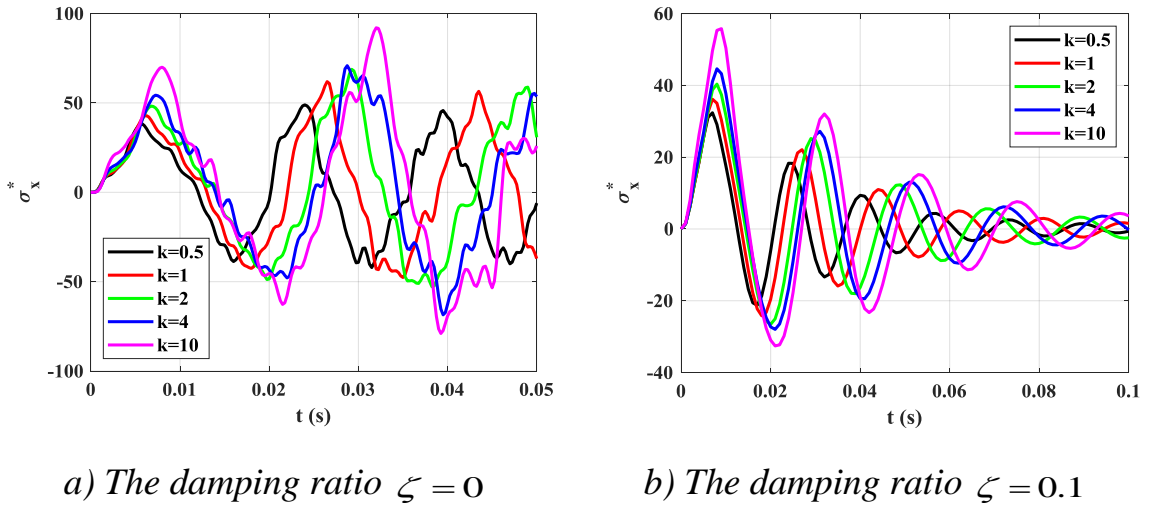
Figure 4.21. The stress response σ_{xx}^* of the A-point over time t at $z = h/2$.

a) The damping ratio $\zeta = 0$ *b) The damping ratio $\zeta = 0.1$*
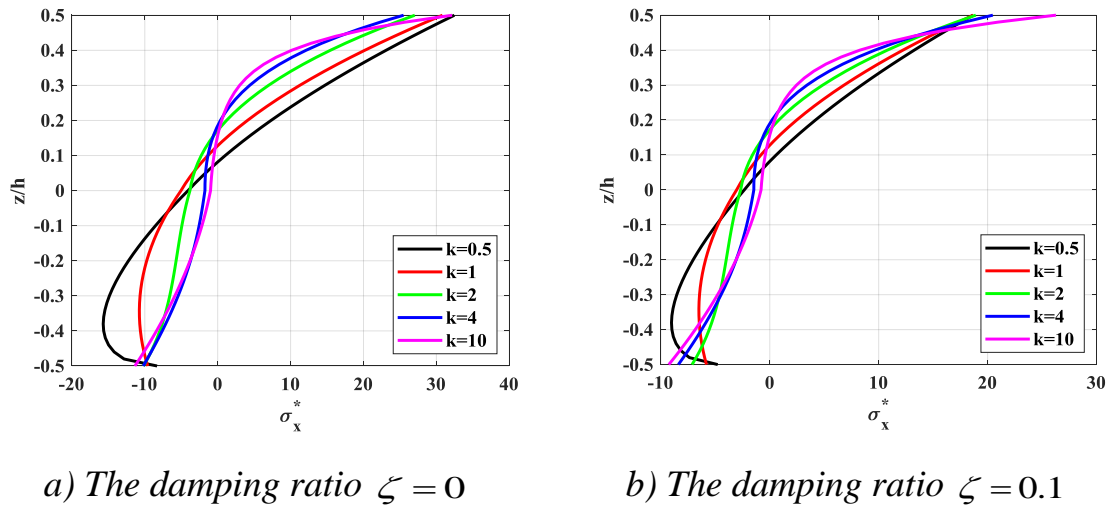
Figure 4.22. The stress σ_{xx}^* of the A-point of nanoplates along thickness at $t = 0.005s$.

4.2.4.3. Annular nanoplate

Consider FGP (Al_2O_3/Al) annular nanoplate with geometric dimensions $R = 2r = 10$ *nm*, $h = 1$ *nm.* The FGP nanoplate is subjected to a load $p(t)$ over time as follows the formula (4.17).

a) Influence of the nonlocal factor

Figure 4.23 presents the effect of the nonlocal factor μ on the displacement response of the completely clamped supported FGP nanoplate with even porosity, porosity factor $\xi = 0.5$, and the power-law index $k = 1$. The foundation stiffness: K_1=100, K_2=10. It can be seen that the vibration is damped after the application time of the load, and the nonlocal factor reduces the stiffness of nanoplate hence the displacement increase.
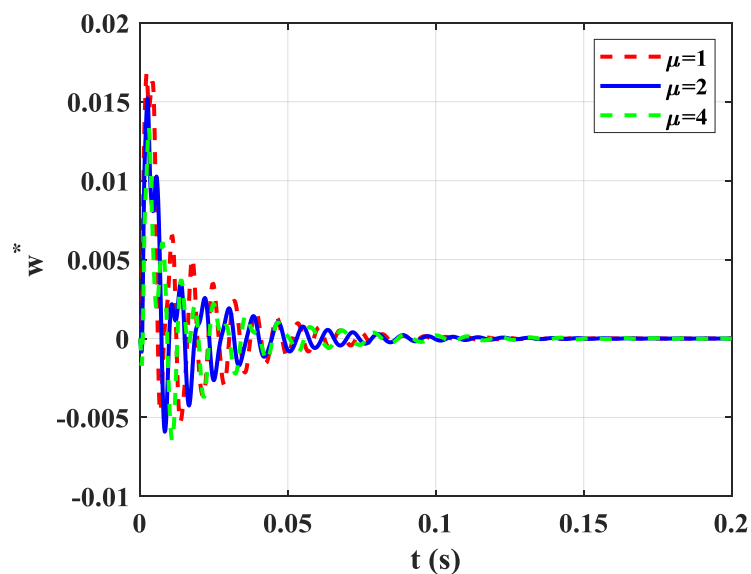
Figure 4.23. The displacement response of the completely clamped supported FGP annular nanoplate with even porosity.

b) Influence of the power-law index

Figure 4.24 displays the influence of the power-law index k on the displacement response of the completely clamped supported FGP nanoplate with uneven porosity, porosity factor $\xi = 0.2$, and nonlocal factor $\mu = 1$. The foundation stiffness: K_1=150, K_2=50. It can be observed that the power-law index k increase makes reduce the stiffness of nanoplate, leading to displacement increase. Besides, rich-metal nanoplate's stiffness is smaller than rich-ceramic nanoplate's stiffness. It can also be seen that, after the time of

application of the load, the displacement response of the plate decreases gradually due to the consideration of the damped structure.
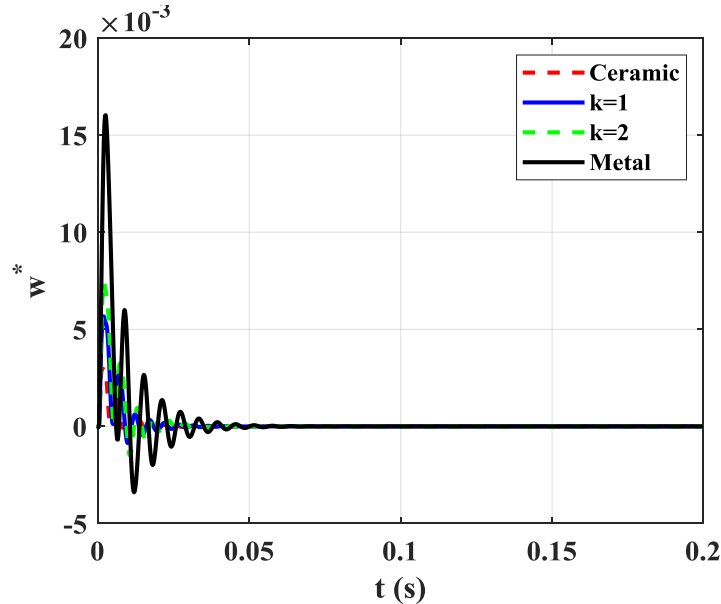
Figure 4.24. The displacement response of the completely clamped supported FGP annular nanoplate with uneven porosity.

c) Influence of the porosity factor

Finally, Figure 4.25 demonstrates the effect of the porosity factor ξ on the displacement response of the completely simply supported FGP nanoplate with two cases of porosity distributions, power-law index $k = 1$, and nonlocal factor $\mu = 2$. The foundation stiffness: K_1=50, K_2=10. It can be found that the increase in porosity factor ξ makes reduce the stiffness of nanoplates resulting in an increase in displacement. Furthermore, the maximum displacement response of the completely simply supported FGP nanoplate with even porosity is larger than the nanoplate with even porosity. In this example, the Rayleigh coefficient $\zeta = 0.1$ is used.

a) Even porosity   *b) Uneven porosity*
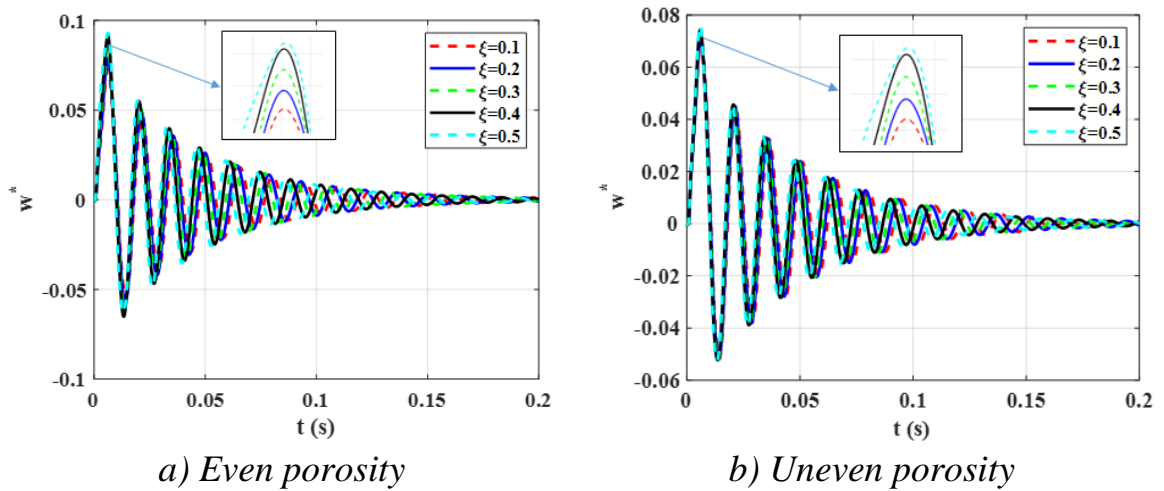
Figure 4.25. The displacement response of the completely simply supported

FGP annular nanoplate.

4.3. Summary of Chapter 4

In this chapter, the author presented the free vibration problem and forced vibration problem. From the proposed formulation and the numerical results, the author can withdraw some following points:

The author has built an algorithm and a calculation program FGP_Nanoplates_FSDT_Nonlocal_Freevibration_2022 (FNFNF_2022) to calculate the free vibration of the FGP nanoplates resting on an elastic foundation. The calculation results of the program are compared with other published results showing accuracy and reliability.

The author has built an algorithm and a calculation program FGP_Nanoplates_FSDT_Nonlocal_Dynamic_2022 (FNFND_2022) to calculate the FGP nanoplates resting on an elastic foundation under dynamic load. The calculation results of the program are compared with other published results showing accuracy and reliability.

The survey results show that there are many factors affecting the free vibration of FGP nanoplates resting on an elastic foundation. However, there

are large influencing factors such as nonlocal factor, the parameters of the functionally graded porous material, stiffness of the elastic foundation

The survey results show that there are many factors affecting the dynamic response of FGP nanoplates resting on an elastic foundation. However, there are large influencing factors, such as the nonlocal factor, the parameters of the functionally graded porous material, and the stiffness of the elastic foundation. Therefore, when designing nanoplates for special requirements, engineers need to pay attention to the above issues for the structure to operate at high efficiency.

The obtained results in this chapter have been shown in papers number 1, number 3, and number 5 (List of publications).

CONCLUSIONS AND RECOMMENDATIONS FOR FUTURE STUDIES

1. Novel contributions of the thesis

Based on the finite element method and nonlocal elastic theory, the static and dynamic responses of FGP nanoplates resting on an elastic foundation have been investigated in this thesis. The following are some of the significant contributions of the thesis:

- The thesis established a model, a finite element algorithm, and a collection of programs to analyze of static bending, free and forced vibration of the FGP nanoplates resting on an elastic foundation with various plate shapes and boundary conditions. The findings demonstrate the difference between nonlocal elasticity theory and local elasticity theory.

- The influence of parameters such as nonlocal coefficients, material properties, geometric dimensions, elastic foundation stiffness, etc., on the static response, and natural and forced vibrations of FGP nanoplates have been examined in this thesis. From there, the thesis provides scientifically and practically relevant commentary.

- The data set of the dissertation may be used as a reference in the computation and design of nanostructures to handle static and dynamic loads encountered in sensors, electronic chips, and sensors.

2. Recommendations for future studies

- Using higher-order shear deformation theories to examine the vibrations of nanoplates and nanoshells subjected to various types of mechanical loads while taking temperature into consideration.

- Investigating the buckling problems of nanoplates in a viscoelastic environment while subjected to a variety of mechanical loads.

- Computing the shape optimization problem and material optimization issue for nanoplates.

- Calculation of nanomaterial-reinforced structures exposed to various sorts of loads.

LIST OF PUBLICATIONS

1) Trac Luat Doan, **Pham Binh Le**, Trung Thanh Tran, Vu Khac Trai, Quoc Hoa Pham (2021). Free Vibration Analysis of Functionally Graded Porous Nano-plates with Different Shapes Resting on Elastic Foundation. *Journal of Applied and Computational Mechanics,* Vol. 7, Issue 3. doi.org/10.22055/JACM.2021.36181.2807, pp. 1593-1605 (SCOPUS).

2) **Le Pham Binh**, Doan Trac Luat, Le Minh Thai, Tran Trung Thanh (2021). Static bending analysis of annular nanoplates resting on elastic foundation using nonlocal elasticity theory. *Journal of Science and Technique – Le Quy Don Technical University, Vol. 16, No. 02, pp. 23-32.*

3) **Le Pham Binh**, Doan Trac Luat, Tran Trung Thanh, Pham Quoc Hoa and Pham Tien Dat, (2021). Forced vibration of FGP nanoplates resting on elastic foundation using finite element formulation. *Proceedings of The 15th National Conference on Solid Mechanics, Thai Nguyen – 2021, pp. 81-90.*

4) **Le Pham Binh**, Le Minh Thai, Pham Tien Dat and Tran Trung Thanh, (2021). Static behavior of FGP half-annular nanoplates resting on elastic foundation using nonlocal elasticity theory. *Proceedings of The 15th National Conference on Solid Mechanics, Thai Nguyen – 2021, pp. 91-99.*

5) Tran Trung Thanh, **Le Pham Binh** (2022). Nonlocal Dynamic Response Analysis of Functionally Graded Porous L-shape Nanoplates Resting on Elastic Foundation Using Finite Element Formulation. *Engineering with Computer. h*ttps://doi.org/10.1007/s00366-022-01679-6, (ISI, Q1).

BIBLIOGRAPHY

[1]. Nguyễn Đức Nghĩa, *Hoá học nano – Công nghệ nền và vật liệu nguồn*, Nhà xuất bản Khoa học Tự nhiên và công nghệ, Hà Nội, 2007.

[2]. Nguyễn Văn Hậu (2017), Nghiên cứu ứng xử tấm composite chức năng (FGM) dưới tác dụng tải trọng cơ nhiệt, Luận án tiến sĩ, Trường Đại học Sư phạm kỹ thuật Thành phố Hồ Chí Minh.

[3]. Phạm Công Hồng (2018), Phân tích phi tuyến tĩnh và động lực học tấm chữ nhật FGM trên nền đàn hồi, Luận án tiến sĩ, Trường Đại học Công nghệ, Đại học Quốc gia Hà Nội.

[4]. Nguyễn Văn Thành (2021), Ổn định và các đáp ứng phi tuyến của kết cấu tấm và vỏ composite gia cường các sợi nano carbon, có cơ lý tính biến đổi (FG-CNTRC), Luận án tiến sĩ, Trường Đại học Công nghệ, Đại học Quốc gia Hà Nội.

[5]. G.B. Sergeev, K.J. Klabunde, *Nanochemistry*, 2nd ed, Elsevier.

[6]. J. Scott Bunch, et al (2007), "Electromechanical resonators from graphene sheets", *Science,* Vol. 315, pp. 490–493.

[7]. Evoy S., Carr D.W., Sekaric L., Olkhovets A., Parpia J.M., Craighead H.G. (1999), "Nanofabrication and electrostatic operation of single-crystal silicon paddle oscillators", *Journal of Applied Physics,* Vol. 86, pp. 6072–6077.

[8]. Ganhua Lu, Leonidas E Ocola, Junhong Chen (2009), "Reduced graphene oxide for room-temperature gas sensors", *Nanotechnology,* Vol. 20, 445502.Arash B, Wang Q, Duan WH. Detection of gas atoms via vibration of graphenes. *Phys Lett* A 2011;375:2411–5.

[9]. Behrouz Arash, Quan Wang, Wen Hui Duan (2011), "Detection of gas atoms via vibration of graphenes", *Physics Letters* A, Vol. 375, pp. 2411–2415.

[10]. A. Sakhaee-Pour, M.T. Ahmadian, A. Vafai (2008), "Applications of single-layered graphene sheets as mass sensors and atomistic dust detectors", *Solid State Communications,* Vol. 145, pp. 168–172.

[11]. Freund LB, Suresh S (2003), *Thin film materials*, Cambridge University Press.

[12]. A. Cemal Eringen (1972), "Linear theory of nonlocal elasticity and dispersion of plane waves", *International Journal of Engineering Science*, Vol. 10, pp. 425-435.

[13]. A. Cemal Eringen (1972), "Nonlocal polar elastic continua", *International Journal of Engineering Science*, Vol. 10, pp. 1-16.

[14]. A. Cemal Eringen, Edelen DGB (1972), "On nonlocal elasticity". *International Journal of Engineering Science*, Vol. 10; pp. 233-248.

[15]. A. Cemal Eringen (1983), "On differential equations of nonlocal elasticity and solutions of screw dislocation and surface waves", *Journal of Applied Physics*, Vol. 54, No. 9, pp. 4703-4710.

[16]. A. Cemal Eringen (2002), *Nonlocal Continuum Field Theories*, Springer, New York.

[17]. Norouzzadeh A, Ansari R, Rouhi H (2007), "Pre-buckling responses of Timoshenko nanobeams based on the integral and differential models of nonlocal elasticity: an isogeometric approach", *Applied Physics A*, Vol.123, pp. 330-341.

[18]. Norouzzadeh A, Ansari R. (2017), "Finite element analysis of nano-scale Timoshenko beams using the integral model of nonlocal elasticity", *Physics E*, Vol. 88, pp. 194-200.

[19]. R. Ansari, J. Torabi, A. Norouzzadeh (2018), "Bending analysis of embebded nanoplates on the integral formulation of Eringen's nonlocal theory using the finite element method", *Phys B: Condensed Matter* Vol. 534, pp. 90-97.

[20]. Yang F., Chong A.C.M., Lam D.C.C., Tong P. (2002), "Couple stress based strain gradient theory for elasticity", *International Journal of Solid and Structures*, Vol. 39, pp. 2731-2743.

[21]. Toupin R.A. (1962), "Elastic materials with couple-stresses", *Archive for Rational Mechanics and Analysis*, Vol. 11, pp. 385-414.

[22]. Mindlin R.D., Tiersten H.F. (1962), "Effects of couple-stresses in linear elasticity", *Archive for Rational Mechanics and Analysis*, Vol. 11, pp. 415-448.

[23]. Koiter W.T. (1964), "Couple stresses in the theory of elasticity", *I and II. Nederl Akad Wetensch Proc Ser B*, Vol. 67, pp.17-44.

[24]. Dehrouyeh-Semnani A.M., Nikkhah-Bahrami M. (2015), "A discussion on evaluation of material length scale parameter based on micro-cantilever test", *Composite Structures*, Vol. 122, pp. 425-429.

[25]. Khajueenejad F., Ghanbari J. (2015), "Internal length parameter and buckling analysis of carbon nanotubes using modified couple stress theory and Timoshenko beam model", *Materials Research Express* 2, 105009.

[26]. Lam D.C.C., Yang F., Chong A.C.M., Wang J., Tong P. (2003), "Experiments and theory in strain gradient elasticity", *Journal of the Mechanics and Physics of Solids*, Vol. 51, pp. 1477-1508.

[27]. Lu P., Zhang P.Q., Lee H.P., Wang C.M., Reddy J.N. (2007), "Non-local elastic plate theories". *Proc R Soc A Math Phys Eng Sci*, Vol. 463, pp. 3225-3240.

[28]. Duan W.H., Wang C.M. (2007), "Exact solutions for axisymmetric bending of micro/nanoscale circular plates based on nonlocal plate theory", *Nanotechnology*, Vol. 18, 385704, pp. 1-5.

[29]. Aksencer T., Aydogdu M. (2011), "Lévy type solution method for vibration and buckling of nanoplates using nonlocal elasticity theory", *Physics E*, Vol. 43, pp. 954-959.

[30]. Shakouri A., Ng TY, Lin R.M. (2011), "Nonlocal plate model for the free vibration analysis of nanoplates with different boundary conditions", *Journal of Computational and Theoretical Nanoscience*, Vol. 8, pp. 2118-2128.

[31]. Phadikar J.K., Pradhan S.C. (2010), "Variational formulation and finite element analysis for nonlocal elastic nanobeams and nanoplates", *Computational Materials Science*, Vol. 49, pp. 492-499.

[32]. Ansari R., Rajabiehfard R., Arash B. (2010), "Nonlocal finite element model for vibrations of embedded multi-layered graphene sheets", *Computational Materials Science*, Vol. 49, pp. 831-838.

[33]. Nguyen N.T., Hui D., Lee J., Nguyen-Xuan H. (2015), "An efficient computational approach for size-dependent analysis of functionally graded nanoplates", *Computer Methods in Applied Mechanics Engineering*, Vol. 297, pp. 191-218.

[34]. Anjomshoa A. (2013), "Application of Ritz functions in buckling analysis of embedded orthotropic circular and elliptical micro/nano-plates based on nonlocal elasticity theory", *Meccanica*, Vol. 48, pp. 1337-1353.

[35]. Anjomshoa A., Shahidi A.R., Shahidi S.H., Nahvi H. (2015), "Frequency analysis of embedded orthotropic circular and elliptical micro/nano-plates using nonlocal variational principle", *Journal of Solid Mechanics*, Vol. 7, pp. 13-27.

[36]. Mohammadi M., Farajpour A., Moradi A., Ghayour M. (2014), "Shear buckling of orthotropic rectangular graphene sheet embedded in an elastic medium in thermal environment", *Composites Part B: Engineering*, Vol. 56, pp. 629-637.

[37]. Ashoori A.R., Salari E., Sadough Vanini S.A. (2016), "Size-dependent thermal stability analysis of embedded functionally graded annular nanoplates based on the nonlocal elasticity theory". *International Journal of Mechanical Sciences*, Vol. 119, pp. 396-411.

[38]. Pradhan S.C., Phadikar J.K. (2009), "Nonlocal elasticity theory for vibration of nanoplates", *Journal of Sound Vibration*, Vol. 325, pp. 206-223.

[39]. Pradhan S.C., Phadikar J.K. (2011), "Nonlocal theory for buckling of nanoplates", *International Journal of Structural Stability Dynamics*, Vol. 11, pp. 411-429.

[40]. Ansari R., Sahmani S., Arash B. (2010), "Nonlocal plate model for free vibrations of single-layered graphene sheets", *Physics Letter A*, Vol. 375, pp. 53-62.

[41]. Ansari R., Arash B., Rouhi H. (2011), "Vibration characteristics of embedded multi-layered graphene sheets with different boundary conditions via nonlocal elasticity", *Composite Structures*, Vol. 93, pp. 2419-2429.

[42]. Hosseini-Hashemi S., Bedroud M., Nazemnezhad R. (2013), "An exact analytical solution for free vibration of functionally graded circular/annular Mindlin nanoplates via nonlocal elasticity", *Composite Structures*, Vol. 103, pp. 108-118.

[43]. Anjomshoa A., Tahani M. (2016), "Vibration analysis of orthotropic circular and elliptical nano-plates embedded in elastic medium based on nonlocal Mindlin plate theory and using Galerkin method", *Journal of Mechanical Science and Technology*, Vol. 30, pp. 2463-2474.

[44]. Golmakani M.E., Rezatalab J. (2014), "Nonlinear bending analysis of orthotropic nanoscale plates in an elastic matrix based on nonlocal continuum mechanics", *Composite Structures*, Vol. 111, pp. 85-97.

[45]. Dastjerdi S., Jabbarzadeh M., Aliabadi S. (2016), "Nonlinear static analysis of single layer annular/circular graphene sheets embedded in Winkler–Pasternak elastic matrix based on non-local theory of Eringen", *Ain Shams Engineering Journal*, Vol. 7, pp. 873-884.

[46]. Dastjerdi S., Jabbarzadeh M. (2017), "Non-linear bending analysis of multi-layer orthotropic annular/circular graphene sheets embedded in elastic matrix in thermal environment based on non-local elasticity theory", *Applied Mathematical Modelling*, Vol. 41, pp. 83-101.

[47]. Ansari R., Norouzzadeh A. (2016), "Nonlocal and surface effects on the buckling behavior of functionally graded nanoplates: an isogeometric analysis", *Physics E*, Vol. 84, pp. 84-97.

[48]. Aghababaei R., Reddy J.N. (2009), "Nonlocal third-order shear deformation plate theory with application to bending and vibration of plates", *Journal of Sound and Vibration*, Vol. 326, pp. 277-289.

[49]. Pradhan S.C. (2009), "Buckling of single layer graphene sheet based on nonlocal elasticity and higher order shear deformation theory. *Physics Letter A*, Vol. 373, pp. 4182-4188.

[50]. Pradhan S.C., Sahu B. (2010), "Vibration of single layer graphene sheet based on nonlocal elasticity and higher order shear deformation theory", *Journal of Computational and Theoretical Nanoscience*, Vol. 7, pp. 1042-1050.

[51]. Ansari R., Sahmani S. (2013), "Prediction of biaxial buckling behavior of single-layered graphene sheets based on nonlocal plate models and molecular dynamics simulations", *Applied Mathematical Modelling*, Vol. 37, pp. 7338-7351.

[52]. Daneshmehr A., Rajabpoor A., Pourdavood M. (2014), "Stability of size dependent functionally graded nanoplate based on nonlocal elasticity and higher order plate theories and different boundary conditions", *International Journal of Engineering Science*, Vol. 82, pp. 84-100.

[53]. Daneshmehr A., Rajabpoor A., Hadi A. (2015), "Size dependent free vibration analysis of nanoplates made of functionally graded materials based on nonlocal elasticity theory with high order theories", *International Journal of Engineering Science*, Vol. 95, pp. 23-35.

[54]. Nami, M. R., M. Janghorban, and M. Damadam (2015), "Thermal buckling analysis of functionally graded rectangular nanoplates based on nonlocal third-order shear deformation theory", *Aerospace Science and Technology*, Vol. 41, pp. 7-15.

[55]. Sobhy M. (2014), "Generalized two-variable plate theory for multi-layered graphene sheets with arbitrary boundary conditions", *Acta Mechanica*, Vol. 225, pp. 2521-2538.

[56]. Thai H.T., Choi D.H. (2013), "Efficient higher-order shear deformation theories for bending and free vibration analyses of functionally graded plates", *Archive of Applied Mechanics*, Vol. 83, pp. 1755-1771.

[57]. Sobhy M. (2015), "Lévy-type solution for bending of single-layered graphene sheets in thermal environment using the two-variable plate theory", *Intenational Journal of Mechanical Science*, Vol. 90, pp. 171-178.

[58]. Sobhy M. (2015), "Hygrothermal deformation of orthotropic nanoplates based on the state-space concept", *Composites Part B: Engineering*, Vol. 79, pp. 224-235.

[59]. Zenkour A.M., Sobhy M. (2013), "Nonlocal elasticity theory for thermal buckling of nanoplates lying on Winkler–Pasternak elastic substrate medium", *Physica E*: *Low-Demensional Systems and Nanostructures,* Vol. 53, pp. 251-259.

[60]. Alzahrani E.O., Zenkour A.M., Sobhy M. (2013), "Small scale effect on hygro-thermo-mechanical bending of nanoplates embedded in an elastic medium", *Composite Structures*, Vol. 105, pp. 163-172.

[61]. Thai H.T., Vo T.P., Nguyen T.K., Lee J. (2014), "A nonlocal sinusoidal plate model for micro/nanoscale plates", *Proceedings of Institution of Mechanical Engineering, Part C: Journal of Mechanical Engineering Science*, Vol. 228, pp. 2652-2660.

[62]. Touratier M. (1991), "An efficient standard plate theory". *International Journal of Engineering Science*. 1991; Vol. 29, pp. 901-916.

[63]. Belkorissat I., Houari M.S.A., Tounsi A., Bedia E.A.A., Mahmoud S.R. (2015), "On vibration properties of functionally graded nano-plate using a new nonlocal refined four variable model", *Steel Composite Structures*, Vol. 18, pp. 1063-1081.

[64]. Phung-Van P., Lieu Q.X., Nguyen-Xuan H., Wahab M.A.. (2017), "Size-dependent isogeometric analysis of functionally graded carbon nanotube-reinforced composite nanoplates", *Composite Structures*, Vol. 166, pp.120–135.

[65]. Zenkour, A., and M. Sobhy (2013), "Nonlocal elasticity theory for thermal buckling of nanoplates lying on Winkler-Pasternak elastic substrate medium", *Physica E: Low-dimensional Systems and Nanostructures*, Vol. 53, pp. 251-259.

[66]. Tran, T. T., Tran, V. K., Pham, Q.-H., and Zenkour, A. M. (2021), "Extended four-unknown higher-order shear deformation nonlocal theory for bending, buckling and free vibration of functionally graded porous nanoshell resting on elastic foundation", *Composite Structures*, 113737.

[67]. Thai, H-T., Vo, T.P., Nguyen, T-K., Kim, S-E. (2017), "A review of continuum mechanics models for size-dependent analysis of beams and plates", *Composite Structures*, doi: http://dx.doi.org/10.1016/j.compstruct.2017.06.040.

[68]. Arash, B., and Q. Wang (2012), "A review on the application of nonlocal elastic models in modeling of carbon nanotubes and graphenes", *Computational materials science*, Vol. 51, pp. 303-313.

[69]. Vikram Singh Chandel, Guannan Wang, and Mohammad Talha (2020), "Advances in modelling and analysis of nano structures: a review", *Nanotechnology Reviews*, Vol. 9, pp. 230-258.

[70]. Shahsavari, D., M. Shahsavari, L. Li, and B. Karami (2018), "A novel quasi-3D hyperbolic theory for free vibration of FG plates with porosities resting on Winkler/Pasternak/Kerr foundation", *Aerospace Science and Technology*, Vol. 72, pp. 134-149.

[71]. Reddy, J. N., *Mechanics of laminated composite plates and shells: theory and analysis*, 2nd ed, CRC Press.

[72]. Amin Anjomshoa, Ali Reza Shahidi, Behrooz Hassani, Emad Jomehzadeh (2014), "Finite element buckling analysis of multi-layered graphene

sheets on elastic substrate based on nonlocal elasticity theory", *Applied Mathematical Modelling,* Vol. 38, pp. 5934–5955.

[73]. Mohammed Sobhy (2015), "A comprehensive study on FGM nanoplates embedded in an elastic medium", *Composite Structures*, Vol. 134, pp. 966-980.

[74]. Thai, H.-T., and D.-H. Choi (2021), "A refined plate theory for functionally graded plates resting on elastic foundation", *Composites Science and Technology*, Vol. 71, pp. 1850-1858.

[75]. Roque, C., D. Cunha, C. Shu, and A. Ferreira (2021), "A local radial basis functions-Finite differences technique for the analysis of composite plates", *Engineering Analysis with Boundary Elements*, Vol. 35, pp. 363-374.

[76]. Thai, C.H., H. Nguyen-Xuan, S. P. A. Bordas, N. Nguyen-Thanh, and T. Rabczuk (2015), "Isogeometric analysis of laminated composite plates using the higher-order shear deformation theory", *Mechanics of Advanced Materials and Structures*, Vol. 22, pp. 451-469.

[77]. I. Belkorissat, M.S.A. Houari, A. Tounsi, E. Bedia, S. Mahmoud (2015), "On vibration properties of functionally graded nano-plate using a new nonlocal refined four variable model", *Steel Composite Structures*, Vol. 18, pp. 1063-1081.

[78]. Aghababaei, R., and J. Reddy (2009), "Nonlocal third-order shear deformation plate theory with application to bending and vibration of plates", *Journal of Sound and Vibration*, Vol. 326, pp. 277-289.

[79]. Qian, L.F. (2003), "Free and Forced Vibrations of Thick Rectangular Plates using Higher-Order Sheara and Normal Deformable Plate Theory and Meshless Petrov-Galerkin (MLPG) Method", *Computer Modeling in Engineering & Sciences*, Vol. 4, pp. 519–534.

[80]. Aifantis, E.C. (1999), *Strain gradient interpretation of size effects, Fracture scaling*, Springer, New York.

[81]. Eringen, A.C. (1983), "On differential equations of nonlocal elasticity and solutions of screw dislocation and surface waves", *Journal of Applied Physics*, Vol. 54, pp. 4703-4710.

[82]. Li, C., C. W. Lim, and J. Yu (2011), "Twisting statics and dynamics for circular elastic nanosolids by nonlocal elasticity theory", *Acta Mechanica Solida Sinica*, Vol. 24, 484-494.

[83]. Ansari, R., S. Sahmani, and B. Arash (2010), "Nonlocal plate model for free vibrations of single-layered graphene sheets", *Physics Letters A*, Vol. 375, pp. 53-62.

[84]. Ana, S. R., and A. Farajpour (2014), "Decoupling the nonlocal elasticity equations for thermo-mechanical vibration of circular graphene sheets including surface effects", *Physica E: Low-dimensional Systems and Nanostructures*, Vol. 60, pp. 80-90.

[85]. Jalali, S., E. Jomehzadeh, and N. Pugno (2016), "Influence of out-of-plane defects on vibration analysis of graphene: Molecular Dynamics and Non-local Elasticity approaches", *Superlattices and Microstructures*, Vol. 91, pp. 331-344.

[86]. Pradhan, S., and T. Murmu (2009), "Small scale effect on the buckling of single-layered graphene sheets under biaxial compression via nonlocal continuum mechanics", *Computational materials science*, Vol. 47, pp. 268-274.

[87]. Reddy, J. (2010), "Nonlocal nonlinear formulations for bending of classical and shear deformation theories of beams and plates", *International Journal of Engineering Science*, Vol. 48, pp. 1507-1518.

[88]. Prandhan, S.C., and Phadikar, J.K. (2011), "Nonlocal theory for buckling of nano-plates", *International Journal of Structural Stability and Dynamics*, Vol. 11, pp. 411-429.

[89]. Farajpour, A., M. Danesh, and M. Mohammadi (2011), "Buckling analysis of variable thickness nanoplates using nonlocal continuum

mechanics", *Physica E: Low-dimensional Systems and Nanostructures*, Vol. 44, pp. 719-727.

[90]. Murmu, T., and S. Adhikari (2011), "Nonlocal vibration of bonded double-nanoplate-systems", *Composites Part B: Engineering*, Vol. 42, pp. 1901-1911.

[91]. Aksencer, T., and M. Aydogdu (2012), "Forced transverse vibration of nanoplates using nonlocal elasticity", *Physica E: Low-dimensional Systems and Nanostructures*, Vol. 44, pp. 1752-1759.

[92]. Satish, N., S. Narendar, and S. Gopalakrishnan (2012), "Thermal vibration analysis of orthotropic nanoplates based on nonlocal continuum mechanics", *Physica E: Low-dimensional Systems and Nanostructures*, Vol. 44, pp. 1950-1962.

[93]. Shen, Z.-B., H.-L. Tang, D.-K. Li, and G.-J. Tang (2012), "Vibration of single-layered graphene sheet-based nanomechanical sensor via nonlocal Kirchhoff plate theory", *Computational Materials Science*, Vol. 61, pp. 200-205.

[94]. Hosseini-Hashemi, S., M. Zare, and R. Nazemnezhad (2013), "An exact analytical approach for free vibration of Mindlin rectangular nano-plates via nonlocal elasticity", *Composite Structures*, Vol. 100, pp. 290-299.

[95]. Fazelzadeh, S. A., and E. Ghavanloo (2014), "Nanoscale mass sensing based on vibration of single-layered graphene sheet in thermal environments", *Acta Mechanica Sinica*, Vol. 30, pp. 84-91.

[96]. Tran, V.-K., Tran, T.-T., Phung, M.-V., Pham, Q.-H., and Nguyen-Thoi, T. (2020), "A Finite Element Formulation and Nonlocal Theory for the Static and Free Vibration Analysis of the Sandwich Functionally Graded Nanoplates Resting on Elastic Foundation". *Journal of Nanomaterials*, 2020.

[97]. Liu, C., Yu, J., Xu, W., Zhang, X., and Wang, X. (2021), "Dispersion characteristics of guided waves in functionally graded anisotropic

micro/nano-plates based on the modified couple stress theory", *Thin-Walled Structures*, Vol. 161, 107527.

[98]. Phung-Van, P., and Thai, C. H. (2021), "A novel size-dependent nonlocal strain gradient isogeometric model for functionally graded carbon nanotube-reinforced composite nanoplates", *Engineering with Computers*, Vol. 2021, pp. 1-14.

[99]. Xinran, Z., M. Huang, A. Dongqi, C. Zhou, and R. Li. (2021), "New analytic bending, buckling, and free vibration solutions of rectangular nanoplates by the symplectic superposition method", *Scientific Reports (Nature Publisher Group)*, Vol. 11(1).

[100]. Ho, D. T., S.-D. Park, S.-Y. Kwon, K. Park, and S. Y. Kim (2014), "Negative Poisson's ratios in metal nanoplates", *Nature communications*, Vol. 5, pp. 1-8.

[101]. Ke, L.-L., Y.-S. Wang, J. Yang, and S. Kitipornchai (2014), "Free vibration of size-dependent magneto-electro-elastic nanoplates based on the nonlocal theory", *Acta Mechanica Sinica*, Vol. 30, pp. 516-525.

[102]. Malekzadeh, P., M. G. Haghighi, and M. Shojaee (2014), "Nonlinear free vibration of skew nanoplates with surface and small scale effects", *Thin-Walled Structures*, Vol. 78, pp. 48-56.

[103]. Lee, Z., C. Ophus, L. Fischer, N. Nelson-Fitzpatrick, K. Westra, S. Evoy, V. Radmilovic, U. Dahmen, and D. Mitlin (2006), "Metallic NEMS components fabricated from nanocomposite Al-Mo films", *Nanotechnology*, Vol. 17, pp. 3063.

[104]. Simsek, M. (2012), "Nonlocal effects in the free longitudinal vibration of axially functionally graded tapered nanorods", *Computational Materials Science*, Vol. 61, pp. 257-265.

[105]. Simsek, M., and H. Yurtcu (2013), "Analytical solutions for bending and buckling of functionally graded nanobeams based on the nonlocal Timoshenko beam theory", *Composite Structures*, Vol. 97, pp. 378-386.

[106]. Natarajan, S., S. Chakraborty, M. Thangavel, S. Bordas, and T. Rabczuk (2012), "Size-dependent free flexural vibration behavior of functionally graded nanoplates", *Computational Materials Science*, Vol. 65, pp. 74-80.

[107]. Nazemnezhad, R., and S. Hosseini-Hashemi (2014), "Nonlocal nonlinear free vibration of functionally graded nanobeams", *Composite Structures*, Vol. 110, pp. 192-199.

[108]. Hosseini-Hashemi, S., I. Nahas, M. Fakher, and R. Nazemnezhad (2014), "Surface effects on free vibration of piezoelectric functionally graded nanobeams using nonlocal elasticity", *Acta Mechanica*, Vol. 225, pp. 1555-1564.

[109]. Hosseini-Hashemi, S., R. Nazemnezhad, and M. Bedroud (2014), "Surface effects on nonlinear free vibration of functionally graded nanobeams using nonlocal elasticity", *Applied Mathematical Modelling*, Vol. 38, pp. 3538-3553.

[110]. Jung, W.-Y., and S.-C. Han (2013), "Analysis of sigmoid functionally graded material (S-FGM) nanoscale plates using the nonlocal elasticity theory", *Mathematical Problems in Engineering*, Vol. 2013.

[111]. Hosseini-Hashemi, S., M. Bedroud, and R. Nazemnezhad (2013), "An exact analytical solution for free vibration of functionally graded circular/annular Mindlin nanoplates via nonlocal elasticity", *Composite Structures*, Vol. 103, pp. 108-118.

[112]. Salehipour, H., H. Nahvi, and A. Shahidi (2015), "Exact analytical solution for free vibration of functionally graded micro/nanoplates via three-dimensional nonlocal elasticity", *Physica E: Low-dimensional Systems and Nanostructures*, Vol. 66, pp. 350-358.

[113]. Salehipour, H., A. Shahidi, and H. Nahvi (2015), "Modified nonlocal elasticity theory for functionally graded materials", *International Journal of Engineering Science*, Vol. 90, pp. 44-57.

[114]. Ansari, R., M. F. Shojaei, A. Shahabodini, and M. Bazdid-Vahdati (2015), "Three-dimensional bending and vibration analysis of functionally graded nanoplates by a novel differential quadrature-based approach", *Composite Structures*, Vol. 131, pp. 753-764.

[115]. Wang, Y.-Z., and F.-M. Li (2012), "Static bending behaviors of nanoplate embedded in elastic matrix with small scale effects", *Mechanics Research Communications*, Vol. 41, pp. 44-48.

[116]. Narendar, S., and S. Gopalakrishnan (2012), "Nonlocal continuum mechanics based ultrasonic flexural wave dispersion characteristics of a monolayer graphene embedded in polymer matrix", *Composites Part B: Engineering*, Vol. 43, pp. 3096-3103.

[117]. Pouresmaeeli, S., E. Ghavanloo, and S. Fazelzadeh (2013), "Vibration analysis of viscoelastic orthotropic nanoplates resting on viscoelastic medium", *Composite structures*, Vol. 96, pp. 405-410.

[118]. Daikh, A. A., and A. M. Zenkour (2020), "Bending of Functionally Graded Sandwich Nanoplates Resting on Pasternak Foundation under Different Boundary Conditions", *Journal of Applied and Computational Mechanics*, Vol. 2020.

[119]. Ebrahimi, F., A. Dabbagh, and T. Rabczuk (2021), "On wave dispersion characteristics of magnetostrictive sandwich nanoplates in thermal environments", *European Journal of Mechanics-A/Solids*, Vol. 85, 104130.

[120]. Panyatong, M., B. Chinnaboon, and S. Chucheepsakul (2015), "Incorporated effects of surface stress and nonlocal elasticity on bending analysis of nanoplates embedded in an elastic medium", *Suranaree Journal of Science and Technology*, Vol. 22, pp. 21-33.

[121]. Anitescu, C., E. Atroshchenko, N. Alajlan, and T. Rabczuk (2019), "Artificial neural network methods for the solution of second order boundary value problems", *Computers, Materials and Continua*, Vol. 59, pp. 345-359.

[122]. Guo, H., Zhuang, X., and Rabczuk, T. (2019), "A deep collocation method for the bending analysis of Kirchhoff plate", *Computers, Materials & Continua*, Vol. 59, pp. 433-456.

[123]. Samaniego, E., C. Anitescu, S. Goswami, V. M. Nguyen-Thanh, H. Guo, K. Hamdia, X. Zhuang, and T. Rabczuk (2020), "An energy approach to the solution of partial differential equations in computational mechanics via machine learning: Concepts, implementation and applications", *Computer Methods in Applied Mechanics and Engineering*, Vol. 362, 112790.

[124]. Vu-Bac, N., T. Lahmer, X. Zhuang, T. Nguyen-Thoi, and T. Rabczuk (2016), "A software framework for probabilistic sensitivity analysis for computationally expensive models", *Advances in Engineering Software*, Vol. 100, pp. 19-31.

[125]. Zhuang, X., H. Guo, N. Alajlan, H. Zhu, and T. Rabczuk (2021), "Deep autoencoder based energy method for the bending, vibration, and buckling analysis of Kirchhoff plates with transfer learning", *European Journal of Mechanics-A/Solids*, Vol. 2021, 104225.

APPENDICES

1. Appendix 1: Matrices and Expressions

$$\mathbf{P}(r,s) = \underset{5\times40}{\begin{bmatrix} [p]_{1\times8} & [0] & [0] & [0] & [0] \\ [0] & [p] & [0] & [0] & [0] \\ [0] & [0] & [p] & [0] & [0] \\ [0] & [0] & [0] & [p] & [0] \\ [0] & [0] & [0] & [0] & [p] \end{bmatrix}}$$

where:

$$\underset{1\times8}{\mathbf{P}} = \underbrace{\begin{bmatrix} 1 & r & s & rs & r^2 & s^2 & r^2s & rs^2 \end{bmatrix}}_{1\times8}$$

$$\underset{1\times8}{[0]} = \underbrace{\begin{bmatrix} 0 & 0 & 0 & 0 & 0 & 0 & 0 & 0 \end{bmatrix}}_{1\times8}$$

- The matrix contains the coordinates of the i node elements

$$\underset{5\times40}{\mathbf{A}_i} = \begin{bmatrix} [P_i] & [0] & [0] & [0] & [0] \\ [0] & [P_i] & [0] & [0] & [0] \\ [0] & [0] & [P_i] & [0] & [0] \\ [0] & [0] & [0] & [P_i] & [0] \\ [0] & [0] & [0] & [0] & [P_i] \end{bmatrix}$$

$$\underset{1\times8}{\mathbf{P}_i} = \begin{bmatrix} 1 & r_i & s_i & r_is_i & r_i^2 & s_i^2 & r_i^2s_i & r_is_i^2 \end{bmatrix}$$

- Jacobi matrix:

$$\mathbf{J} = \begin{bmatrix} -\frac{1}{4}(1-s)(1-2r-s) & -\frac{1}{4}(1-s)(s-2r) & -\frac{1}{4}(1+s)(-2r-s) & -\frac{1}{4}(1+s)(s-2r) & \frac{1}{2}(1-s)(-2r) & \frac{1}{2}(1-s^2) & \frac{1}{2}(-2r)(1+s) & -\frac{1}{2}(1-s^2) \\ -\frac{1}{4}(1-r)(1-2s-r) & -\frac{1}{4}(1+r)(r-2s) & -\frac{1}{4}(1+r)(-2s-r) & -\frac{1}{4}(1-r)(r-2s) & -\frac{1}{2}(1-r^2) & \frac{1}{2}(1+r)(-2s) & \frac{1}{2}(1-r^2) & \frac{1}{2}(1-r)(-2s) \end{bmatrix} \begin{bmatrix} x_1 & y_1 \\ x_2 & y_2 \\ x_3 & y_3 \\ x_4 & y_4 \\ x_5 & y_5 \\ x_6 & y_6 \\ x_7 & y_7 \\ x_8 & y_8 \end{bmatrix}$$

- Functional partial derivatives in the form of variables r, s:

$$\frac{\partial N_1}{\partial r} = -\frac{1}{4}(1-s)(1-2r-s); \qquad \frac{\partial N_2}{\partial r} = \frac{1}{2}(1-s)(-2r);$$

$$\frac{\partial N_1}{\partial s} = -\frac{1}{4}(1-r)(1-2s-r); \qquad \frac{\partial N_2}{\partial s} = -\frac{1}{2}(1-r^2);$$

$$\frac{\partial N_3}{\partial r} = -\frac{1}{4}(1-s)(s-2r); \qquad \frac{\partial N_4}{\partial r} = \frac{1}{2}(1-s^2);$$

$$\frac{\partial N_3}{\partial s} = -\frac{1}{4}(1+r)(r-2s); \qquad \frac{\partial N_4}{\partial s} = \frac{1}{2}(1+r)(-2s);$$

$$\frac{\partial N_5}{\partial r} = -\frac{1}{4}(1+s)(-2r-s); \qquad \frac{\partial N_6}{\partial r} = \frac{1}{2}(-2r)(1+s);$$

$$\frac{\partial N_5}{\partial s} = -\frac{1}{4}(1+r)(-2s-r); \qquad \frac{\partial N_6}{\partial s} = \frac{1}{2}(1-r^2);$$

$$\frac{\partial N_7}{\partial r} = -\frac{1}{4}(1+s)(s-2r); \qquad \frac{\partial N_8}{\partial r} = -\frac{1}{2}(1-s^2);$$

$$\frac{\partial N_7}{\partial s} = -\frac{1}{4}(1-r)(r-2s); \qquad \frac{\partial N_8}{\partial s} = \frac{1}{2}(1-r)(-2s);$$

2. Appendix 2: The calculation programs

2.1. The calculation programs for solving static behavior of FGP nanoplate resting on elastic foundation: FGP_Nanoplates_FSDT_Nonlocal_Static_2022 (FNFNS_2022)

```
%-------------------------------------------------------------------------
clear
clc

disp('Please wait Programme is under Run')
%-------------------------------------------------------------------------
%   Input data % Geometrical and material properties of plate
%-------------------------------------------------------------------------
material=[1 2];
for dem=1:length(material)
    mater=material(dem)
% file_name='tamchuL'
% eval(file_name);        % Read input file
a=10; % nm
b=a/1; % nm
h=a/10;% nm
nX=8;
```

```
nY=nX;
%-------------------------------
Ec=380e9;
Em=70e9;
rhoc=3800;
rhom=2707;
nuc=0.3;
num=0.3;
nu=0.3;
muy=4;
k=5;
phii=0.2;
kss=5/6;
%----------------
%% He so nen
D11=Em*h^3/12/(1-nu^2);
Kw=100;
K1=Kw*D11/a^4;
Gb=10;
K2=Gb*D11/a^2;

alphac=3.3e-6;
alpham=17.3e-6;

P0=-1;
dz=h/1e5;
hesom=zeros(5);
Dm=zeros(3);
Dmb=Dm;
Db=Dm;
Ds=zeros(2);

tu=0;
mau=0;

NxT=0;
NyT=0;
if mater==1
material_porous_1;
elseif mater==2
    material_porous_2;
else
material_porous_3;
end
h0=0;
 [coordinates, nodes] = rectangularMesh8nut(a,b,nX,nY);
%
nel = length(nodes);                  % number of elements
nnel=8;                               % number of nodes per element
ndof=5;                               % number of dofs per node
nnode = length(coordinates) ;         % total number of nodes in system
sdof=nnode*ndof;                      % total system dofs
edof=nnel*ndof;                       % degrees of freedom per element
%------------------------------------------------------------------------
% PlotMesh8node(coordinates,nodes);
%------------------------------------------------------------------------
[pointb,weightb]=GaussQuadrature('night');
```

```
[points,weights] = GaussQuadrature('second');
%-----------------------------------------------------------------------
force = zeros(sdof,1) ;              % System Force Vector
stiffness=zeros(sdof,sdof);         % system stiffness matrix
mass=zeros(sdof,sdof);              % system stiffness matrix
index=zeros(edof,1);                % index vector
%-----------------------------------------------------------------------

for iel=1:nel                       % loop for the total number of
elements
for i=1:nnel
node(i)=nodes(iel,i);               % extract connected node for (iel)-th
element
xx(i)=coordinates(node(i),1);       % extract x value of the node
yy(i)=coordinates(node(i),2);       % extract y value of the node
P(i) = P0*1; sin(xx(i)*pi/a)*sin(yy(i)*pi/b);
Px(i)=-01*(pi/a)^2*P(i);
Py(i)=-01*(pi/b)^2*P(i);
end
knenw = zeros(edof,edof);
knens = zeros(edof,edof);
ke = zeros(edof,edof);              % initialization of element stiffness
matrix
me = zeros(edof,edof);              % initialization of element stiffness
matrix
kb = zeros(edof,edof);              % initialization of bending matrix
ks = zeros(edof,edof);              % initialization of shear matrix
f = zeros(edof,1) ;                 % initialization of force vector
k_T = zeros(edof,edof);
%-----------------------------------------------------------------------
%-----------------------------------------------------------------------
for intx=1:9
xi=pointb(intx,1);                          % sampling point in x-axis
wtx=weightb(intx,1);                        % weight in x-axis
% for inty=1:3
eta=pointb(intx,2);                         % sampling point in y-axis
wty=weightb(intx,2) ;                       % weight in y-axis
% [shape,dhdr,dhds,shapeQ]=Shapefunctions(xi,eta); % compute shape
functions and derivatives at sampling point
[shape,dhdr,dhds,d2hdr2,d2hdrds,d2hds2,shapeQ]=Shapefunctions8nut(xi,eta)
;
% [dhdr,dhds,d2hdr2,d2hdrds,d2hds2]=Shapefunctions1(xi,eta);
% [detjacobian,invjacobian]=Jacobian(nnel,dhdr,dhds,xx,yy);  % compute
Jacobian
[jacobian,detjacobian,invjacobian]=Jacobian1(nnel,dhdr,dhds,xx,yy);
[dhdx,dhdy,dshapex,dshapey]=ShapefunctionDerivatives(nnel,dhdr,dhds,invja
cobian);
%
[d2xdr,dNx,dNy,d2Nxx,d2Nyy,d2Nxy,d2hdx2,d2hdxdy,d2hdy2]=ShapefunctionDeri
vatives2(nnel,...
%
dhdr,dhds,d2hdr2,d2hdrds,d2hds2,jacobian,detjacobian,invjacobian,xx,yy);
[d2hdx2,d2hdxdy,d2hdy2]=ShapefunctionDerivatives22(nnel,...

dhdr,dhds,d2hdr2,d2hdrds,d2hds2,jacobian,detjacobian,invjacobian,xx,yy);
 %---------------
```

```
 Nw=[0 0 shapeQ(1) 0 0, 0 0 shapeQ(2) 0 0,0 0 shapeQ(3) 0 0,0 0 shapeQ(4)
0 0,...
     0 0 shapeQ(5) 0 0, 0 0 shapeQ(6) 0 0,0 0 shapeQ(7) 0 0,0 0 shapeQ(8)
0 0];
 Nwxx=[0 0 d2hdx2(1) 0 0, 0 0 d2hdx2(2) 0 0,0 0 d2hdx2(3) 0 0,0 0
d2hdx2(4) 0 0,...
       0 0 d2hdx2(5) 0 0, 0 0 d2hdx2(6) 0 0,0 0 d2hdx2(7) 0 0,0 0
d2hdx2(8) 0 0];
Nwyy=[0 0 d2hdy2(1) 0 0, 0 0 d2hdy2(2) 0 0,0 0 d2hdy2(3) 0 0,0 0
d2hdy2(4) 0 0,...
       0 0 d2hdy2(5) 0 0, 0 0 d2hdy2(6) 0 0,0 0 d2hdy2(7) 0 0,0 0
d2hdy2(8) 0 0];


[B1,B2]=PlateBending8nut(nnel,dhdx,dhdy);
Bs=PlateShear8nut(nnel,dhdx,dhdy,shape);
fe = Force(nnel,shapeQ,P,Px,Py,muy);
% fe = ForcePBD(nnel,shapeQ,P,Px,Py,muy);
% fe = ForceNano(nnel,shapeQ,P,Px,Py,muy,d2hdx2,d2hdy2);
kb=kb+[B1' B2']*[Dm Dmb;
                 Dmb Db]*[B1; B2]*wtx*wty*detjacobian;
% k_T= k_T +
NxT*(dshapex(3,:)'*dshapex(3,:)+dshapey(3,:)'*dshapey(3,:))*wtx*wty*detja
cobian;
ks=ks+Bs'*Ds*Bs*wtx*wty*detjacobian;
knenw = knenw + K1*(Nw'*Nw + muy*(dshapex(3,:)'*dshapex(3,:) +
dshapey(3,:)'*dshapey(3,:)))*wtx*wty*detjacobian;
knens = knens +
K2*(dshapex(3,:)'*dshapex(3,:)+dshapey(3,:)'*dshapey(3,:)...
    +muy*(Nwxx'*Nwxx + Nwyy'*Nwyy + Nwxx'*Nwyy +
Nwyy'*Nwxx))*wtx*wty*detjacobian;
f = f+fe*wtx*wty*detjacobian ;
me=me+(shape'*hesom*shape+...
        muy*dshapex'*hesom*dshapex+...
        muy*dshapey'*hesom*dshapey)*wtx*wty*detjacobian;
end  % end of numerical integration loop for bending term
 ke = kb+ks+knenw+knens;
 index=elementdof(node,nnel,ndof);% extract system dofs associated with
element
 stiffness(index,index) = stiffness(index,index) + ke;
 mass(index,index) =  mass(index,index) + me;
 force(index,1) = force(index,1) + f;
end
%-------------------------------------------------------------------------
%% Boundary conditions
typeBC = 'ssss' ;        % Boundary Condition type
% typeBC = 'cccc'
% typeBC = 'cscs' ;
% typeBC = 'sssc' ;
% typeBC = 'sfsc' ;
bcdof = BoundaryCondition(typeBC,coordinates) ;
btd=setdiff([1:sdof]',[bcdof]);
displacement = zeros(sdof, 1);
displacement(btd,1) = stiffness(btd, btd)\(force(btd,1)) ;
w = displacement(3:5:sdof) ;
format short
% D1 = 100*Ec*h^3/12/(1-nuc^2) ;
% D2 = 100*Ec*h^3 ;
```

```
maxw2 = 100*Ec*h^3*min(w)/(P0*a^4)
% PlotFieldonDefoMesh(coordinates,nodes,w,w)
% colormap HSV
% return
%% Tinh ung suat
% Sigma_xx
demus=0;
dzz=h/20;
for z=-h/2:dzz:h/2
demus=demus+1;
if mater==1
    Eus=(Em +(Ec-Em)*(0.5+z/h)^k -0.5*phii*(Ec+Em));
elseif mater==2
    Eus=(Em +(Ec-Em)*(0.5+z/h)^k -0.5*phii*(Ec+Em)*(1-2*abs(z)/h));
else
    Eus=(Em +(Ec-Em)*(0.5+z/h)^k -log10(0.5*phii+1)*(Ec+Em)*(1-
2*abs(z)/h));
end
    nu=num;
    C11=Eus/((1-nu)*(1+nu));
    C22=C11;
    C12=nu*C11;
    C66=Eus/2/(1+nu);
Dus1=[C11 C12 0;
     C12 C22 0;
     0   0   C66];
Dus2=[C66 0;
     0 C66];
phantu=  nX/2 + nX*(nX/2 -1);
for i=2
node(i)=nodes(phantu,i);         % extract connected node for (iel)-th
element
xx(i)=coordinates(node(i),1);    % extract x value of the node
yy(i)=coordinates(node(i),2);    % extract y value of the node
end
xi=0;eta=-1;
% [shape,dhdr,dhds,shapeQ]=Shapefunctions(xi,eta); % compute shape
functions and derivatives at sampling point
[shape,dhdr,dhds,d2hdr2,d2hdrds,d2hds2,shapeQ]=Shapefunctions8nut(xi,eta)
;
[detjacobian,invjacobian]=Jacobian(nnel,dhdr,dhds,xx,yy);  % compute
Jacobian
[dhdx,dhdy,dshapex,dshapey]=ShapefunctionDerivatives(nnel,dhdr,dhds,invja
cobian);
[B1,B2]=PlateBending8nut(nnel,dhdx,dhdy);
% kinmtps=shearNaturalStrain(nnel,xx,yy,dhdr,dhds);
% Bs=invjacobian*kinmtps;
Bs=PlateShear8nut(nnel,dhdx,dhdy,shape);
 index=elementdof(node,nnel,ndof);
ungsuat1=  Dus1*[B1 + (z-h0)*B2]*(displacement(index));
ungsuat2=  Dus2*Bs*(displacement(index));
xichma_xx(dem,demus) =10* ungsuat1(1)*h/P0/a;
xichma_yy(dem,demus) =10* ungsuat1(2)*h/P0/a;
xichma_xy(dem,demus) =10* ungsuat1(3)*h/P0/a;
xichma_xz(dem,demus) =10* ungsuat2(1)*h/P0/a;
xichma_yz(dem,demus) =10* ungsuat2(2)*h/P0/a;
end
end
```

```
zz = [-h/2:dzz:h/2];
figure(3);
plot(xichma_xx(1,:),zz/h,'*-
r','MarkerIndices',1:1:length(xichma_xx(1,:)),'LineWidth',1.5);
hold on
plot(xichma_xx(2,:),zz/h,'-
<b','MarkerIndices',1:1:length(xichma_xx(2,:)),'LineWidth',1.5);
 set(gca,...
    'Units','normalized',...
    'Position',[0.15 0.2 .7 .75],...
    'FontUnits','points',...
    'FontWeight','bold',...
    'FontSize',14, ...
    'FontName','Times');
xlabel('\sigma^*_{xx}','Fontsize',14, 'FontName','times');
yticks([-0.5 :0.1: 0.5]);
ylabel('z/h','Fontsize',14, 'FontName','times');
grid on
legend({'Case 1','Case 2'},'Fontsize',12, 'FontName','times')

figure(4);
plot(xichma_xy(1,:),zz/h,'*-
r','MarkerIndices',1:1:length(xichma_xy(1,:)),'LineWidth',1.5);
hold on
plot(xichma_xy(2,:),zz/h,'-
<b','MarkerIndices',1:1:length(xichma_xy(2,:)),'LineWidth',1.5);
 set(gca,...
    'Units','normalized',...
    'Position',[0.15 0.2 .7 .75],...
    'FontUnits','points',...
    'FontWeight','bold',...
    'FontSize',14, ...
    'FontName','Times');
xlabel('\sigma^*_{xy}','Fontsize',14, 'FontName','times');
yticks([-0.5 :0.1: 0.5]);
ylabel('z/h','Fontsize',14, 'FontName','times');
grid on
legend({'Case 1','Case 2'},'Fontsize',12, 'FontName','times')


return
```

2.2. The calculation programs for solving free vibration of FGP nanoplate resting on elastic foundation:

FGP_Nanoplates_FSDT_Nonlocal_Freevibration_2022 (FNFNF_2022)

```
%-------------------------------------------------------------------------
clear
clc
%
disp('Please wait Programme is under Run')
%-------------------------------------------------------------------------
%  Input data % Geometrical and material properties of plate
```

```
%------------------------------------------------------------------

file_name='tamchuL111'
eval(file_name);        % Read input file
a=1; % nm
b=a/1; % nm
h=a/5;% nm
nX=8;
nY=nX;
%------------------------------
Ec=1;
Em=Ec;
rhoc=1;
rhom=1;
nuc=0.3;
num=0.3;
nu=0.3;
muy=0;
k=0;
phii=0.0;
kss=1;
%----------------
%% He so nen
D11=Em*h^3/12/(1-nu^2);
Kw=0;
K1=Kw*D11/a^4;
Gb=0;
K2=Gb*D11/a^2;

alphac=3.3e-6;
alpham=17.3e-6;

P0=-1;
dz=h/4;
hesom=zeros(5);
Dm=zeros(3);
Dmb=Dm;
Db=Dm;
Ds=zeros(2);

tu=0;
mau=0;

NxT=0;
NyT=0;

material_porous_1;
% material_porous_2;
% material_porous_3;

%   [coordinates, nodes] = rectangularMesh8nut(a,b,nX,nY);
%
nel = length(nodes) ;             % number of elements
nnel=8;                           % number of nodes per element
ndof=5;                           % number of dofs per node
nnode = length(coordinates) ;     % total number of nodes in system
```

```
sdof=nnode*ndof;                        % total system dofs
edof=nnel*ndof;                         % degrees of freedom per element
%------------------------------------------------------------------------
PlotMesh(coordinates,nodes);
%------------------------------------------------------------------------
[pointb,weightb]=GaussQuadrature('night');
[points,weights] = GaussQuadrature('second');
%------------------------------------------------------------------------
force = zeros(sdof,1) ;             % System Force Vector
stiffness=zeros(sdof,sdof);         % system stiffness matrix
mass=zeros(sdof,sdof);              % system stiffness matrix
index=zeros(edof,1);               % index vector
%------------------------------------------------------------------------

for iel=1:nel                      % loop for the total number of
elements
for i=1:nnel
node(i)=nodes(iel,i);              % extract connected node for (iel)-th
element
xx(i)=coordinates(node(i),1);      % extract x value of the node
yy(i)=coordinates(node(i),2);      % extract y value of the node
P(i) = P0*sin(xx(i)*pi/a)*sin(yy(i)*pi/b);
Px(i)=-01*(pi/a)^2*P(i);
Py(i)=-01*(pi/b)^2*P(i);
end
knenw = zeros(edof,edof);
knens = zeros(edof,edof);
ke = zeros(edof,edof);             % initialization of element stiffness
matrix
me = zeros(edof,edof);             % initialization of element stiffness
matrix
kb = zeros(edof,edof);             % initialization of bending matrix
ks = zeros(edof,edof);             % initialization of shear matrix
f = zeros(edof,1) ;                % initialization of force vector
k_T = zeros(edof,edof);
%------------------------------------------------------------------------
%------------------------------------------------------------------------
for intx=1:9
xi=pointb(intx,1);                 % sampling point in x-axis
wtx=weightb(intx,1);               % weight in x-axis
% for inty=1:3
eta=pointb(intx,2);                % sampling point in y-axis
wty=weightb(intx,2) ;              % weight in y-axis
% [shape,dhdr,dhds,shapeQ]=Shapefunctions(xi,eta); % compute shape
functions and derivatives at sampling point
[shape,dhdr,dhds,d2hdr2,d2hdrds,d2hds2,shapeQ]=Shapefunctions8nut(xi,eta)
;
% [dhdr,dhds,d2hdr2,d2hdrds,d2hds2]=Shapefunctions1(xi,eta);
% [detjacobian,invjacobian]=Jacobian(nnel,dhdr,dhds,xx,yy);  % compute
Jacobian
[jacobian,detjacobian,invjacobian]=Jacobian1(nnel,dhdr,dhds,xx,yy);
[dhdx,dhdy,dshapex,dshapey]=ShapefunctionDerivatives(nnel,dhdr,dhds,invja
cobian);
[d2xdr,dNx,dNy,d2Nxx,d2Nyy,d2Nxy,d2hdx2,d2hdxdy,d2hdy2]=ShapefunctionDeri
vatives2(nnel,...

dhdr,dhds,d2hdr2,d2hdrds,d2hds2,jacobian,detjacobian,invjacobian,xx,yy);
```

```
[B1,B2]=PlateBending8nut(nnel,dhdx,dhdy);


Bs=PlateShear8nut(nnel,dhdx,dhdy,shape);
fe = Force(nnel,shapeQ,P,Px,Py,muy);
% fe = ForceNano(nnel,shapeQ,P,Px,Py,muy,d2hdx2,d2hdy2);
kb=kb+[B1' B2']*[Dm Dmb;
                 Dmb Db]*[B1; B2]*wtx*wty*detjacobian;
% k_T= k_T +
NxT*(dshapex(3,:)'*dshapex(3,:)+dshapey(3,:)'*dshapey(3,:))*wtx*wty*detja
cobian;
ks=ks+Bs'*Ds*Bs*wtx*wty*detjacobian;
knenw=knenw+K1*(muy*(dshapex(3,:)'*dshapex(3,:)+dshapey(3,:)'*dshapey(3,:
))+...


shape(3,:)'*shape(3,:))*wtx*wty*detjacobian;
knens=knens+K2*(dshapex(3,:)'*dshapex(3,:)+dshapey(3,:)'*dshapey(3,:))*wt
x*wty*detjacobian;
f = f+fe*wtx*wty*detjacobian ;
me=me+(shape'*hesom*shape+...
       muy*dshapex'*hesom*dshapex+...
       muy*dshapey'*hesom*dshapey)*wtx*wty*detjacobian;
end
% end  % end of numerical integration loop for bending term
 ke = kb+ks+knenw+knens;
 index=elementdof(node,nnel,ndof);% extract system dofs associated with
element
 stiffness(index,index) = stiffness(index,index) + ke;
 mass(index,index) =  mass(index,index) + me;
 force(index,1) = force(index,1) + f;
end
%-------------------------------------------------------------------------
%% Boundary conditions
% typeBC = 'ssss' ;         % Boundary Condition type
typeBC = 'cccc'
% typeBC = 'cscs' ;
% typeBC = 'sssc' ;
% typeBC = 'sfsc' ;
bcdof = BoundaryConditionL(typeBC,coordinates) ;
bcval = zeros(1,length(bcdof)) ;
activeDof=setdiff([1:sdof]',[bcdof]);
%-------------------------------------------------------------------------
% Solution
w2 =
eigs(stiffness(activeDof,activeDof),mass(activeDof,activeDof),4,'sm');
% w2 = diag(w2);
w2=sqrt(w2);
Gc=Ec/2/(1+nuc);
omega_ktn=w2*a*sqrt(rhoc/Gc)
return
%-------------------------------------------------------------------------
[Fi, w2] = eig(stiffness(activeDof,activeDof),mass(activeDof,activeDof));
w2 = diag(w2);
[w2,tt]=sort(w2);
w2=sqrt(w2);
% omega_ktn=w2(1:6)*a*sqrt(rhom/Em)
Fi=Fi(:,tt);
%  break
```

```
for k=1:length(activeDof);
    ak=sqrt(Fi(:,k)'*mass(activeDof,activeDof)*Fi(:,k));
    Fi(:,k)=Fi(:,k)/ak;
end

Dang_DD = zeros(sdof, length(activeDof));
Dang_DD(activeDof,:) = Fi;
% Ve dang dao dong rieng
mod1 = Dang_DD(3:5:sdof, 1);
mod2 = Dang_DD(3:5:sdof, 2);
mod3 = Dang_DD(3:5:sdof, 3);
mod4 = Dang_DD(3:5:sdof, 4);
mod5 = Dang_DD(3:5:sdof, 5);
mod6 = Dang_DD(3:5:sdof, 6);
% mod7 = Dang_DD(3:5:sdof, 7);
% mod8 = Dang_DD(3:5:sdof, 8);
% mod9 = Dang_DD(3:5:sdof, 9);
% mod10 = Dang_DD(3:5:sdof, 10);

PlotFieldonDefoMesh(coordinates,nodes,mod1,mod1)
%       title('Mode 1');
colormap HSV
     PlotFieldonDefoMesh(coordinates,nodes,mod2,mod2)
%       title('Mode 2');
colormap HSV
     PlotFieldonDefoMesh(coordinates,nodes,mod3,mod3)
%       title('Mode 3');
colormap HSV
     PlotFieldonDefoMesh(coordinates,nodes,mod4,mod4)
%       title('Mode 4');
colormap HSV
```

2.3. The calculation programs for solving dynamic behavior of FGP nanoplate resting on elastic foundation: FGP_Nanoplates_FSDT_Nonlocal_Dynamic_2022 (FNFND_2022)

```
%------------------------------------------------------------------------
clear
clc
disp('Please wait Programme is under Run')
%------------------------------------------------------------------------
%  Input data % Geometrical and material properties of plate
%------------------------------------------------------------------------
a=10;   % nm
b=a/1;  % nm
h=a/10; % nm
nX=8;
nY=nX;
%------------------------------
Ec=380e9;
Em=70e9;
rhoc=3800;
rhom=2707;
```

```
nuc=0.3;
num=0.3;
nu=0.3;
muy=1;
k=1;
phii=0.2;
kss=5/6;
%-----------------
%% He so nen
D11=Em*h^3/12/(1-nu^2);
Kw=100;
K1=Kw*D11/a^4;
Gb=10;
K2=Gb*D11/a^2;

alphac=3.3e-6;
alpham=17.3e-6;

P0=-1;
dz=h/1000;
hesom=zeros(5);
Dm=zeros(3);
Dmb=Dm;
Db=Dm;
Ds=zeros(2);

tu=0;
mau=0;

NxT=0;
NyT=0;

% material_porous_1;
material_porous_2;
% material_porous_3;

[coordinates, nodes] = rectangularMesh8nut(a,b,nX,nY);
nel = length(nodes) ;                    % number of elements
nnel=8;                                  % number of nodes per element
ndof=5;                                  % number of dofs per node
nnode = length(coordinates) ;            % total number of nodes in system
sdof=nnode*ndof;                         % total system dofs
edof=nnel*ndof;                          % degrees of freedom per element
%-------------------------------------------------------------------------
--
% PlotMesh(coordinates,nodes)
%-------------------------------------------------------------------------
--
[pointb,weightb]=GaussQuadrature('night');
[points,weights] = GaussQuadrature('second');
%-------------------------------------------------------------------------
--
force = zeros(sdof,1) ;                  % System Force Vector
stiffness=zeros(sdof,sdof);              % system stiffness matrix
mass=zeros(sdof,sdof);                   % system stiffness matrix
index=zeros(edof,1);                     % index vector
```

```
%--------------------------------------------------------------------

for iel=1:nel                          % loop for the total number of
elements
for i=1:nnel
node(i)=nodes(iel,i);                  % extract connected node for (iel)-th
element
xx(i)=coordinates(node(i),1);          % extract x value of the node
yy(i)=coordinates(node(i),2);          % extract y value of the node
P(i) = P0*sin(xx(i)*pi/a)*sin(yy(i)*pi/b);
Px(i)=-01*(pi/a)^2*P(i);
Py(i)=-01*(pi/b)^2*P(i);
end
knenw = zeros(edof,edof);
knens = zeros(edof,edof);
ke = zeros(edof,edof);                 % initialization of element stiffness
matrix
me = zeros(edof,edof);                 % initialization of element stiffness
matrix
kb = zeros(edof,edof);                 % initialization of bending matrix
ks = zeros(edof,edof);                 % initialization of shear matrix
f = zeros(edof,1) ;                    % initialization of force vector
k_T = zeros(edof,edof);
%--------------------------------------------------------------------
%--------------------------------------------------------------------
for intx=1:9
xi=pointb(intx,1);                     % sampling point in x-axis
wtx=weightb(intx,1);                   % weight in x-axis
% for inty=1:3
eta=pointb(intx,2);                    % sampling point in y-axis
wty=weightb(intx,2) ;                  % weight in y-axis
% [shape,dhdr,dhds,shapeQ]=Shapefunctions(xi,eta); % compute shape
functions and derivatives at sampling point
[shape,dhdr,dhds,d2hdr2,d2hdrds,d2hds2,shapeQ]=Shapefunctions8nut(xi,eta)
;
% [dhdr,dhds,d2hdr2,d2hdrds,d2hds2]=Shapefunctions1(xi,eta);
% [detjacobian,invjacobian]=Jacobian(nnel,dhdr,dhds,xx,yy);  % compute
Jacobian
[jacobian,detjacobian,invjacobian]=Jacobian1(nnel,dhdr,dhds,xx,yy);
[dhdx,dhdy,dshapex,dshapey]=ShapefunctionDerivatives(nnel,dhdr,dhds,invja
cobian);
[d2xdr,dNx,dNy,d2Nxx,d2Nyy,d2Nxy,d2hdx2,d2hdxdy,d2hdy2]=ShapefunctionDeri
vatives2(nnel,...

dhdr,dhds,d2hdr2,d2hdrds,d2hds2,jacobian,detjacobian,invjacobian,xx,yy);

% [d2hdx2,d2hdxdy,d2hdy2]=ShapefunctionDerivatives22(nnel,...
%
dhdr,dhds,d2hdr2,d2hdrds,d2hds2,jacobian,detjacobian,invjacobian,xx,yy);

 %---------------
 Nw=[0 0 shapeQ(1) 0 0, 0 0 shapeQ(2) 0 0,0 0 shapeQ(3) 0 0,0 0 shapeQ(4)
0 0,...
      0 0 shapeQ(5) 0 0, 0 0 shapeQ(6) 0 0,0 0 shapeQ(7) 0 0,0 0 shapeQ(8)
0 0];
 Nwxx=[0 0 d2hdx2(1) 0 0, 0 0 d2hdx2(2) 0 0,0 0 d2hdx2(3) 0 0,0 0
d2hdx2(4) 0 0,...
```

```
       0 0 d2hdx2(5) 0 0, 0 0 d2hdx2(6) 0 0,0 0 d2hdx2(7) 0 0,0 0
d2hdx2(8) 0 0];
Nwyy=[0 0 d2hdy2(1) 0 0, 0 0 d2hdy2(2) 0 0,0 0 d2hdy2(3) 0 0,0 0
d2hdy2(4) 0 0,...
       0 0 d2hdy2(5) 0 0, 0 0 d2hdy2(6) 0 0,0 0 d2hdy2(7) 0 0,0 0
d2hdy2(8) 0 0];


[B1,B2]=PlateBending8nut(nnel,dhdx,dhdy);
Bs=PlateShear8nut(nnel,dhdx,dhdy,shape);
fe = Force(nnel,shapeQ,P,Px,Py,muy);
% fe = ForceNano(nnel,shapeQ,P,Px,Py,muy,d2hdx2,d2hdy2);
kb=kb+[B1' B2']*[Dm Dmb;
                 Dmb Db]*[B1; B2]*wtx*wty*detjacobian;
% k_T= k_T +
NxT*(dshapex(3,:)'*dshapex(3,:)+dshapey(3,:)'*dshapey(3,:))*wtx*wty*detja
cobian;
ks=ks+Bs'*Ds*Bs*wtx*wty*detjacobian;
knenw = knenw + K1*(Nw'*Nw + muy*(dshapex(3,:)'*dshapex(3,:) +
dshapey(3,:)'*dshapey(3,:)))*wtx*wty*detjacobian;


knens = knens +
K2*(dshapex(3,:)'*dshapex(3,:)+dshapey(3,:)'*dshapey(3,:)...
    +muy*(Nwxx'*Nwxx + Nwyy'*Nwyy + Nwxx'*Nwyy +
Nwyy'*Nwxx))*wtx*wty*detjacobian;
f = f+fe*wtx*wty*detjacobian ;
me=me+(shape'*hesom*shape+...
       muy*dshapex'*hesom*dshapex+...
       muy*dshapey'*hesom*dshapey)*wtx*wty*detjacobian;
end
% end  % end of numerical integration loop for bending term
 ke = kb+ks+knenw+knens;
 index=elementdof(node,nnel,ndof);% extract system dofs associated with
element
 stiffness(index,index) = stiffness(index,index) + ke;
 mass(index,index) =  mass(index,index) + me;
 force(index,1) = force(index,1) + f;
end
%------------------------------------------------------------------
%% Boundary conditions
typeBC = 'ssss' ;          % Boundary Condition type
% typeBC = 'cccc'
% typeBC = 'cscs' ;
% typeBC = 'sssc' ;
% typeBC = 'sfsc' ;
bcdof = BoundaryCondition(typeBC,coordinates) ;
bcval = zeros(1,length(bcdof));
btd=setdiff([1:sdof]',[bcdof]);
so_btd=sdof;
%------------------------------------------------------------------
% Solution
w2 = eigs(stiffness(btd,btd),mass(btd,btd),2,'sm');
% w2 = diag(w2);
ww=sqrt(w2);
betaR=2*0.0/(ww(1)+ww(2)); % 0.008, 0.1; 0.25
alphaR=betaR*ww(1)*ww(2);
C0=alphaR*mass+betaR*stiffness;
C0=C0;
```

```
C=zeros(sdof,sdof);
TT=2*pi/ww(1);
%% programe moving load
 t_max=TT*20;
 t1=t_max/1;
%  thd=0.028;
%  deltaPhi=0.20679*1e6;

 t=0:t_max/500:t_max;
 nt=length(t);
 F0=zeros(sdof,1);
 beta=1/4;
 gamma=1/2;
 for i=1:nt-1

      M=mass;
      C=C0;
      K=stiffness;
      %--------Force------------
      if   t(i)<=t1
     epsilon=0.05*ww(1); Omega=ww(1)+2*epsilon;
      Ft(i)=sin(Omega*t(i));
      else
      Ft(i)=0;
      end
      F=force*Ft(i);

    if i==1

       U = zeros(so_btd, nt);
       V = zeros(so_btd, nt);
       A = zeros(so_btd, nt);

       u0 = zeros(so_btd, 1);
       v0 = zeros(so_btd, 1);
       a0 = zeros(so_btd, 1);

       U(:,1) = u0;
       V(:,1) = v0
       A(:,1) = a0;

       dt = t(2)-t(1);
    end;
    % giai bai toan dong
%      Keff = M + 0.5*dt*C + 0.25*(dt^2)*K;
%
%      A(btd,i+1) = Keff(btd,btd)\(F(btd) - C(btd,btd)*(V(btd,i) +
0.5*dt*A(btd,i)) ...
%                   - K(btd,btd)*(U(btd,i) + dt*V(btd,i) +
0.25*(dt^2)*A(btd,i)));
%      V(btd,i+1) = V(btd,i) + 0.5*dt*A(btd,i) + 0.5*dt*A(btd,i+1);
%      U(btd,i+1) = U(btd,i) + dt*V(btd,i) + dt^2*0.25*A(btd,i) +
dt^2*0.25*A(btd,i+1);
    Keff = M + gamma*dt*C + beta*(dt^2)*K;
    A(btd,i+1) = Keff(btd,btd)\(F(btd) - C(btd,btd)*(V(btd,i) + (1-
gamma)*dt*A(btd,i)) ...
```

```
                          - K(btd,btd)*(U(btd,i) + dt*V(btd,i) + (1/2-
beta)*(dt^2)*A(btd,i)));
    V(btd,i+1) = V(btd,i) + (1-gamma)*dt*A(btd,i) + gamma*dt*A(btd,i+1);
    U(btd,i+1) = U(btd,i) + dt*V(btd,i) + dt^2*(1/2-beta)*A(btd,i) +
dt^2*beta*A(btd,i+1);
 end
figure(1);
Dofs=floor(nnode/2)*ndof+3;
% Dd = E*h^3/12/(1-nu^2);
ktn=10*Ec*h^3/P0/a^4;
plot(t/TT,-U(Dofs,:)*ktn,'-r','LineWidth',2);

%  ylim([-0.35 0.22]);
set(gca,...
 'Units','normalized',...
    'Position',[0.15 0.2 .72 .72],...
    'FontUnits','points',...
    'FontWeight','bold',...
    'FontSize',13, ...
    'FontName','Times')
xlabel('t (s)');
ylabel('w')
% legend('Present','[44]','Fontsize',16, 'FontName','times');
grid on
hold on
box on
```